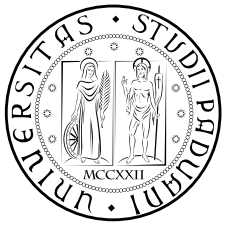

Università degli Studi di Padova

Dipartimento di Scienze Chimiche

Scuola di Dottorato in Scienze Molecolari

XXV Ciclo

Thermodynamic studies on Cu(I) and Ag(I) phosphino complexes with potential anti-tumor activity

Direttore: Prof. Antonino Polimeno

Supervisore: Prof. Plinio Di Bernardo

Dottorando: Francesco Endrizzi

GENNAIO 2013

A Carla e Giuliano, miei mentori e guide

Ai miei amici, sorriso nei momenti felici,
sostegno nelle difficoltà

Alla mia famiglia, la parte migliore di me

Acknowledgments

I would like to express my sincere gratitude to the people of the research group of "Thermodynamics of Lanthanides and Actinides Elements", I worked in ("Dipartimento di Scienze Chimiche", University of Padova). In particular my PhD supervisor, Prof. Plinio Di Bernardo and Prof. Pier Luigi Zanonato for their supervision, their help and the attention devoted to my thesis work.

I am grateful to the many coworkers who have contributed to this three-year project: the people of the Bioinorganic Chemistry group of I.C.I.S.–CNR, Padova, in particular Dr. Francesco Tisato, Dr. Marina Porchia, Dr. Laura Crociani, Dr. Carlo Santini, Dr. Roberta Seraglia for their ESI–MS studies on the copper and silver phosphino complexes, and Prof. Cristina Marzano and coworkers ("Dipartimento di Scienze del Farmaco", University of Padua), for the *in vitro* cytotoxicity assays.

I am grateful to Dr. Andrea Melchior ("Dipartimento di Scienze e Tecnologie Chimiche", University of Udine) for his contribution with the theoretical DFT studies on copper phosphino complexes.

I would like to thanks the "Electrocatalysis and Applied Electrochemistry" group of the University of Padua, in particular the group head, Prof. Armando Gennaro and Dr. Abdirisak Ahmed Isse for their contribution with the cyclic voltammetric studies on copper phosphino complexes.

I would like to express my gratitude to mrs Gabriel Walton, for her assistance for the editing of this thesis manuscript, and to prof. Marilena Tolazzi ("Dipartimento di Scienze e Tecnologie Chimiche", University of Udine) for her reviewing hints.

Finally, I am grateful to the Scientific Board of the PhD School in Molecular Sciences of the University of Padova, in particular the Chairmans of the School, Prof. Antonino Polimeno and Prof. Maurizio Casarin, and mrs Daniela Longo of the Scientific Secretariat ("Dipartimento di Scienze Chimiche", University of Padova).

Abstract

Interest in copper-based compounds in medicine is due to the fact that copper, unlike platinum and gold, often employed in cancer chemotherapy, is a ubiquitous bioelement involved in several processes of metabolic enzymes in living organisms. In addition, altered levels of intracellular copper are often known to be related to both some genetic disorders and other serious pathologies such as prostate and lung cancer. On the basis of this evidence, several therapies based on administration of copper salts in the presence of chelating agents capable of transporting the bioelement have recently been developed. Intracellular copper intake in living organisms is strictly regulated by a complex membrane protein system with an active transport function. In humans, these proteins, hCTR1, are characterized by several methionine- and histidine-rich aminoacidic sequences, putative binding sites for Cu(I). Several studies, based on in vitro and competition experiments in solution between these substrates and monovalent Cu(I) and Ag(I) and divalent Cu(II) and Zn(II), have demonstrated that these transport proteins have a specific affinity for the unstable Cu(I) rather than for the more stable Cu(II) ion. Despite this, most research in the past on the development of copper compounds with potential anti-tumor activity mainly focused on Cu(II) derivatives. However, in the last few years scientific attention has also been devoted to Cu(I) compounds. In particular, a new class of Cu(I) compounds with hydrophilic phosphines, characterized by both high thermodynamic stability and good solubility in aqueous solution (see figure below), has recently been proposed. Among these compounds, the monodentate species exhibit good to moderate cytotoxic activity in vitro, whereas the activity of the chelate complex and that of the free phosphines are negligible. The cytotoxic activity of Cu(I) complexes seems to be linked to the complex abilities of binding biological substrates after dissociation of one or more phosphine ligands. Matching this suggestion, some preliminary ESI-MS experiments show that, at the high dilutions required by in vitro and MS experiments ($10^{-5} - 10^{-6}$ mol/L) the chelate complex **(1)** retains its tetracoordination, whereas complexes including monodentate phosphines **(2)**, **(3)** are partially dissociated. This result reveals the importance of obtaining more information about the Structure/Stability-Activity Relationship (SSAR) of these compounds in biological environments. With this aim, our work focused on two main topics: 1) study of the formation equilibria of Cu(I) complexes with PTA in aqueous solution; 2) extension of

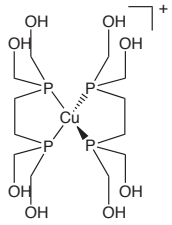

(1) $[Cu(bhpe)_2]^+$

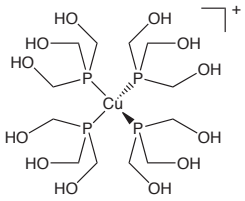

(2) $[Cu(thp)_4]^+$

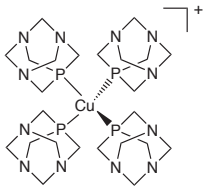

(3) $[Cu(PTA)_4]^+$

study to the formation of analogous complexes of Ag(I). This cation is isoelectronic with Cu(I) and may form phosphine complexes with similar cytotoxic activity. In order to carry out this study, a series of microcalorimetric, spectrophotometric and potentiometric experiments was designed to find the stability constants and thermodynamic functions (ΔG, ΔH, ΔS) concerning the formation of both Cu(I)- and Ag(I) - PTA complexes in solution. In addition, for more information on the interactions of Cu(I) and Ag(I) with residues present in the binding sites of copper-transport membrane proteins hCTR1, solution studies were extended to the interactions between Cu(I) and Ag(I) and the amino acids methionine and histidine. To date, there are very few studies on this topic, although they are essential to acquire the necessary information to clarify the still not fully understood mechanisms of intracellular copper intake.

Contents

Acknowledgments v

Abstract vii

1. Introduction 1

1.1. The use of metal-based compounds in medicine 1

1.2. The use of copper compounds in medicine 3

1.2.1. Inorganic chemistry of copper compounds 3

1.2.2. Biochemistry of copper uptake and its distribution 6

1.2.3. Copper and human health disorders 9

1.3. The role of biologic copper in cancer and copper-based anticancer drugs . . 12

1.3.1. Cu(I) phosphino complexes as anticancer agents 16

1.4. Recent Cu(I) phosphino complexes with potential anti-tumor activity, and introduction to the present work 17

Aim of the work 19

2. Experimental 21

2.1. Techniques 22

2.1.1. Potentiometry 22

2.1.2. UV-Vis spectrophotometry 24

2.1.3. Cyclic voltammetry 25

2.1.4. Microcalorimetry 26

2.2. Formation of Cu(I)–PTA complexes 31

2.2.1. Chemicals 34

2.2.2. Interaction between Cu(II) and PTA in aqueous solution 36
2.2.3. Formation of Cu(I)–PTA complexes in aqueous solution 43
2.2.4. Results 46
2.2.5. Theoretical DFT calculations on Cu(I)–Cl–PTA complexes 52
2.2.6. Results. 53
2.3. Formation of Ag(I)–PTA complexes 58
2.3.1. Results 60
2.3.2. Comparisons between Cu(I) and Ag(I) complexes of PTA 65
2.4. Formation of Cu(II), Ag(I), Cu(I) complexes with the amino acid methionine in aqueous solution 67
2.4.1. Protonation of methionine in aqueous solution 68
2.4.2. Formation of Cu(II) complexes with methionine 70
2.4.3. Formation of Cu(I) complexes with methionine 72
2.4.4. Formation of Ag(I) complexes with methionine 75

3. Relationship between ESI behavior, stability and cytotoxic activity of M(I) phosphino complexes 79
3.1. Experimental 80
3.1.1. Results and discussion 81
3.2. *In vitro* cytotoxicity assays of phosphino complexes 85

Conclusions 89

Bibliography 91

A. Analytical details of the experiments 101

B. The solution chemistry of *soft* transition metal complexes 105
B.1. *Hard* and *soft* complexes 105
B.2. Enthalpy and entropy of formation of hard and soft complexes 109

C. Effect of the ionic medium on the solution equilibria 113
C.1. The Debye–Hückel limiting Law. 113

C.2. The Specific ion Interaction Theory (SIT) 114
C.3. The Pitzer models 116
C.3.1. Application in the study of Cu(I)–chloride complexes 116

D. Numerical methods **119**

D.1. The method of least-squares 119
D.2. Calculating the concentrations of the species at the equilibrium 125
D.3. The program Hyperquad: the minimization of potentiometric and spectrophotometric data 126
D.4. The program Letagrop: the minimization of microcalorimetric data 129

CHAPTER 1

Introduction

1.1. The use of metal-based compounds in medicine

Since the early 1970s, following the discovery of the anti-tumor properties of cisplatin, several metal-based compounds have been developed as potential anticancer agents.

The anti-tumor neoplastic activity of a metal compound depends on the nature of the metal itself, its oxidation state, and coordination chemistry: the coordinative mechanisms which occur in vivo between the metal cation and the biological substrates are the key processes of the biological activity of these compounds, the chemistry of which cannot be mimicked by organic compounds. Among several metal-based compounds, those of platinum(II) have been the most frequently used in the clinical treatment of several types of cancers, including those of the genito-urinary and colorectal tracts and non-small cell lung cancers [1, 2]. As an ancestor of platinum-based drugs, cis-diamino dichloro platinum(II), commonly known as cisplatin (figure 1.1) has been used for decades in clinical practice, in view of its remarkably efficacy in the treatment of several neoplastic diseases, particular those of the genito-urinary tract [3].

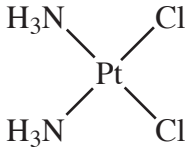

Figure 1.1.: Structure of cisplatin.

However, the efficacy of cisplatin is severely limited by several serious drawbacks [4]: several cancers have intrinsic resistance to treatment with this drug, whereas acquired resistance is observed after early treatment cycles in other clinical cases [5, 6]. In addition, collateral toxicity is the factor that most limits the use of cisplatin: nephrotoxicity and neurotoxicity are particularly important [7]. Lastly, the poor solubility of cisplatin is another problem which makes its administration difficult.

In view of these considerations, thousands of alternative platinum-based compounds as potential anticancer agents have been studied and developed in the last few decades [5, 8, 9]. Several complexes of group 11 metal cations have also been studied, including gold(I), gold(III) and copper(II) compounds. In particular, Auranofin, a thioglucose derivative of triethylphosphine gold(I) used as an anti-arthritic drug [10], showed in vivo anti-tumor activity against P388 leukemia when tested on a panel of murine models [11]. With the aim of finding new compounds with cytotoxic activity toward a wider range of cancer diseases, P. Sadler et al. tested the toxicity of a series of monocationic bis-diphosphine gold(I) compounds, such as $[Au(dppe)_2]Cl$, toward a panel of human tumor cell lines including M5076 reticulum cell carcinoma, B16 melanoma and P388 leukemia [12, 13]. The results of the trials indicated that these gold(I) derivatives have good cytotoxicity toward the cell lines tested and, remarkably, higher drug tolerance profiles compared with those of cisplatin. These encouraging results paved the way for research on new gold-based compounds as potential anticancer drugs and, as a rational extension, also on copper(II) and copper(I) derivatives. Researches on copper compounds for clinical use, are also aimed by the fact that copper, unlike platinum and gold, is an endogenous metal cation. As it will be discussed in the next section, copper is a fundamental cofactor of several metalloproteins and is involved in several metabolic processes. Therefore, due to the ubiquity of copper in our organism, the copper-based drugs potentially have a wide spectrum of biological substrates to target, unlike those of platinum and gold, which exert their cytotoxic activity toward a relatively small number of biomolecules.

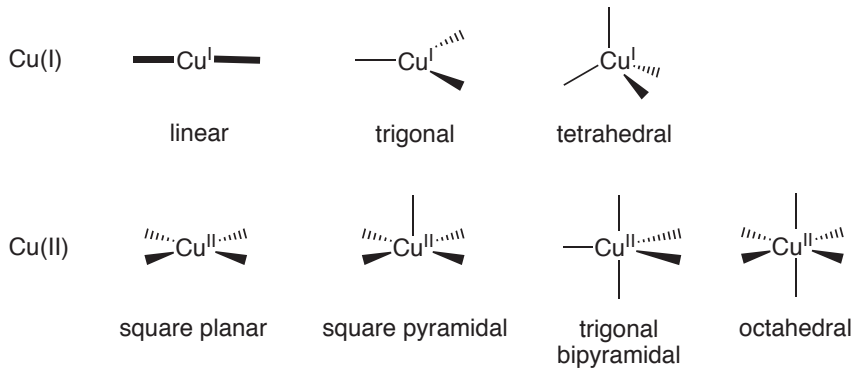

Figure 1.2.: Most common coordinative geometries in Cu(I) and Cu(II) complexes. Most favored Cu(I) geometries are linear (CN = 2), trigonal (CN = 3) and tetrahedral (CN = 4). Cu(II) forms tetracoordinate complexes (CN = 4), usually with square-planar arrangement. Other common geometries are square-pyramidal and trigonal bipyramidal (CN = 5) and octahedral (CN=6).

1.2. The use of copper compounds in medicine

1.2.1. Inorganic chemistry of copper compounds

Copper is the 29$^{\text{th}}$ element of the periodic table and the first of the three transition metals of the group 11, further including silver and gold. Cu(I) and Cu(II) are the two most important and common oxidation states in compounds of this metal, although some examples of Cu(III) and Cu(IV) compounds are known too [14].

The chemistry of Cu(I)

Cu(I) and Cu(II) have both the typical behavior of *soft* cations (for more details see appendix section B on page 105). Cu(I) has a d^{10} electronic configuration, and strongly prefers to form covalent compounds with neutral or low-charged anionic ligands containing sulfur-donor groups, such as thiolates and thioethers, aromatic sp^2 amines and phosphines. Due to the d^{10} configuration (which corresponds to a ground state term ^1S), Cu(I) compounds typically show diamagnetic properties and are generally colorless, except if the ligand itself is colored or if color derives from charge-transfer bands. The relative stabilities of Cu(II) and Cu(I) are indicated by the following potential data:

$$Cu^{+} + e^{-} = Cu, \quad E^{0} = 0.52\,V \tag{1.1}$$

$$Cu^{2+} + e^{-} = Cu^{+}, E^{0} = 0.153V \tag{1.2}$$

whence:

$$Cu + Cu^{2+} = 2Cu^{+}, E^{0} = -0.37V, K = \frac{[Cu^{2+}]}{[Cu^{+}]^{2}} = 10^{6} \tag{1.3}$$

As implied by the last expression, in aqueous solutions only low equilibrium concentrations of Cu(I) ($< 10^{-2}$ M) can exist. The chemical equilibrium between the two species strongly depends on the nature of the solvent, and on the nature of the ligands and coordinating anions present in solution. For example, Cu(I) in aqueous environments is known to be stabilized by chloride anions (> 0.1 M), with which it forms a series of stable chloro complexes [15], as reported in equation (1.4):

$$Cu^{+} + nCl^{-} = [CuCl_{n}]^{1-n}; n = 1 - 3 \tag{1.4}$$

In these complexes, the Cu(I) center has the typical linear or trigonal coordinative geometries. Another example is the stabilization of the Cu(I) oxidation state in an acetonitrile solution: in this solvent Cu(I) is highly stabilized by formation of a tetracoordinate adduct with the –CN group of acetonitrile. This complex has a characteristic tetrahedral geometry and can be isolated as a solid compound with formula $[Cu(MeCN)_4][X]$, where X is a non-coordinating anion such as ClO_4^-, $[BF_4]^-$, $[PF_6]^-$ [16].

The chemistry of Cu(II)

Most Cu(I) compounds are easily oxidized to Cu(II) compounds, which are more stable. The aqueous solution chemistry of Cu(II) is well-known, and a large number of salts, many of which are water-soluble, exist in addition to a wealth of complexes. In water solutions Cu(II) forms stable complexes with both amines and carboxylate organic anions. Several

examples of Cu(II) chloro complexes, weaker than those of Cu(I), are also known.

Stereochemistry and properties of Cu(II) compounds. The d^9 configuration makes Cu(II) subject to Jahn-Teller distortion: according to the Crystal Field Theory, a Cu(II) ion placed in a field with cubic symmetry (i.e., regular octahedral or tetrahedral) undergoes deep modifications in its stereochemistry. In a strong octahedral field, d-valence orbitals are split into a doubly degenerate (ground state) set and a triple-degenerate set. When Cu(II) is six-coordinated, the octahedron is severely distorted. The most frequently observed effect is elongation along one fourfold axis, leading to coordinative geometry characterized by a planar array of four short and two long Cu(II)–ligand bonds. In the limit case, the elongation leads to the removal of the apical ligands, with the formation of a tetracoordinate square-planar complex.

Due to the Jahn-Teller distortion, a characteristic absorbance band corresponding to the transition $e_g \rightarrow t_{2g}$ is generally observable in the region between 600 and 900 nm. This absorption gives to Cu(II) complexes their typical blue or greenish colors.

Another important characteristic of Cu(II) compounds is their paramagnetic behavior in a magnetic field. This is due to the presence of an unpaired electron in the d^9 configuration. The magnetic moments of simple Cu(II) complexes (those lacking Cu–Cu interactions) are generally in the range of 1.75 to 2.20 BM, regardless of stereochemistry and independent of temperature, except at very low temperatures (< 5 K) [16].

Aqueous chemistry and complexes of Cu(II). Most Cu(II) salts dissolve easily in water, giving the aqua ion $[Cu(H_2O)_6]^{2+}$. Addition of ligands to such aqueous solutions leads to the formation of complexes by successive displacement of water molecules. For example, it is known that Cu(II) in aqueous solution forms up to four complexes with ammonia: $[Cu(H_2O)_6]^{2+} + nNH_3 \rightleftarrows [Cu(NH_3)_n(H_2O)_{6-n}]^{2+}$, n = 1–4. Due to the Jahn-Teller effect Cu(II) does not bind fifth and sixth ammonia molecules in octahedral complexes. Stepwise stability constants for to the formation of 5– or 6– coordinate Cu(II) complexes with different ligands are consequently characterized by very low values. reflecting the weak nature of complexes of these species.

1.2.2. Biochemistry of copper uptake and its distribution

Copper is an essential trace element common in all living organisms. It is present as a cofactor in several metalloproteins with enzymatic functions: its unique redox chemistry, based on the easily reversible couple Cu(II)/Cu(I), is crucial for several biochemical processes, including iron trafficking, DNA synthesis and mitochondrial respiration [17]. Copper is also found in several enzymes, such as cytochrome oxidase and ascorbate oxidase, and is also present in superoxide dismutase (SOD), the biochemical role of which, as the name implies, is to catalyze the dismutation of superoxide ions. This task in particular is very delicate, because it involves the production of free radicals and *reactive oxygen species* (ROS) which, if not properly handled by the enzymatic systems, can cause serious damage to several biological substrates, including lipid peroxidation in membranes, direct oxidation of proteins, and cleavage of DNA and RNA chains. Copper levels in human organism therefore need to be strictly regulated by several homeostatic mechanisms, in order to ensure a proper intracellular supply of the metal without reaching toxic concentrations.

At the protein level, two families of membrane proteins control copper homeostasis [18]: copper excretion is governed by the ATP-dependent pumps ATP7A and ATP7B [19, 20], and copper uptake is mediated by the copper transport proteins (Ctr). This family of transporters is widely present in all eukaryotic organisms. In humans, protein hCtr1 consists in a chain of 190 amino acid residues arranged in a main intermembrane domain of three alpha helices (3TMDs) [21, 22] with amino and carboxyl groups located on the opposite sides of the hydrophobic membrane environment.

The homotrimeric structure of the three TMD domains of hCtr1 has recently been resolved [18]. TMD2, which is crucial for copper binding, has a conserved “Mets” motif, a methionine-rich sequence of the form MXXXM, where M is a methionine residue and “X” indicates one of several other amino acids. Various studies concur that this aminoacidic cluster is a critical site for copper uptake [23, 24].

The extracellular domain of hCtr1 is composed of a N-terminal tail of 66 amino acids containing two Mets methionine-rich motifs, whose thioether groups are binding sites for the biometal, and also histidine residues, which may also be putative binding sites for copper. The cytosolic portion presents a His-Cys-His sequence which XAS study indicates

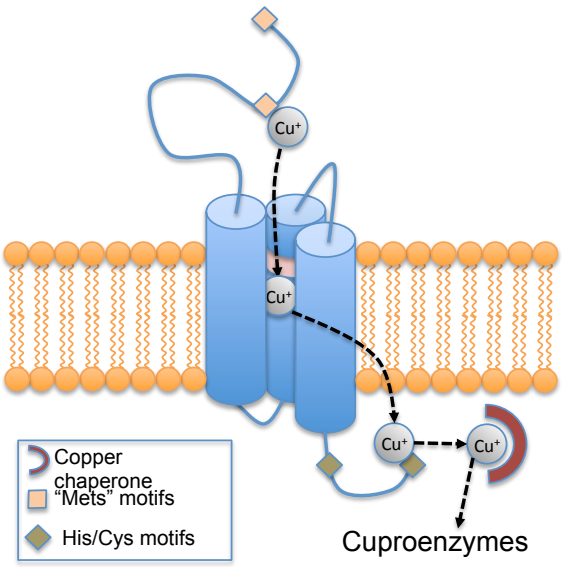

Figure 1.3.: Sketch of mammalian copper transport protein (Ctr1). Mets sequences in extracellular tail bind Cu(I) through histidine and methionine groups, thus stabilizing cation in monovalent state. Cu(I) is transported inside cell, where it is bound by cysteine/histidine motifs which pass metal to a copper chaperone which finally delivers copper to cytosolic metalloproteins.

is a coordination site for copper via cysteine residues, or histidine if cysteine is not present [25].

According to the current hypotheses [26, 27], Ctr1 specifically binds the monovalent Cu(I) rather than Cu(II), with the methionine residues of the Mets motifs in the extracellular domain. The cuprous cation passes through the 3TMD domains and is coordinated by the cysteine/histidine residues of the intracellular tail. The membrane protein then releases the metal to the cytosolic copper chaperones, which deliver the biometal to the cuproenzymes [28, 29] (sketch in figure 1.3).

Methionine residue is known to be a prominent binding site for a metal cation with *soft* properties such as Cu(I), which prefers coordination through the sulfur-donor group rather than oxygen- and nitrogen-containing ligands [30]. Since Cu(II) the thermodynamically stable copper species in aqueous environments, it is still not completely clear why biological systems choose to acquire copper in its monovalent state. In a biological perspective, one explanation is the need to achieve high specificity toward copper rather than other metals present in aqueous environments, to ensure close regulation of the bioelement. Biological binding sites such as the thiolate and thioether groups do show high specificity

toward monovalent *soft* cations such as Cu(I), which are relatively uncommon in aqueous environments, whereas divalent cations such as Cu(II) and Zn(II), the coordination chemistry of which is similar, are more common, so that specificity toward a particular divalent cation is lower. Matching this observation, experiments on yeast have shown that Cu(II) is reduced to Cu(I) prior to its intracellular acquisition [31]. A recent study in solution also proved that methionine-rich Mets sequences bind monovalent cations Ag(I) and Cu(I) selectively, rather than the divalent Zn(II), and no competition is observable between divalent and monovalent cations [21].

Once the cell membrane has been passed, copper ions are bound by cytosolic chaperone proteins which play a crucial role: on one hand, they must bind the metal cation tightly enough to avoid its premature release into the cytosolic environment; on the other, they must do so quite weakly, to allow the chaperone to exchange the biometal for the target metalloproteins where copper is required. Many studies confirm the critical role of the several specific chaperones in copper delivery [32]. It should be noted that, although this task requires fine tuning of the coordinative properties of the copper binding site, the number of possible amino acid residues capable of binding copper is rather limited: the list includes the methionine thioether group, cysteine thiolate, histidine imidazole nitrogens, and the carboxylate group of aspartate and glutamate. Interestingly, copper can form an arene-complex with an aromatic ring such as that of a tryptophan residue [33]. Less common are examples of complexes with the serine hydroxyl group and tyrosine phenolic oxygen [34]. In addition to the various chemical properties of the ligand groups themselves, copper trafficking proteins possess complex secondary structures which can finely tune coordination sites, for selectivity and a suitable affinity for the metal [34]. In fact, as in the more general context of inorganic chemistry, copper ions also have different coordinative geometries in biological environments. For instance, the most common arrangements of Cu(I) in some cupro-enzymes include dicoordinate linear complexes with two cysteinate residues in Atx1 (see figure 1.4 a) [35], trigonal distorted geometry presumed for the Cu(I) core in the mitochondrial assembly protein, SCO1 (fig. 1.4 b) [36], and a distorted tetrahedral arrangement in the periplasmic copper binding protein Cusf in prokaryotic cells (fig. 1.4 c).

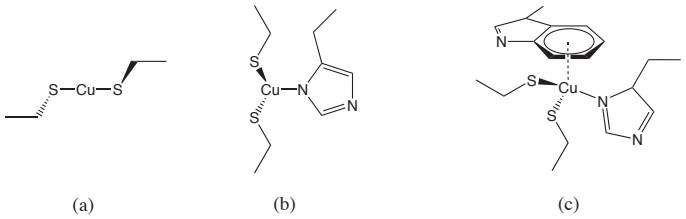

Figure 1.4.: Examples of coordinative geometries of copper found in biological adducts: (a) linear geometry in cysteinate-copper adducts in Atx1; (b) trigonal complex of copper with two cysteinate residues and a histidine (presumed structure in SCO1 protein); (c) distorted tetrahedral geometry in Cusf prokaryotic binding proteins)

1.2.3. Copper and human health disorders

Copper, like iron and zinc, is one of the various trace elements required by our organism for several biological processes. However, as previously noted, due to the critical role played by copper in oxidation processes involving the production of ROS, its intracellular levels must be closely regulated. For instance, in *Esherichia coli* models, homeostatic levels of Fe(III) and Zn(II) cations are known to be allowed to reach concentrations within 100 μmol/dm^3, whereas copper must be strictly maintained below 100 μmol/dm^3. Disrupted copper homeostasis, which is often due to genetic dysfunctions of some of the various mechanisms of intake, transport, delivery and excretion, can lead to serious disorders, such as Menkes' and Wilson's diseases, caused respectively by decreased and enhanced systemic copper acquisition. Other pathologies, such as the neurodegenerative Alzheimer's disease and some cancer malignancies are related to altered copper levels in the human organism [37].

The Wilson's Disease (WD)

Wilson's disease is an autosomal recessive genetic disorder, caused in the ATP7B gene, which encodes for a copper transport protein, located in the trans-Golgi network, and involved in copper excretion into bile [38, 39]. The main pathophysiology linked to copper toxicity in the development of WD includes copper-mediated oxidative damage, activation of cell death pathways, and release of copper in the plasma pool into extra-hepatic tissues. As a consequence, general increment of copper levels in liver is observed, while the levels of ceruloplasmin (Cp) protein, which is the main copper transport protein in blood, decrease

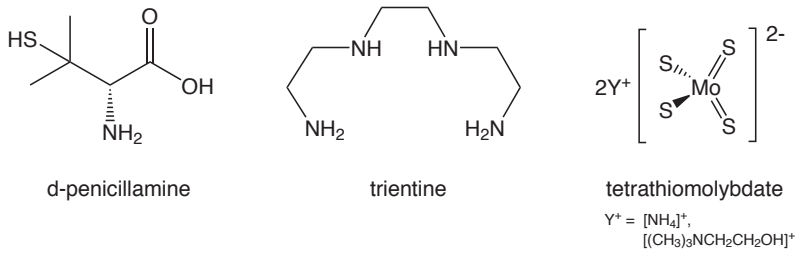

Figure 1.5.: Copper chelators used in clinical WD treatment.

as an effect of the diminished function of the ATP7B protein [40].

Therapies for patients with WD include oral administration of chelating agents to capture the copper excess. In particular, three compounds, d-penicillamine, trientine and ammonium tratrathiomolybdate (figure 1.5) are used to treat WD [41] of patients with symptoms of hepatic insufficiency or chronic active hepatitis. D-penicillamine was the first drug to be used, but it has several limitations due to its toxic side-effects [41, 42]. Although trientine and ammonium tetrathiomolybdate have fewer potential side-effects, they must still be carefully monitored. A second generation of tetrathiomolybdate with chinoline (fig. 1.5) has been reported to stabilize the disease, primarily by SOD inhibition [43, 44].

The Menkes' Disease (MD)

Menkes' disease (MD) is a genetic disorder caused by dysfunction in the ATP7A gene encoding for ATPase, a copper transport protein [45]. ATPase is a pump protein which plays the role of transporting copper into the trans-Golgi network. Copper is then delivered to the proper copper enzymes, including dopamine-β-hydroxylase; ATPase is also involved in copper excretion from the cell. As a result of the mutation in the ATP7A gene, copper excretion and trafficking mechanisms are greatly altered, leading to copper accumulation in peripheral tissues in the form of copper metallothionein.

Patients with MD undergo progressive neurological impairments due to copper deficiency in the brain. Although in MD patients unaltered mechanisms of copper uptake and excretion in liver are observed, as well as normal levels of hepatic cuproenzymes, copper absorption in gastrointestinal tract is greatly decreased. In particular, diminished uptake of the metal in the intestinal tract results in a shortage of exchangeable copper and therefore a deficiency of copper proteins, which play critical roles at developmental level [46].

The most frequent clinical treatment for MD patients consists of intravenous or subcutaneous administration of copper salts, to compensate for copper deficiency due to decreased uptake [47]. A further identification of the copper-histidine system in normal human serum and acquired knowledge about its biochemistry and physiological significance led to treatment of MD with copper-histidine formulations [43, 48]. Although most of the copper in human serum is bound to Cp even when not in an exchangeable form, the formation of the albumin-copper-histidine ternary complex provides the actual carrier necessary for the regulation and control of copper transport across the cell membrane [43, 48].

The Alzheimer Disease (AD)

Alzheimer's disease is a well-known neurodegenerative disease, characterized by progressive patterns of cognitive and functional impairments. Altered levels of copper in the human organism have been related to the physiopathology of AD: one study reports that elevated free copper plasma concentrations were found in AD patients [37], and increased concentrations of copper have also been found in cerebrospinal fluid together with normal plasma copper levels [49].

Although copper is known to be involved in the development of degeneration, its role it is not completely clear. A prominent suggestion about copper involvement in AD may be via its interaction with amyloid precursor protein and β-amyloid peptide in self-aggregating plaques and neurofibrillary tangles, which may contribute to the pathogenesis of the disorder via cellular oxidative stress [50, 51]. Copper can induce aggregation of amyloidogenic peptide and the production of ROS, which oxidize β-amyloid peptide [52]. Patients with AD reveal extracellular deposition of Aβ peptides in senile plaques and intracellular accumulation of hyperphosphorylated τ-protein in neuronal cells as neurofibrillary tangles [43].

Treatment for AD consists of the administration of copper chelators to sequester copper. In particular, some derivatives of 8-hydroxy quinoline (see figure 1.6), i.e., P-OHQ, have recently been proposed [53]. It has been proven that these compounds act as strong tetradentate ligands toward divalent cations such as Cu(II) and Zn(II) and they have been assessed as potential metal-chelating agents in AD treatment.

A recent study suggested that P-OHQ chelates can dissolve Aβ deposits by removing

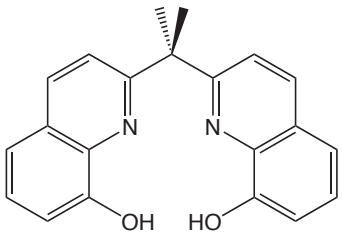

P-OHQ

Figure 1.6.: Chemical structure of P-OHQ.

copper from amyloid aggregates [53]. P-OHQ can also inhibit the production of hydrogen peroxide induced by the formation of copper adducts with Aβ proteins, and involved in the toxicity of the peptide [54].

1.3. The role of biologic copper in cancer and copper-based anticancer drugs

Cancer diseases are generally accompanied by significant changes in metabolic rates in cells. Such altered states have been related, among other factors, to deregulated copper handling by proteins involved in the uptake and trafficking of copper ions [55]. Since down-regulated cell respiration has been found in many types of cancer, the involvement of copper in angiogenesis is under investigation [43], and many Cu(II) chelate compounds showing cytotoxic activity have been extensively developed in the last few decades [50].

In general, copper-based drugs show a wide range of various biological pharmacodynamics and thus possible diverse mechanisms lying behind their cytotoxicity: for example, chelate compounds of curcuminoids significantly reduce solid tumors in mice. Complexes of pyridine-2-carbohydrazide have quite prominent cytotoxic activity against colon cancer cell lines, according to a mechanism which inhibits the expression of c-Src, a non-receptor tyrosine kinase involved in the growth-mediated signaling pathway [56]. The varying biological activity of these copper-based drugs, compared with those of the well-praised platinum ones, not only implies diverse pharmacodynamics but also a considerable spectrum of biological targets. As previously mentioned, this is not surprising, in view of the ubiquity of copper in our organism and its many biological roles. In general, platinum-based compounds

interact with DNA, inducing crosslinks, whereas copper compounds more probably interact with enzymes and inhibit vital cell functions. The next sections provide some examples of copper-based drugs with potential anticancer activity and the biological targets with which they interact.

Copper compounds as proteasome inhibitors.

Proteasome is a large protein complex present in both the nucleus and cytosol of cells. It represents the main part of a biological enzymatic system which is used by eukaryotic organisms to regulate intracellular levels of proteins. The role of proteasome is to catalyze the hydrolytic degradation of unneeded or damaged proteins. Prior to being degraded, proteins are "flagged" by a ubiquitin tail, a chain of 76 amino acid residues. The flag is used by proteasome to identify the protein and to start hydrolysis. Proteasome is essential for many cellular roles, including response to oxidative stress, regulation of gene expression and induction of apoptosis [57, 58]. Deregulated function of the ubiquitin-proteasome system may lead to accumulation of unwanted proteins and to the incapability of eliminating damaged proteins with aberrant functions. Therefore, inhibition of the proteasome-ubiquitin pathway may be a key factor for the anti-tumor activity of a drug.

Several studies in the field of medicinal bioinorganic chemistry have established a relationship between proteasome inhibition, cancer and copper, so that a new class of so-called organic copper compounds has been developed in the last ten years [59]. In these drugs, copper is coordinated either to neutral heteroatomic molecules such as phenanthroline, or to anionic organic ligands such as 8-hydroxyquinolinate, pyrrolidine dithiocarbamate or (pyridine-2-yl methylamino) methyl phenolate (fig. 1.7). These compounds are efficient inhibitors of the chymotrypsin-like activity of proteasome, whereas the free ligands in themselves are not particularly good inhibitors. This result shows that copper plays a crucial role in the proteasomal function inhibition induced by these compounds. It has also been found that organic complex formation is essential for copper uptake and transportation in cells [60].

More recently, some new ternary copper complexes with 1,10-phenanthroline and indole-3-acetate (fig. 1.8) have been reported as potential anticancer agents acting via proteasome

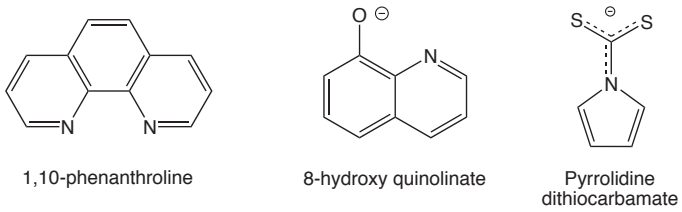

Figure 1.7.: Ligands used to design Cu(II) organic compounds with proteasomal inhibitor functions.

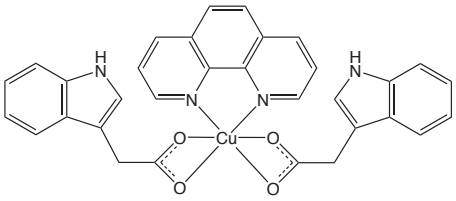

Figure 1.8.: chemical structure of bis-indole acetate phenanthroline Cu(II), a novel potent inhibitor of proteasome activity and apoptosis-inducer.

inhibition [61]. It has been found that this complex is a potent inhibitor of the proteasomal activity and induces apoptosis in MDA-MB-231 human breast cancer cells.

Copper and angiogenesis

Angiogenesis is the biological process of creation of new blood vessels from the existing vascular bed. In normal health conditions this is a tightly regulated process and its up-regulation is usually interpreted as a signal of a pathological condition. Angiogenesis is an essential process for cancer development and metastasis [62], since the creation of new vessels is essential for the diffusion of tumors during the metastatic process. On this basis have been developed in the last decades several therapies based on anti-angiogenetic drugs. Among different strategies several drugs that could act as potential copper scavengers have been developed. It is known that copper deficiency can inhibit angiogenesis, preventing the growth of tumor cells or an inflammation to spread [50], but, since the role of copper in the angiogenetic process is not yet fully understood, further research is needed for this purpose. Anyway copper was found to be a cofactor required by several angiogenetic mediators, including Vascular Endothelial Growth Factor (VEGF), basic Fibroblast Growth Factor (bFGF), and Interleukine 1 and 8 (IL-1, IL-8) [63–65].

Copper compounds in cancer chemotherapy

The first treatments of several types of cancer have been made with copper chelators such as 8-OHQ and tetrathiomolybdate derivatives, known to be copper-scavengers and yet successfully employed in Wilson disease treatment. These compounds were reported to be of therapeutic value in the treatment of several types of cancer diseases, for their anti-angiogenetic and anticancer effects.

Binary Cu(II) complexes. Several binary complexes of Cu(II) with N, O or S donor ligands have been synthesized and their biological activity tested.

The binary complex 2,6-bis(benzimidazo-2-yl)pyridine Cu(II) chloride exhibit a cytotoxicity through metalloprotease activity [66]: experiment showed that the complex binds bovine serum albumin causing site-specific cleavages, in the protein when the system is incubated in atmospheric conditions. The cleavage and thus the biological activity seem to be related to the activation of dioxygen by the metal bound to the protein.

A series of copper(II) complexes with thiosemicarbazone derivatives have been reported to inhibit enzymatic activity of DNA ribonucleotide diphosphate reductase and to induce cell apoptosis, thus suggesting these derivatives are potential anticancer drugs [67]. Similarly Cu(II) nitrophenone thiosemicarbazone complexes have been found to show cytotoxic activity against tripanosoma *in vitro*.

Ternary Cu(II) complexes. Several Cu(II) ternary complexes bearing one or two N, N- and N, O- bidentate ligands have been synthesized and their biological activity tested. In these complexes, copper binds a N, N-donor chelate ligand such as 1,10-phenanthroline or 2,2'-bipyridine and a N, N- or a O, O- chelate ligand such acetyl acetonate or glycinate. Such class of compounds exhibits antineoplastic activity against a variety of tumor cell lines both *in vitro* and *in vivo*. It has been found that they interact with mitochondria of both healthy and tumor cells inhibiting the oxidative phosphorylation process and the mitochondrial respiration [68]; moreover they exhibit high affinity towards plasmid, genomic and internucleosomal DNA.

Finally a number of complexes of Cu(II) with Schiff bases derivatives and 2-amino-2-

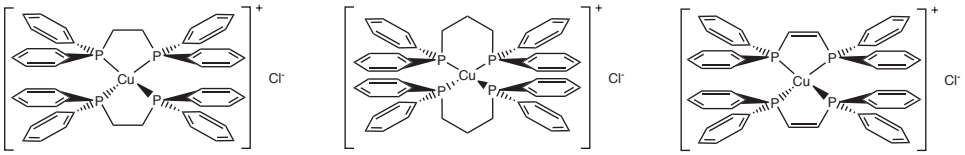

[Cu(dppe)$_2$]Cl [Cu(dppp)$_2$]Cl [Cu(dppey)$_2$]Cl

Figure 1.9.: Examples of Cu(I) – diphenyl phosphine chelate compounds prepared in the last decades and tested ad anticancer agents in vitro.

thiazoline have been reported to show significant anti-inflammatory and anticancer activity against various cell lines [69].

1.3.1. Cu(I) phosphino complexes as anticancer agents

Most of the research done until now on the design of new copper compounds with potential anti-tumor activity has been mainly focused on Cu(II) derivatives, more likely than on Cu(I) ones, even if the experimental evidences, yet discussed in the previous sections, confirm that copper is acquired by cells, and trafficked, in its monovalent oxidation state. According to that, Cu(I) derivatives might be indeed of interest as prominent anticancer drugs. However, Cu(I) derivatives are generally unstable in aqueous environments, especially in the presence of potentially oxidant species that can promote Cu(I) oxidation. Cu(I) complexes designed in order to obtain anticancer drugs, should bear ligands able both to strongly bind Cu(I), in order to stabilize it in its monovalent state, and meanwhile to ensure a good hydrosolubility to the whole metal compound.

With this aim, several phosphino Cu(I) compounds of the type [Cu(P–P)$_2$][Cl] P–P = dppe: 1,2-bis(diphenylphosphino)ethane, dppp = 1,2-bis(diphenylphosphino)propane, dppey = 1,2-bis(diphenylphosphino)ethylene, were designed in these last decades (figure 1.9). These compounds showed cytotoxic activity against several tumor cell lines, including B16 melanoma, P388 leukemia, and M5076 reticulum cell carcinoma [13, 70].

Despite the encouraging results obtained by the preliminary *in vitro* assays, the presence of a number of phenyl groups appended to the phosphorous atom determined a strong lipophilic character to the resulting metal complexes, thus causing undesired toxicity in animal models and precluding clinical trials in humans [71].

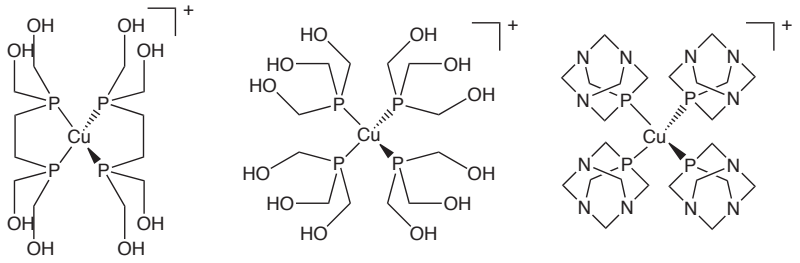

Figure 1.10.: Structures of the Cu(I) phosphino complexes recently prepared as anti-tumor agents.

1.4. Recent Cu(I) phosphino complexes with potential anti-tumor activity, and introduction to the present work

In order to obtain Cu(I) compounds with potential anticancer activity, characterized by higher hydrophilicity and lower systemic toxicity *in vivo* than the diphenylphosphine chelate derivatives previously studied, Tisato et al. [72] prepared a new class of tetra-coordinated Cu(I) complexes with monodentate or chelate phosphine ligands (fig. 1.10). These compounds proved to be easier to handle during *in vitro* tests and, more importantly, retained their cytotoxic activity against a panel of human tumor cell lines.

These complexes are bis-substituted or tetra-substituted derivatives $[Cu(bhpe)_2][PF_6]$ and $[Cu(thp)_4][PF_6]$, $[Cu(PTA)_4][PF_6]$ (bhpe = bis[bis(hydroxymethyl)phosphino] ethane), thp = tris(hydroxymethyl)phosphine, PTA = 1,3,5-triaza-7-phosphaadamantane) (see Figure 1.10). They are examples of fully phosphinated Cu(I) compounds, perfectly soluble in aqueous solutions. Phosphinic hydrophilic ligands are also characterized by high stability in aqueous environments and low cytotoxicity. The metal ion coordination sphere of these complexes, as assessed both in the solid state by X-ray crystallographic analyses and in solution by multinuclear NMR spectroscopy, is identical, presenting four equivalent phosphorus donors in a tetrahedral arrangement. However, the *in vitro* cytotoxic activity of the above complexes is very different: **(1)** in the figure exhibits negligible cytotoxicity [73], whereas **(3)** and **(2)** respectively show moderate and good cytotoxic activity *in vitro*. In particular compound **(2)** is an effective anti-tumor agent toward various tumor cell lines, including cisplatin-resistant ones [73].

Preliminary physicochemical characterization of these tetracoordinate Cu(I) compounds was made by electron spray ionization mass spectrometry (ESI-MS). The results obtained with this technique were not consistent with some NMR experiments. As a matter of fact, NMR studies showed that Cu(I) is always tetracoordinated (to four monodentate ligands in **(2)**, **(3)** (Figure 1.10) or to two bidentate chelate ligands in **(1)**) in aqueous solutions and at the relatively high concentration required by this technique ($10^{-2} - 10^{-3}$ M). The fragmentation patterns of the complexes in ESI experiments indicated that, at ESI concentrations ($10^{-5} - 10^{-6}$ M), chelate complex **(1)** retains its tetracoordinate "CuP_4" arrangement, whereas monodentate complexes **(2)** and **(3)** are partially dissociated to lower stoichiometry species [72].

A further UV-Vis spectrophotometry study carried out in acetonitrile (AN) [72] gave a convincing interpretation of the difference between the results obtained by the two techniques, and deeper insight into the differing *in vitro* cytotoxicity of these compounds. Speciation plots, calculated by the formation constants of the complexes $[Cu(PTA)_n]^+$ (n = 1–4) in AN showed that, although very strong, $[Cu(PTA)_4]^+$ complex is partially dissociated at high dilution. In particular, the much more stable chelate complex **(1)** (fig. 1.10) is not dissociated and, having all its coordination sites occupied, is characterized by modest cytotoxic activity *in vitro*. Conversely, complexes **(2)** and **(3)**, monodentate and less stable, can dissociate at high dilutions one or more of the phosphinic ligands thereby allowing copper to interact with biologically important substrates. This is a convincing demonstration that studies of this type, giving an accurate description of the relative stabilities of the complexes in the prevailing conditions of use, should always integrate the design of new metal-based compounds with potential therapeutic effects.

Given the attractive cytotoxic properties shown by $[Cu(thp)_4]^+$ and $[Cu(PTA)_4]^+$, the synthetic and biological studies of Cu(I) phosphine compounds have been recently widen to isostructural Ag(I) and Au(I) analogs [74]. Three series of water soluble complexes, namely $[M(thp)_4]^+$, $[M(PTA)_4]^+$, $[M(thpp)_4]^+$ (thpp = tris(hydroxyphosphyl)phosphine), have been prepared (Fig. 1.11), in order to obtain metal derivatives with steric-electronic as well as hydrophilic-lipophilic properties which could be tuned by modification of the ligand. These new derivatives were tested as cytotoxic agents against a panel of several

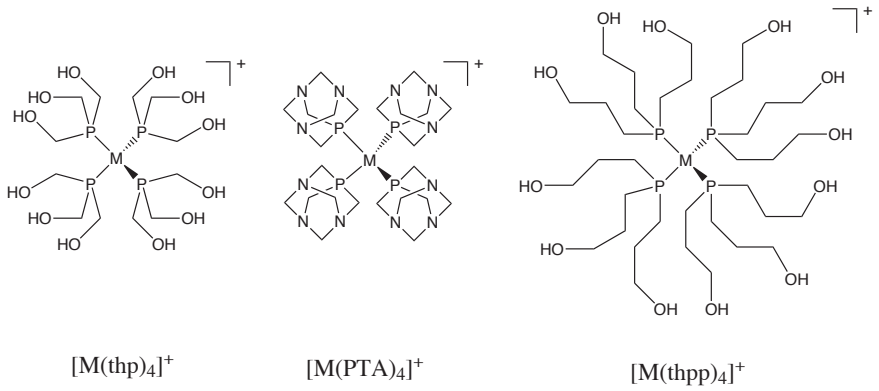

Figure 1.11.: Structures of the coinage metal-phosphine complexes recently synthesized (M = Cu^+, Ag^+, Au^+).

human tumor cell lines also including a defined cisplatin resistant cell line. The best results in term of *in vitro* anti-tumor activity were achieved with the metal-thp derivatives and, among the coinage metal complexes, copper derivatives proved to be the most efficient [74].

Aim of the work

The first aim of this research focused on two main objectives: 1) to extend the study on formation equilibria of $[Cu(PTA)_n]^+$ complexes (Figure 1.12) in water, and 2) to amplify studies to novel compounds of Ag(I). Ag(I) is isoelectronic with Cu(I), therefore the two cations should have similar coordination chemistry and their compounds characterized by comparable cytotoxic activity. This notwithstanding, studies on the speciation and biological activity of Ag(I)–phosphine complexes, similar to those of Cu(I) already tested, are not reported in literature to the best of our knowledge.

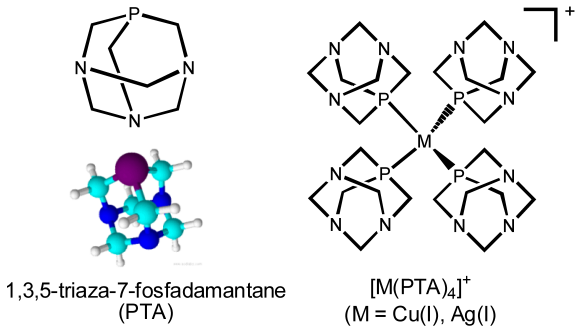

Figure 1.12.: structure of the hydrophilic phosphine PTA and of the complexes Cu(I), Ag(I)–PTA.

Although it is known that bioabsorption of copper occurs by complexation of the monovalent metal cation by the thioether group of methionine residues in the copper transport proteins of the cell membrane [21, 22], the scientific literature does not yet contain rigorous studies on quantification of the affinity of Cu(I) toward mehionine. In addition, only few and not conclusive, investigations about the competition between Cu(I) and Ag(I) toward methionine are found in the literature [21]. Therefore, the second aim of this thesis work was the determination of the thermodynamic parameters (ΔG, ΔH, ΔS) for the complex formation of Cu(I) and Ag(I) with this amino acid in aqueous solution.

Studies were carried out by means of potentiometry, microcalorimetry and UV-Vis spectrophotometry at 25 °C. In all cases, to keep the activity coefficients of the species in solution constant, all the solutions were prepared in a proper ionic medium with a constant concentration 0.1 or 1.0 M.

CHAPTER 2

Experimental

A first series of experiments on the Cu(I)–PTA system, carried out by means of spectrophotometric titrations, allowed the determination of the stability constants of the complexes formed by the metal cation and the phosphine in the experimental conditions used. The results obtained were then used to correlate the composition of species in solution at different concentrations of total metal (speciation), with the biological activity of the compounds *in vitro*. The speciation model obtained for the Cu(I)–PTA system by means of the spectrophotometric approach was then confirmed, and integrated, with a series of microcalorimetric experiments. Microcalorimetry allowed a further and independent determination of the formation constants for the Cu(I)–PTA complexes in the same conditions of the UV-Vis experiments as well as the direct determination of the enthalpies of formation of the complexes in solution, successively used to build a complete set of complex formation thermodynamic functions (ΔG, ΔH, TΔS) necessary for a complete description of the systems in solution.

A series of potentiometric and microcalorimetric experiments were also performed in order to study the formation of the analogous Ag(I)–PTA complexes, $[Ag(PTA)_n]^+$ (n = 1–4), in aqueous solution.

The results of the thermodynamic and ESI-MS studies [72] concerning the stability of tetracoordinated $[M(PTA)_4]^+$ (M = Cu(I), Ag(I)) complexes in aqueous solution [75] are compared and discussed in Chapter 3.

In view of the good results obtained by microcalorimetry in studying the M–PTA systems,

the same technique was also employed to investigate the formation of adduct of Cu(I) and Ag(I) whith methionine, the prominent binding site for these *soft* cations in the copper trasport proteins of the cell membrane.

The speciation model suggested by these studies are well consistent with some recent data concerning the interaction between Cu(I) and the h-Ctr proteins in solution [21, 22].

2.1. Techniques

2.1.1. Potentiometry

Potentiometry is one of the most frequently used method to determine the stability constants of complex species in solution, because of its great accuracy and precision [76]. Potentiometry consists of measuring the potential between two electrodes in contact with the solution. The potential is affected by the presence of the analytes in solution, and its value is related to their concentration. Experiments are usually carried out at a constant temperature, since the value of the electrodic potential also depends on temperature. To perform a potentiometric measurement, an indicator electrode, which must be sensitive to any variation in the concentration of the analyte, and a reference electrode, the potential of which remains constant during measurement, are required. Potentiometry uses electrodes which are selectively sensitive to one ion of interest: in this study, glass membrane and silver electrodes were used, since they are sensitive to the concentration of hydrogen and silver ions respectively. The main limitation of potentiometry is the essential requirement of a suitable reversible electrode sensitive to the ion to be analyzed. However, studying a system at equilibrium can often be achieved, although a suitable reversible electrode is not available for direct measurement of the analyte concentration. For example, although the formation of a complex between a metal ion and a ligand cannot be directly evaluated with an electrode sensitive to changes in the concentration of the metal ion, it is possible to assess the competition between that metal and the hydrogen ion toward ligand complexation, if the ligand is both a basic species and a Lewis donor. In this case, the system can be studied by means of a series of properly designed potentiometric titrations, with a glass electrode to measure the pH of the solution.

Electrodic potentials depend on the activity of the species in solution and originate from two main factors: the redox equilibrium of the analyte and its concentration in solution. Given a general analytical species M^{n+}, which can undergo the following reversible equilibrium of reduction:

$$M^{z+} + n\mathbf{e}^- \rightarrow M^{(z-n)+} \tag{2.1}$$

The observed electrodic potential, E, of a solution in which the above equilibrium takes place is given by the Nernst equation:

$$E = E^0 + \frac{RT}{nF} \ln \frac{\{M^{z+}\}}{\{M^{(z-n)+}\}} \tag{2.2}$$

Where E^0 is the standard potential of the redox couple at 298.15 K, F is one Faraday charge, 96,485 C, n is the number of electrons involved in the reduction process and {X} is the activity of species X. Equation (2.2) provides the relationship between the measured potential and the activity of the species in solution. During experiments, however, we do not deal with the activities of the species but with their concentrations. Activities and concentrations are related to each other by the expression:

$$\{X\} = \gamma_X \cdot [X] \tag{2.3}$$

Where term γ is the activity coefficient of species X, which depends on the temperature of the solution and its ionic strength.

For reliable thermodynamic data for describing a chemical equilibrium, it is therefore necessary to keep activity coefficients γ of the species in solution constant during the experiments. The experiments must therefore be carried out at a constant temperature, using a thermostatic control apparatus. In addition, to keep the ionic strength of the solution constant, a sufficiently high concentration of an inert background electrolyte must be used. In experiments carried out in aqueous solution, 0.1 or 1.0 M sodium perchlorate or nitrate are usually employed.

In the case of constant activity coefficients, equation (2.2) may be rewritten in terms of concentrations, replacing standard potential E^0 with formal potential, $E^{0\prime}$:

$$E = E^{0'} + \frac{RT}{nF} \ln \frac{[\mathrm{M}^{z+}]}{[\mathrm{M}^{(z-n)+}]}, \text{ where : } E^{0'} = E^{0} + \frac{RT}{nF} \ln \frac{\gamma_{\mathrm{M}^{z+}}}{\gamma_{\mathrm{M}^{(z-n)+}}} \tag{2.4}$$

Methods. Experiments performed to study the protonation of PTA and its complexation by Ag(I) were carried out by means of a series of potentiometric titrations (see section 2.3). A glass membrane electrode (*Metrohm Unitrode*) was used to study phosphine protonation, and the formation of silver(I) complexes of PTA was followed by a massive silver electrode (*Metrohm Combined Ag-ring*). Titrant volumes were added with an automatic burette (*Metrohm Dosimat 665*). Experimental data (E, mV vs V_{added}, mL) were collected with home-made software (*WinTit*) and processed with the *Hyperquad 2006* minimization program [77, 78], in order to find the speciation model for the best description of the experimental data (for details, see appendix section D.3 on page 126).

2.1.2. UV-Vis spectrophotometry

Ultraviolet and visible spectrophotometry (UV-Vis) is a technique generally less accurate and precise than potentiometry [79]. Therefore, if potentiometry can be used to investigate the system, spectrophotometry should be regarded as a complementary technique.

Spectrophotometric investigation of chemical equilibria is based on changes in the UV-Vis absorption spectrum of an analyte when it forms complexes in solution. The Lambert-Beer Law governs the light absorption of a specific absorber in spectrophotometry. This law states that a linear relationship exists between the absorbance of an analyte in solution and the product between its concentration and the path length of the measurement cell, according to the well-known expression:

$$A_\lambda = \varepsilon_\lambda \cdot C \cdot l \tag{2.5}$$

where: A_λ is the absorbance of the analyte at wavelength λ, C is its molar concentration, l is cell path length (usually expressed in centimeters) and ε_λ is the molar absorbance of the analyte at the wavelength of λ. Now, in a solution where the absorbing analyte, a_0, forms n complexes (a_1, $a_2, \ldots,$ a_n), each of them with a characteristic absorption spectrum,

the absorbance of the solution at a given wavelength λ is:

$$A_\lambda = l \cdot (\varepsilon_{\lambda,0} \cdot C_0 + \varepsilon_{\lambda,1} \cdot C_1 + \cdots + \varepsilon_{\lambda,n} \cdot C_n) \tag{2.6}$$

where $\varepsilon_{\lambda,0}$, $\varepsilon_{\lambda,1}, \ldots$ are the molar absorbances of species a_0, $a_1, \ldots$ and C_n are their concentrations in solution.

Methods. In this study, spectrophotometry was used to study the complex formation between Cu(I) and PTA in aqueous solution. Experiments were carried out in a series of *batch* titrations (see section 2.2.3 on page 43). The absorbance spectra of the solutions were collected on a *Varian Cary 4000* spectrophotometer equipped with a thermostatic Peltier system, which ensures temperature control during experiments. Experimental data were collected with the instrument software and processed with the *Hyperquad 2006* minimization program to obtain the speciation model which best reproduces the experimental data.

2.1.3. Cyclic voltammetry

Cyclic voltammetry (CV) is another electrochemical technique used to study equilibrium systems and chemical kinetics in solution. A cyclic voltammetry experiment is usually carried out at constant temperature in a thermostated cell not stirred during experiments. Measurements require three electrodes: a working electrode, a counter-electrode and a reference electrode. In a typical CV experiment, the potential of the working electrode is ramped linearly with time to a chosen potential and then lowered to the initial value in the same way. The electric current through the working electrode versus the applied voltage is recorded, and the diagram of the electric current *vs* applied potential is called *voltammogram*. Voltammograms are typically characterized by anodic and cathodic peaks with potential values related to the processes of oxidation and reduction of the species in solution. A voltammetric study can generally provide information about the complexes formed in solution and their redox stability.

Methods. CV was used here for a preliminary investigation on the equilibria of formation of Cu(I)–PTA complexes in aqueous solution and to evaluate their redox stability in the

operating conditions.

2.1.4. Microcalorimetry

Calorimetry is an experimental technique used to measure the reaction heat of a chemical process. Isothermal calorimetry means that the reaction heats involved are studied in isothermal conditions, recording the heat exchange between the reaction vessel and a thermostated bath. Isothermal microcalorimetry is an advanced calorimetric method used to measure reaction heats within the microjoule range. It is thus a very useful technique, suitable to study reactions involving even very small quantities of reagents. A typical microcalorimetric experiment consists of measuring the reaction heat generated when known volumes of titrant (of the order of tenths of μL) are added to a reaction cell containing 1–3 mL of titrand. The application field of isothermal microcalorimetry in chemical equilibrium studies is very attractive, because it offers the possibility of using a single technique to determine the thermodynamic properties (ΔG, ΔH and ΔS) of a wide range of different types of interactions, including the formation of inorganic complexes in water or in non-aqueous solvents, and the binding between small organic molecules such as medicinal compounds with larger biological substrates as proteins.

Given the great sensitivity of this technique, microcalorimetry is suitable to determine the stability constants of very weak complexes [80, 81], since these processes usually involve the development of small amounts of reaction heats. In the present work, it is also shown that microcalorimetry is an excellent technique for studying the formation of strong complexes, since such studies usually require low concentrations of the complexing species in solution and imply low or very low reaction heats.

When solutions of a metal ion M and a ligand L are mixed in a microcalorimeter reaction cell to form a series of successive complexes according toM + nL $\rightleftarrows$ ML_n, reaction heat Q, released or absorbed, is given by:

$$\begin{gathered} Q = V\left([ML]\Delta H_{ML} + [ML_2]\Delta H_{ML_2} + \cdots + [ML_n]\Delta H_{ML_n}\right) + \Delta H_{dil}, \\ \text{and}: \ [ML_n] = \beta_n [M][L]^n \end{gathered} \tag{2.7}$$

where V is the total volume of the cell solution, ΔH_{ML_i} is the molar formation enthalpy of

the ML_i complex, and ΔH_{dil} is dilution heat. Since the formation of every complex implies a definite reaction heat, microcalorimetry is usually employed to measure the enthalpies of formation of the complexes once their stability constants are known. However, in some cases as previously noted, the microcalorimetric approach also allows the direct and simultaneous determination of reaction enthalpies ΔH_n and stability constants β_n of the complex species formed in solution. The values of formation enthalpies obtained by direct calorimetric measurements are much more accurate than those obtained by measuring the temperature dependence of the stability constants with the Vant' Hoff relationship.

Methods. A *Thermometric TAM III* isothermal microcalorimeter (Figures 2.1 and 2.2) was used to study the formation of Cu(I), Ag(I) complexes with PTA (sections 2.2, 2.3) and with the amino acid methionine (see section 2.4). The instrument is composed of two cylindrical metal housings containing the measure and reference cells. The two calorimeter units (Fig. 2.2) are housed in an aluminum holder block in contact with a thermostatic bath (Fig. 2.1). The bath temperature is maintained constant within variations of $\pm 2 \cdot 10^{-4}$ K by a series of fine thermostatic regulation systems, and the aluminum holder block ensures that temperature fluctuations are even smaller than 1 μK in the calorimeter units, within the working range of 278–353 K. Sensitive thermocouple circuits lying on the bottom of the unit are used to detect temperature differences within 10^{-6} K between reference and measure cells.

The reference cell is usually filled with water, or preferably with a solution of the same ionic medium employed during the experiments, so that the reference solution has the same vapor pressure as the solution in the measure cell. The reference and measure cells are made of an inert *Hastelloy* alloy. The measure cell is usually filled with an initial volume of 2.50 – 2.75 mL of the titrand solution. It is then sealed and fixed to a vertical metal tree equipped with a Hastelloy stirrer to mix the reactants. A *Hamilton gastight* glass syringe (V = 0.250 – 0.500 mL) connected to a gold capillary cannula is used as a burette to add the titrant to the cell solution. A stepping motor controls the volume dispensed by the burette. In a typical experiment, successive volumes of 5 – 20 μL of titrant are added to the measure cell.

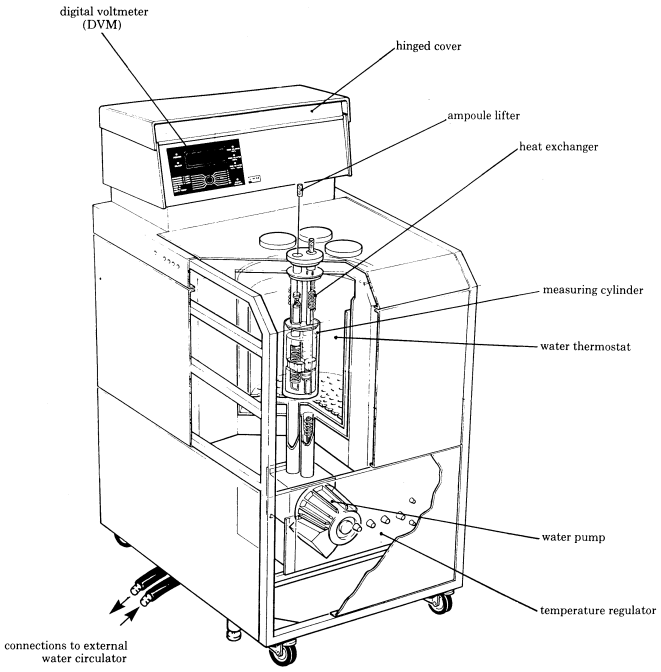

Figure 2.1.: *TAM III* (*Thermal Activity Monitor*) isothermal microcalorimeter.

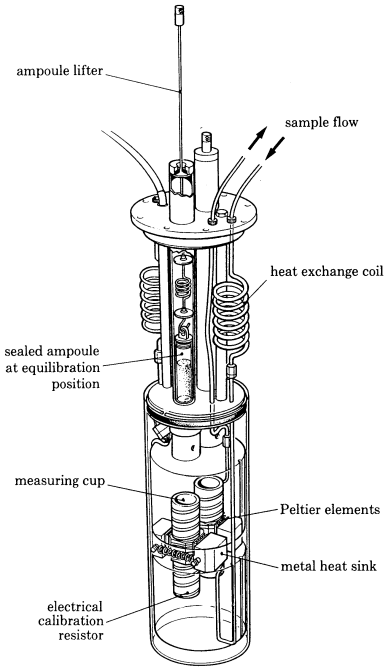

Figure 2.2.: detail of *TAM III* measuring unit cylinder

System calibrations. Before each experiment, the system must be calibrated, for correct information about thermal variations in the measure cell during a thermal event, i.e., when a chemical reaction in solution takes place, after the addition of a certain amount of titrant.

A precision calibration heater resistor is built into the measuring unit. The calibration resistor is integral with the measuring cup, to simulate a thermal event as closely as possible. This ensures that the output from the detector is also as near as possible identical when the same power is dissipated from both resistor and the reaction cell. During calibration, a known current is passed through the appropriate heater resistor and, because the resistor value is known, the thermal power dissipated is also known. The recorder deflection due to the thermal power dissipated gives the calibration level, which may then be used to determine quantitative experimental results.

The instrument has several power amplifiers with different full-scale offsets. During our experiments, power ranges of 30, 100 and 300 μW were used.

Figure 2.3 shows an example of the output of dynamic calibration in the range scale of 100 μW. During dynamic calibration, the dedicated resistors are first supplied with 40% of the selected full-scale power value for a fixed time (Figure 2.3, A). This is then increased to 95% (Figure 2.3, B), and the response rate of the system is stored in memory. This operation proceeds automatically, until sufficient information has been taken into memory. As the figure shows, the output response of the corrected signal (red curve) of a titration peak after calibration is quite fast, and takes into account all the reaction heat due to the addition of a volume of titrant in the course of a few minutes.

A good standard practice which we adopt is to perform several automatic calibrations of the system during an experiment, especially in the case of long-running measurements lasting several hours, during which both external conditions and calorimeter cell thermal capacity may vary. An example of an output of a microcalorimetric titration is shown in Figure 2.4. The enthalpy graph refers to acid-base titration of phosphine PTA. In this experiment, a dynamic calibration was performed every ten additions of titrand. The reaction heat decreases near the equivalent point, and the last small titration peaks simply provide the dilution heat of the titrant in the cell solution.

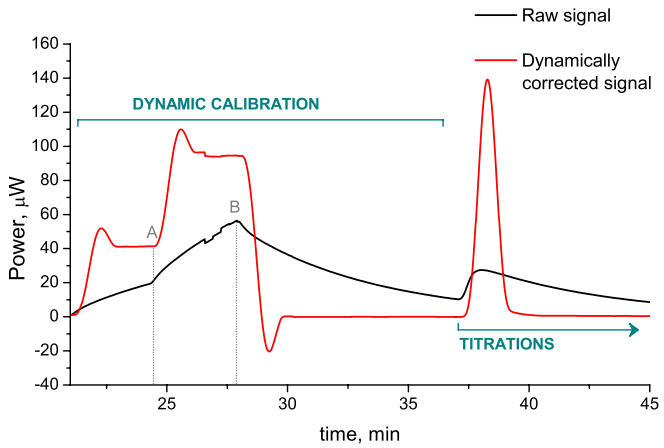

Figure 2.3.: example of dynamic calibration during microcalorimetric titration.

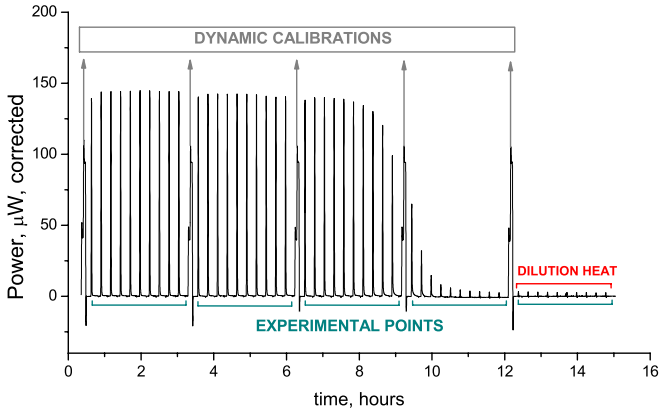

Figure 2.4.: example of microcalorimetric corrected output (acid-base titration of amino functions of phosphine PTA).

Data processing. Experimental data from microcalorimetric titrations (Q_{ex}, mJ) were collected with the instrument software *Win DigiTam* and corrected for dilution heat ($Q_{reaction} = Q_{ex} - Q_{dil}$). The stepwise reaction heats ($Q_{reaction,i}$) and volume of titrant added during titration (V_{add}, µL) were then processed with minimization software based on the *Letagrop* approach [82–86] (see appendix section D.4 for further details) in order to obtain the reaction enthalpies and stability constants which best reproduce the experimental data, according to a given speciation hypothesis.

2.2. Formation of Cu(I)–PTA complexes

The formation of complexes between Cu(I) and PTA was studied by both spectrophotometric and microcalorimetric approaches.

This study presented considerable difficulties, because Cu(I) is a thermodynamically unstable species in aqueous solution and spontaneously tends to undergo fast disproportionation to Cu(II) and metallic copper. An affordable method used to stabilize the monovalent oxidation state of the cation, among those reported in the literature, is to use the chloride ion as a complexing (and thus stabilizing) agent. In chloride solutions, copper(I) forms a series of successive complexes, stable to disproportionation, with general formula $[CuCl_n]^{1-n}$.

Several studies show that, in aqueous solutions with low concentrations of chloride ions (< 0.1 M), Cu(I) mainly forms 1:1 and 1:2 complexes $[CuCl]_{(aq)}$ and $[CuCl_2]^-$ [15, 87–97], whereas the formation of a third 1:3 complex is ascertained with higher chloride concentrations (≥ 1.0 M). Recently, Brugger et al. [15] determined the structure of complexes $[CuCl_2]^-$ and $[CuCl_3]^{2-}$ in an XAS study in solution. The results show that Cu(I) has a slightly distorted linear geometry in $[CuCl_2]^-$ and a trigonal planar arrangement in $[CuCl_3]^{2-}$. The same authors also verified that, in solutions with higher chloride concentration (> 3 M), no complexes after $[CuCl_3]^{2-}$ form at all.

A recent theoretical molecular dynamics study, comprising *ab-initio* calculations, by Sherman [98], also confirmed these data. The most comprehensive study of the speciation of chlorocomplexes in solution was that of Sharma and Millero [92], who evaluated the stability constants of three successive chlorocomplexes with general formula $[CuCl_n]^{1-n}$ (β_n, with n = 1 – 3), forming in solution at relatively high concentrations of chloride (0.100

Table 2.1.: calculated formation constants of complexes $[CuCl_n]^{1-n}$ (n = 1 – 3) at in infinite dilution and NaCl 0.1 and 1.0 M.

species	$\log \beta^0$ [92]	$\log \beta_n$ (NaCl 0.1 M)	$\log \beta_n$ (NaCl 1.0 M)
$[CuCl]_{(aq)}$	3.10	2.87	**2.68**
$[CuCl_2]^-$	5.42	5.20	**5.07**
$[CuCl_3]^{2-}$	4.75	4.72	**4.78**

– 5.00 M). For these species, the same authors also calculated stability constants at infinite dilution (thermodynamic stability constants, β_n^0), providing for each of the species in solution the related Pitzer's parameters [99, 100] which describe variations in the activity coefficients of species γ_n with the ionic medium (for a detailed discussion of the relationship between γ_n and ionic strength of solution, see appendix C on page 113).

The thermodynamic formation constant of the generic complex $[CuCl_n]^{1-n}$ is given by:

$$Cu^+ + nCl^- \rightleftarrows [CuCl_n]^{1-n},\ \beta_n^0 = \frac{\{[CuCl_n]^{1-n}\}}{\{Cu^+\}\{Cl^-\}^n} \tag{2.8}$$

where {X} is the activity of species X. The value of the constant refers to ideal conditions of infinite dilution. Working with an ionic medium of defined concentration, in our case NaCl 1.0 M, the formation constants of complexes β_n^0 can therefore be calculated by substituting in equation (2.8) the values of the activity coefficients of the individual species, according to:

$$\beta_n^0 = \frac{\gamma_{CuCl_n}^{(1\,M)}\,[[CuCl_n]^{1-n}]}{\gamma_{Cu}^{(1\,M)}\,[Cu^+]\cdot(\gamma_{Cl}^{(1\,M)})^n\,[Cl^-]^n},\ \text{whence:}\ \beta_n^{(1\,M)} = \beta_n^0 \cdot \frac{\gamma_{CuCl_n}^{(1\,M)}}{\gamma_{Cu}^{(1\,M)}\cdot(\gamma_{Cl}^{(1\,M)})^n} \tag{2.9}$$

Using Pitzer's parameters [92], we therefore calculated the formation constants of the three $[CuCl_n]^{1-n}$ (n = 1 – 3) complexes in 1.0 M NaCl, the ionic medium used to carry out later experiments with PTA. The calculated values of the formation constants are listed in Table 2.1 (for details of the calculation, see appendix section C.3.1 on page 116).

Figure 2.5 shows the variations in the relative abundances of species $[CuCl_n]^{1-n}$ as a function of total chloride concentration, in a solution containing a total concentration of metal ion 1.00 mM. The speciation plot shows that, in 1.0 M NaCl, Cu(I) is quantitatively

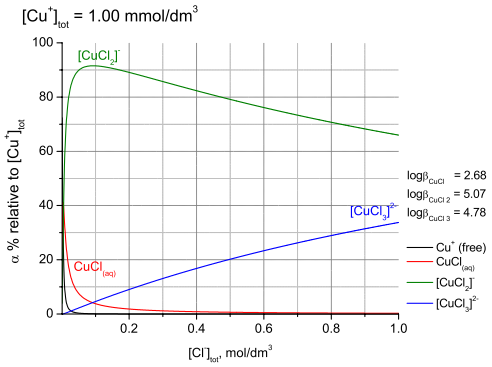

Figure 2.5.: relative abundances of copper(I) chloride complexes at various chloride concentrations for $[Cu^+]_{tot}$ = 1.0 mM and μ = 1.0 M at 25.0 °C.

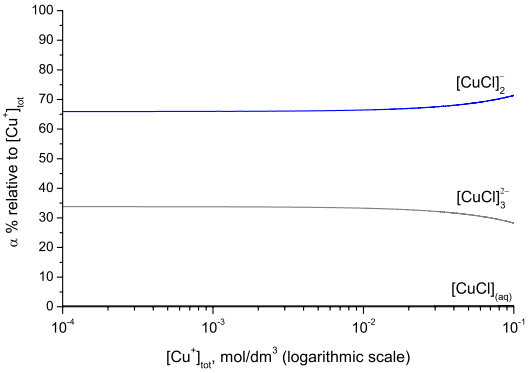

Figure 2.6.: relative abundance of copper(I) chloride complexes at $[Cl^-]_{tot}$ = 1.0 M, T = 25.0 °C.

complexed by chloride forming $[CuCl_2]^-$ (67%) and $[CuCl_3]^{2-}$ (33%). It should be emphasized that in this case (1 M NaCl) the relative abundance of the complexes in solution remains constant with the concentration of the metal, although the total concentration of Cu(I) is significantly lowered (see figure 2.6).

It is of interest to note that, as the aim of the study was to evaluate the stability of copper(I) complexes in conditions close to those of biological systems, the most suitable ionic medium for these experiments would have been NaCl 0.1 M, closer to that of biological environments. However, it was necessary to work in 1.0 M NaCl, not only to avoid Cu(I) disproportionation, but also to achieve the best experimental conditions to minimize Cu(I) oxidation by atmospheric oxygen. Sharma and Millero [101] did point out that Cu(I), although stabilized in its monovalent state by chloride, is subject to oxidation by atmospheric oxygen even at high chloride concentrations (0.1 – 6 M), according to the reactions:

$$\begin{aligned} Cu^+ + O_2 &\rightarrow Cu^{2+} + O_2^{\cdot -} \\ 2O_2^{\cdot -} + 2H^+ &\rightarrow H_2O_2 + O_2 \\ Cu^+ + H_2O_2 &\rightarrow Cu^{2+} + OH^{\cdot} + OH^- \end{aligned} \tag{2.10}$$

To overcome the considerable difficulties due to the instability of the metal ion in aqueous systems, we devised various experimental approaches (see later), in order to carry out

thermodynamic studies in experimental conditions avoiding both the disproportionation of Cu(I) and its possible oxidation by oxygen. Because of the special affinity of Cu(I) for chloride ion, the formation of copper(I)–PTA complexes in NaCl 1M should occur by displacement of one or more chlorides from the coordination sphere of the metal ion. As a result, the stability constants obtained in this work do not refer to equation (2.11), but rather to the processes of substitution of chloride ions in the coordination sphere of Cu(I) by PTA, shown in eq. (2.12):

$$Cu^{+} + nPTA \rightleftarrows [Cu(PTA)_n]^{+} \tag{2.11}$$

$$[CuCl_m]^{1-m} + nPTA \rightleftarrows [CuCl_{m-x}(PTA)_n]^{x-m+1} + xCl^{-} \tag{2.12}$$

With: n = 1– 4, m = 2 – 3, x = 0 – 3. For this reason, our stability constants must be regarded as *conditional stability constants*, referring to a system in which total chloride concentration was 1.0 M.

Because of the easy oxidation of Cu(I) in these equilibrium systems, in order to verify whether the presence of Cu(II) in solution could interfere with complexation, it was first necessary to study the Cu(II)/PTA system.

2.2.1. Chemicals

PTA

1,3,5-triaza-7-phosphadamantane (PTA) was prepared according to published procedures [102, 103], with slight modifications done in order to obtain the compound with a high purity and to minimize its oxidation during the purification process. 50 g (210 mmol) of tetra hydroxyethyl phosphonium chloride (THPC, *Aldrich*, 80% water solution) and 25 g of ice were weighed in a 200 mL beaker. THPC salt was neutralized to tris hydroxyethyl

phosphine by dropwise addition of 17 g of a 50% NaOH aqueous solution under vigorous stirring. In this and in the following preparation steps it was important to not exceed pH 8–9 to avoid unwanted phosphine oxidation. 90 g (900 mmol) of formaldehyde (30% water solution, *Fluka*) and 30 g (214 mmol) of hexamethylene tetramine (HMTA, assay > 99%, *Fluka*) were then added to the basic solution. The reactions leading to the formation of the product are exothermic therefore, in order to avoid unwanted PTA oxidations, it was important to prevent warming of the reaction mixture above room temperature. To do this, the reactants were added dropwise and the reaction vessel was cooled into a ice/water bath.

The reaction mixture was kept under stirring for 12 h at room temperature. The product was concentrated by evaporation of the solvent at room temperature. Crystals of PTA were then separated by the mother liquors and rapidly washed with cold ethanol. The product, once dried under vacuum, was dissolved in chloroform and filtered to separate any trace of NaCl. Chloroform was then evaporated under vacuum and phosphine dissolved in methanol to eliminate any trace of its oxidation product, insoluble in this alcohol. The product obtained after the solvent evaporation was again purified by a second slow recrystallization from water at room temperature. The final product so obtained had a very good purity (>99.5%), suitable for thermodynamic studies, even if the reaction yield was low (3-5%).

Elemental analysis: PTA, $C_6H_{12}N_3P$, FW = 157.15 g/mol. % calculated (% found): C 45.86 (45.77), H 7.70 (7.46), N 26.74 (26.52).

CuCl

The solid salt used to prepare stock solutions of Cu(I) was obtained by an easy procedure that involves a comproportionation reaction between Cu(II) and metallic copper.

Preparation. 10 g of $CuCl_2$ ($\approx$ 74 mmol) (*Aldrich*, pur > 99.0 %) were dissolved in 100 mL of a 10% HCl aqueous solution containing 10 g of metallic copper (beads, *Aldrich*). The comproportionation reaction was completed in 1 h by heating the solution near to the boiling point, under stirring. The reaction mixture was concentrated to small volume and the white solid obtained was filtered, washed (first with several portions of a cold 0.1 M HCl solution and then twice with ethanol and diethyl ether) and dried under vacuum.

The final product was a crystalline white powder that was stored under nitrogen to avoid copper(I) oxidation by the atmospheric oxygen.

2.2.2. Interaction between Cu(II) and PTA in aqueous solution

To check in advance if Cu(II) could react with PTA, we made some preliminary tests, during which known quantities of PTA were added to solutions of Cu(II) (0.5–5 mM in NaCl 1.0 M) to PTA:Cu(II) molar ratios up to 10:1. In all cases, a rapid color fading of the solution was observed, from light blue (typical of that of the cupric aquoion) to colorless. In addition, the formation of a white precipitate was always observed in the solutions with a higher metal ion concentration (1–5 mM). These experiments suggested that a reaction occurred, possibly involving the Cu(II)-promoted phosphine oxidation, leading to the formation of stable $[Cu(PTA)_n]^+$ complexes according to the reactions:

$$\begin{aligned} 2Cu^{2+} + PTA + H_2O &\rightleftarrows 2Cu^+ + PTA_{ox} + 2H^+ \\ Cu^+ + mCl^- &\rightleftarrows [CuCl_m]^{1-m} \\ [CuCl_m]^{1-m} + nPTA &\rightleftarrows [CuCl_{m-x}(PTA)_n]^{1-m+x} + xCl^- \end{aligned} \tag{2.13}$$

The heat involved in these processes was also measured by means of some microcalorimetric titrations. Figure 2.7 shows, as an example, that the amount of heat evolved per volume of PTA added to the metal solution is almost constant and independent from the PTA to Cu molar ratio. The slope of the line Q_{tot}. *vs* V_{added} (see plot (b) in Figure 2.7) indicate an average reaction heat of 44.7 kJ per mole of PTA.

In order to provide a rational description of the reactions occurring when PTA is mixed with solutions of Cu(II), we carried out some cyclic voltammetry (CV) experiments. In these experiments we obtained information about: a) the stability of Cu(I) in NaCl 1.0 M; b) the stability of PTA under the same conditions; c) the reaction between Cu(II) and PTA.

All the CV experiments were performed in a thermostated cell at 25 °C. The solutions in the measuring cell were prepared by dissolving weighed quantities of CuCl or $CuCl_2$ in a known volume of NaCl 1.0 M. Increasing amounts of a PTA solution (50.0 mM) were then added to the cell solution. Before each experiment all the solutions were thoroughly

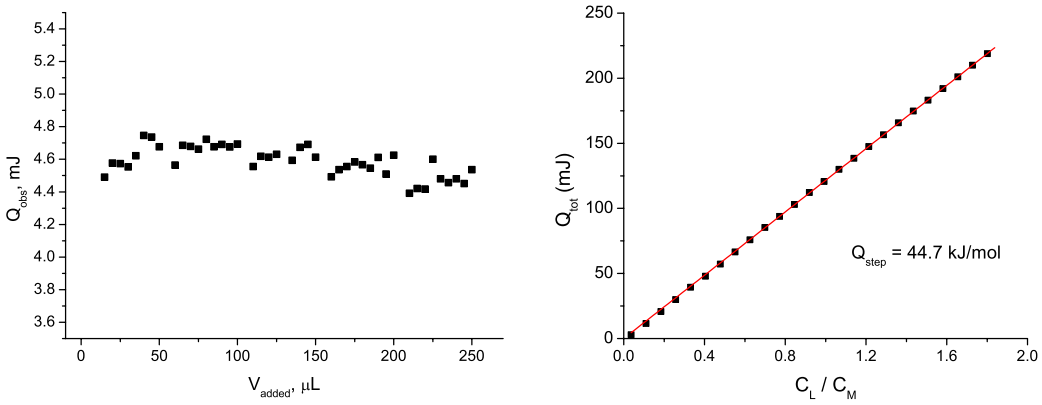

(a) **(b)**

Figure 2.7.: microcalorimetric titration, 2.74 mL of a Cu(II) solution 0.985 mM titrated with successive additions of 10 µL of a 20.0 mM PTA solution in NaCl 1.0 M.

degassed by an argon flux in order to protect them from the atmospheric oxygen.

Two platinum electrodes (working electrode and counter electrode) and a reference electrode (saturated calomel, SCE) were used to carry out the voltammetric measurements. The CV curves (*current intensity*, A, *vs. potential*, V), which show characteristic peaks in the correspondence of the oxidation and reduction potentials of the species investigated, were collected and processed with the *GPES* software provided by the manufacturer.

Two preliminary experiments were carried out in order to study the redox system Cu(II)/Cu(I) in NaCl 1.0 M. During these experiments, the cyclic voltammograms of solutions of CuCl or $CuCl_2$ in the range of potentials of 0.0–0.5 V were collected with a fixed scan rate of 0.1 V/s. The voltammograms are shown in Figure 2.8.

The black curve in the figure is the voltammogram of a copper(I) solution, the red one is that of a copper(II) solution. The two curves show that the redox system is reversible and independent of the particular oxidation state of the species in the starting solution. This result was expected, and is a proof of the particular stability of Cu(I) in NaCl 1.0 M. In both experiments, marked and distinct oxidation/reduction waves are shown, characterized by well-defined anodic and cathodic potential peaks.

A second series of experiments was dedicated to the study of the electrochemical behavior

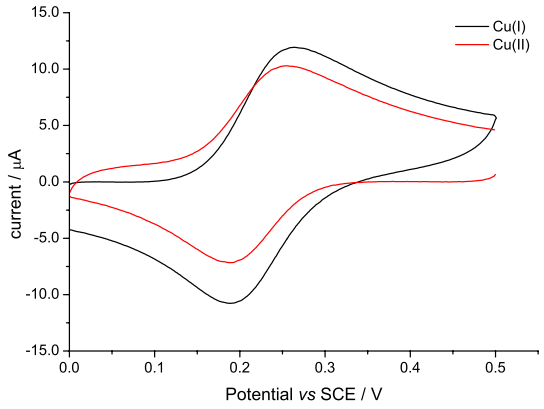

Figure 2.8.: voltammograms of Cu(I) (1.0 mM) and Cu(II) (1.0 mM) in NaCl 1.0 M.

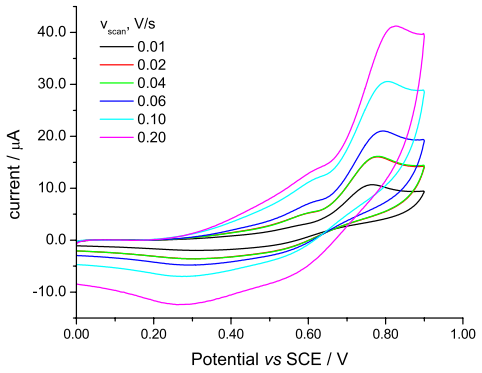

Figure 2.9.: voltammograms of PTA solutions in NaCl 1.0 M at different scan rates (from 0.02 to 0.10 V/s).

of the phosphine. In this case, a series of voltammograms were collected for a 1.0 mM solution of PTA degassed with anoxic argon. The voltammograms were recorded at different scan rates (see Figure 2.9). The results of these experiments show that the phosphine can be oxidized in aqueous solution and that this oxidation occurs in an irreversible manner, since the reduction peaks are not observable in the voltammetric curves.

A third set of CV experiments was carried out in order to study the formation of Cu(I)–PTA complexes in NaCl 1.0 M. For this purpose, a solution of CuCl 1.0 mM in NaCl 1.0 M was prepared in the cell, then successive volumes of a solution of PTA 20.0 M were added until the molar ratio Cu(I):PTA in the measuring cell was 1:4. The CV curves are shown in Figure 2.10. Two distinct oxidation peaks of Cu(I) are observable in the voltammograms

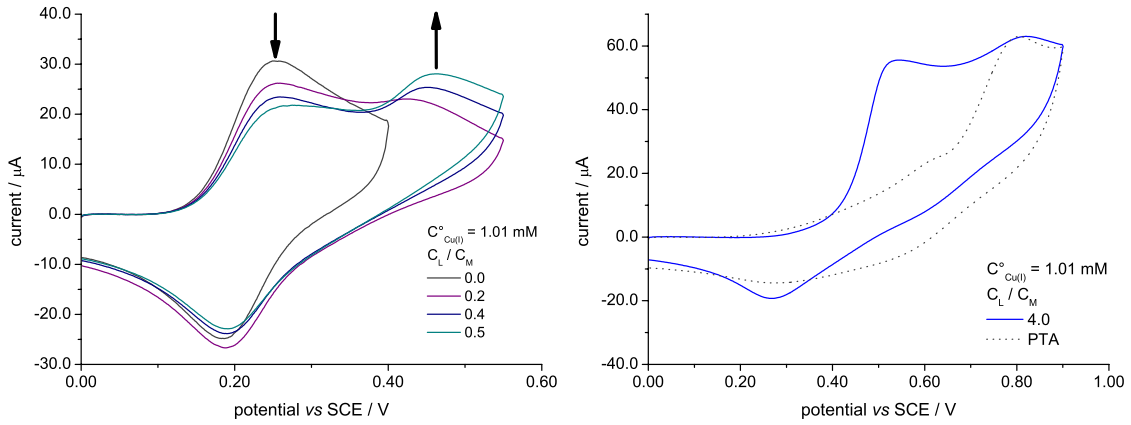

(a) **(b)**

Figure 2.10.: voltammograms of a 1.0 mM Cu(I) solution containing increasing amounts of PTA (NaCl 1.0 M).

in Fig. 2.10(a). The first peak occurs at a potential corresponding to the oxidation of $[CuCl_m]^{1-m}$ complexes (0.189 V), as previously observed, whereas the second is shifted toward more positive potentials (0.425 V). In addition, as the concentration of PTA is increased, the second anodic peak gradually shifts towards higher potentials (0.460 V). More important, the peak current for the oxidation of $[CuCl_m]^{1-m}$ decreases while that of the Cu(I)–PTA complexes increases as the concentration of PTA is increased. This confirms the formation of successive Cu(I)–PTA complexes which stabilize the monovalent oxidation state of the metal ion, shifting the redox potential to more positive values. Oxidation of Cu(I)–PTA complexes is an irreversible process; there is no reduction peak coupled with the oxidation one observed for Cu(I)–PTA to be assigned to the reduction of Cu(II)–PTA. This is a clear indication that no complexation reactions between Cu(II) and PTA take place.

As observed in the preliminary experiments, also in this case, when the molar ratio PTA to Cu(I) in solution was higher than 0.5 and the copper concentration was greater than 1.0 mM, a white precipitate formed in solution. The elemental analysis revealed that the solid compound was a coordination compound with formula [Cu(PTA)]Cl. It was also observed that the quantity of precipitate did not increase as the PTA/copper molar ratio

was further increased. On the contrary, the precipitate was dissolved rapidly in water when the ligand to metal ratio was 4. This observation suggests that Cu(I) should form up to four mononuclear successive complexes in NaCl 1.0 M and that the highest of these complexes is more soluble than the lowest.

The blue curve in Figure 2.10(b) is the voltammogram of the solution in which the molar ratio PTA:Cu(I) is 4. Interestingly, the oxidation peak of the copper chloride complex does not appear in this voltammogram. The anodic peak at 0.460 V also disappeared; it is replaced by a new anodic peak at 0.543 V to be attributed to stable Cu(I)–PTA complexes with stoichiometry higher than 1:1. This voltammogram was extended up to a final potential in the region of PTA oxidation. A comparison of the voltammetric pattern of the CuCl – PTA system with that of PTA alone (dotted curve) shows the presence of a small quantity of free PTA in the system, which confirms the formation of complexes of the type $[Cu(I)(PTA)_n]^+$, with $n > 1$.

It should be noticed that the Cu(I) – PTA system at a 1:4 molar ratio shows a cathodic peak at 0.268 V, which might be assigned to the reduction Cu(II) to Cu(I). The potential of this peaks is significantly more positive than that observed for Cu(II) in the absence of PTA (0.190 V). Moreover, the anodic peak at 0.543 V, arising from oxidation of the Cu(I)–PTA species prevailing in the presence of excess PTA, is shifted by about +0.080 V with respect to the peak initially observed for the Cu(I)/PTA system under 1:1 ratio. These data may be wrongly ascribed to an interaction between Cu(II) and PTA due, for example, to the formation of Cu(II) – PTA complexes by coordination of the metal ion by an amino nitrogen of the phosphine. This possibility was however excluded by the subsequent calorimetric measurements, which show that Cu(II) does not form any complexes with PTA.

The voltammetric response recorded for Cu(I) oxidation in the presence of 4-fold excess of PTA suggests the presence of a catalytic reaction in which PTA is oxidized by Cu(II) generated at the electrode. First, the oxidation peak in Fig. 2.10(b) does not present its anodic partner for the reduction of the electrogenerated Cu(II). Second, and more important, the anodic peak current is much higher (55 µA) than that recorded for the same redox species in the absence of PTA (30 µA, compare the grey curve in Fig 2.10(a) with the blue one in Fig. 2.10(b)). This behavior is typical of electrocatalytic systems in

which an electrogenerated species is involved in a rapid redox reaction occurring in solution. The rate of oxidation of Cu(I) at the electrode is enhanced by the fast regeneration Cu(I) near the electrode as a result of the redox reaction of Cu(II) with PTA. In other words, once Cu(I) is oxidized at the electrode, instead of definitively leaving the vicinity of the electrode it reacts with PTA whereby it is reduced back to Cu(I), which is forced to return to the electrode where it gets oxidized again, thus starting a new cycle. The result of this alternating electro-oxidation and homogenous reduction involving the Cu(II)/Cu(I) couple is an increase of the anodic peak current for Cu(I).

In order to get details on the reactions occurring when Cu(II) and PTA are mixed in aqueous solution and to verify the initial hypothesis concerning the solution redox behavior, a final set of CV experiments was carried out. For this purpose, a solution of 1.0 mM $CuCl_2$ in NaCl 1.0 M was prepared in the CV cell and increasing volumes of PTA 20.0 mM were added to the solution cell until the PTA:Cu(II) molar ratio was 1. The voltammograms were recorded in the range of potentials from 0.00 to 1.10 V. After each addition of the phosphine, the solution was stirred for few minutes to allow completion of the eventual reaction. The voltammograms (Fig. 2.11) show that the successive additions of phosphine bring about a progressive decrease of the intensity of both the anodic and cathodic peaks of the redox couple Cu(II)/$[Cu(I)Cl_m]^{1-m}$, clearly indicating a decrease of Cu(II) concentration, presumably because of its reaction with PTA. In concomitance with the decrease of the peak couple for Cu(II)/$[Cu(I)Cl_m]^{1-m}$, ill-defined broad reduction peaks attributable to the oxidation of Cu(I) appear in the range from 0.5 V to 0.8 V and increase with increasing PTA concentration. This is indicative of the formation of Cu(I)–PTA complexes, which stabilize the monovalent state of copper shifting its oxidation potential to values to 0.5–0.8 *V*.

Some ^{31}P-$\{^1H\}$–NMR measurements were also run. A Cu(II) 1.0 mM solution in NaCl 1.0 M (D_2O) with an excess of PTA (1:10) was prepared and filled in a NMR tube. After verifying that the solution did not contain any trace of precipitate, the spectrum was collected. In Figure 2.12 the spectrum of this solution is reported in blue whereas, for comparison, the PTA NMR spectrum is reported in grey. The blue spectrum strongly suggests that all the Cu(II) in the initial solution reacted with PTA to form Cu(I). In

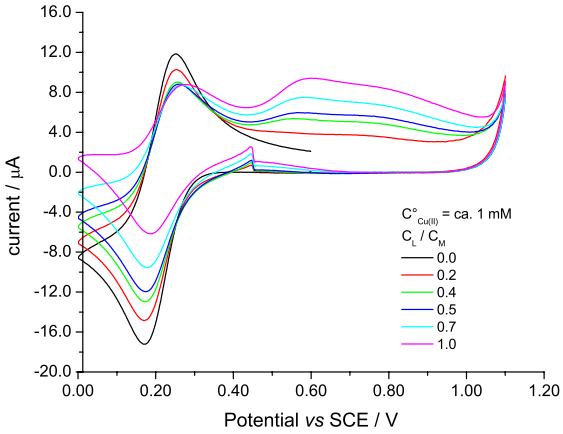

Figure 2.11.: cyclic voltammetry of 1 mM Cu(II) in 1 M NaCl, in the absence and presence of different amounts of PTA. $v_{scan} = 0.2$ *V/s*.

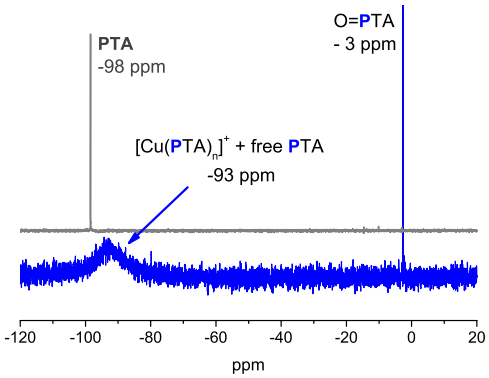

Figure 2.12.: ^{31}P-{^{1}H}–NMR spectrum of a PTA solution (gray) and of a Cu(II)/PTA solution (1:10) in NaCl 1 M.

fact, if the paramagnetic ion Cu(II) would have been present in solution, it would have prevented the acquisition of the spectrum. Otherwise, even if the spectrum could have been collected, the peak positions would have been shifted to ppm ranges very different from those observed. The signal at –98.5 ppm, characteristic of the phosphorus of PTA not complexed (grey in the figure), does not appear in the spectrum of the Cu(II)/PTA solution (blue), while the intense signal at –3 ppm, characteristic of the oxidation product O=PTA, is observable. The broad peak at –93 ppm finally indicates the presence of PTA involved in the Cu(I) complex formation.

In conclusion, different experimental techniques confirmed the initial hypothesis which

admit a series of reactions between Cu(II) and PTA according to the scheme in equation (2.13) on page 36. The total heat developed in these reactions is about 45 kJ/mol.

These evidences also point out another interesting consequence: Cu(I), even if stabilized by chloride, may undergo oxidation to Cu(II) by oxygen in aqueous solution. It turns out that, if Cu(I) is oxidized by unwanted traces of oxygen in solution, the Cu(II) so formed can, in turn, oxidize the phosphine and form copper(I). This process becomes Cu(II)-catalyzed in the presence of O_2 and continues till all the oxygen dissolved in solution disappears. This latter consideration is valuable, because it gives an indication of how much care is needed to carry out experiments on these systems. Moreover it could have considerable effects on the biological tests of the $[Cu(PTA)_4]^+$ compounds, as the presence, even in traces, of Cu(II) during the biological tests (which cannot be carried out in anoxic atmosphere) could bring to an oxidation of the phosphines coordinated to Cu(I), progressively reducing the concentration of the complex and possibly inhibiting its cytotoxic effect.

2.2.3. Formation of Cu(I)–PTA complexes in aqueous solution

Methods. Stock solutions of CuCl 50 mM were prepared by dissolution of the salt in 1.0 M NaCl. The milliQ-grade water employed for the preparation of the stocks was freshly boiled, degassed under anoxic nitrogen and stored in a oxygen-free drybox (*Braun MB II*) prior to use. To avoid Cu(I) hydrolytic reactions the acidity of the stock solutions was adjusted to pH 4 by addition of HCl. Moreover, the stock solutions were stored in sealed bottles and maintained in drybox under stirring in the presence of metallic copper. Such precaution ensured that any unwanted trace of copper(II), spontaneously would comproportionate to Cu(I) in the presence a high chloride concentration. In his way, Cu(II) concentration in solution becomes of course negligible, however Cu(I) concentration may vary slightly. Therefore, the real concentration of Cu(I) was determined by spectrophotometry prior to the preparation of each dilute solution. To do this, the Cu(I) present in weighed quantities of the stock solutions was oxidized to Cu(II) and diluted in known volumes of 1.0 M ammonia solutions, where Cu(II) forms the amino complex, characterized by a blue color. The spectrum of the solution was collected, the absorbance at 607.0 nm was measured and the copper concentration was calculated on the basis of the known value of the molar

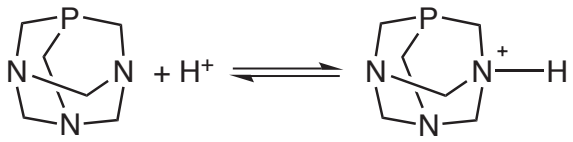

$$PTA + H^+ \rightleftarrows H(PTA)^+$$

Figure 2.13.: PTA protonation.

absorbivity of copper(II) amine complexes at this wavelength: 52.6 ± 0.2 cm^{-1} mol^{-1} dm^{-3} (this work).

The study concerning the formation of Cu(I) and PTA complexes was undertaken by means of spectrophotometric and microcalorimetric techniques. Experiments were carried out in aqueous solutions at 25 °C, in NaCl 1.0 M.

PTA is a basic species in solution and it is quantitatively protonated at pH lower than 5.5 at one of its aminic nitrogens (see Figure 2.13). Therefore, the UV-Vis spectroscopic experiments have been designed to study the complex formation at neutral or weakly basic pHs where PTA does not present protonated amine functions. In this way the study of the system was considerably simplified, since it was focused only on the formation of the four successive complexes $[Cu(PTA)_n]^+$ (n = 1–4), according to the reaction (2.14). Microcalorimetric experiments were instead carried out in solutions with different acidity in order to study also the equilibrium (2.15), concerning the formation of phosphine protonated complexes.

$$Cu^+ + nPTA \rightleftarrows [Cu(PTA)_n]^+ \tag{2.14}$$

$$Cu^+ + n(HPTA) \rightleftarrows [Cu(HPTA)_n]^{n+1} \tag{2.15}$$

Throughout the spectrophotometric study we adopted a series of methodological approaches to avoid Cu(I) oxidation by the atmospheric oxygen. In particular, we took care to carry out all the operations necessary for the preparation of the solutions and the filling of the cuvette in a controlled-atmosphere drybox. Accordingly, all the titrations of Cu(I) were carried out *batchwise*. First by preparing in drybox, by dilution of a stock solution, several solutions of Cu(I) (0.05 - 4.5 mM). Then by transferring the same known volume of these

solutions into a series of vials to which different amounts of a standard solution of PTA were added in order to realize solutions with PTA/Cu(I) molar ratios from 0 to 10. Aliquots of the solutions so prepared were then filled into the spectrophotometric cell. The cell was sealed, taken out from the drybox and the absorption spectrum of the solution collected. Always operating in this way we collected 67 absorption spectra in the wavelength range 210–340 nm. The spectra are characterized by a strong charge-transfer absorption band of the phosphine (210–220 nm) and of the complexes $[Cu(PTA)_n]^+$ (220–300 nm, analytical data of the experiments in Table A.2 on page 102).

The spectral data were then used to obtain the data-input files for the minimization program *Hyperquad*, by which we obtained the stability constants for the formation of the four Cu(I)/PTA complexes (see Table 2.2 on page 46). Once verified that the values of the stability constants obtained by spectrophotometry were of an order of magnitude suitable to allow the study of the system by microcalorimetry (see next section), we used this technique to confirm the spectrophotometry results. For this purpose, we designed a series of microcalorimetric titrations which allowed us to obtain simultaneously the enthalpies and the stability constants for the complex formations. A first series of experiments was carried out at pH close to the neutrality, to study formation of phosphine unprotonated complexes; a second series of titrations was performed in acidic conditions, to study also the formation of complexes with the protonated PTA. Typically, the microcalorimetric titrations were carried out by adding increasing volumes of PTA (30–50 mM) to solutions of Cu(I) (0.2–0.5 mM). However, a series of titrations during which PTA solutions 0.5–10 mM were added to known volumes of CuCl 10 mM, were also performed in order to obtain accurate values of the formation enthalpies of the complexes $[Cu(PTA)_3]^+$ and $[Cu(PTA)_4]^+$. A total of 15 titrations were carried out to perform this part of the study (analytical data in Table A.1 on page 101). Also in this case, in order to minimize the risk of reagent contamination by atmospheric oxygen, the whole set of operations necessary to perform the calorimetric experiments (the cell loading and its connection to the calorimeter head, the burette filling and the insertion of the capillary cannula of the burette into the calorimeter head) were carried out in drybox.

Table 2.2.: Formation (stability) constants and corresponding thermodynamic functions for Cu(I)–PTA and Cu(I)–(HPTA) complexes (NaCl 1.0 M, T = 25 °C). Comparison between $\log K$ values obtained by spectrophotometry (*UV-Vis*) and microcalorimetry (*microcal.*) is shown. In the Table: M = Cu^+, L = PTA, H = H^+. Ionic charges omitted for convenience.

Species	$\log\beta \pm 3\sigma$	$\log\beta \pm 3\sigma$	$\Delta G \pm 3\sigma$	$\Delta H \pm 3\sigma$	$T\Delta S \pm 3\sigma$
	UV-Vis	*microcal.*	kJ/mol	kJ/mol	kJ/mol
HL	5.94 ± 0.25(*)		-33.9 ± 1.4	-17.8 ± 0.6	16.1 ± 1.5
ML	6.36 ± 0.11	6.3 ± 0.6	-36.0 ± 3.3	-53.0 ± 1.7	-17 ± 4
ML_2	12.0 ± 0.6	12.1 ± 0.4	-69.3 ± 2.5	-110 ± 5	-41 ± 6
ML_3	18.2 ± 0.2	17.7 ± 0.6	-101 ± 3	-148.0 ± 1.2	-47 ± 4
ML_4	22.5 ± 0.2	21.4 ± 0.6	-122 ± 4	-188.0 ± 0.8	-66 ± 6
HML	–	11.2 ± 0.8	-64 ± 4	-67.5 ± 1.2	-3 ± 4
H_2ML_2	–	20.8 ± 0.7	-118 ± 4	-160 ± 4	-41 ± 5
HML_3	–	22.0 ± 0.8	-125 ± 4	-170 ± 7	-45 ± 8
reaction		$\log K \pm 3\sigma$	$\Delta G^{step} \pm 3\sigma$	$\Delta H^{step} \pm 3\sigma$	$T\Delta S^{step} \pm 3\sigma$
		(*microcal.*)	kJ/mol	kJ/mol	kJ/mol
$H + L \rightleftarrows HL$		5.94 ± 0.25(*)	-33.9 ± 1.4	-17.8 ± 0.6	16.1 ± 1.5
$M + L \rightleftarrows ML$		6.3 ± 0.6	-36.0 ± 3.3	-53.0 ± 1.7	-17 ± 4
$ML + L \rightleftarrows ML_2$		5.8 ± 0.7	−33.3 ± 4.2	−57.0 ± 5.3	−24 ± 7
$ML_2 + L \rightleftarrows ML_3$		5.6 ± 0.7	−31.7 ± 4.2	−38.0 ± 5.1	−6 ± 6
$ML_3 + L \rightleftarrows ML_4$		3.7 ± 0.8	−21.1 ± 4.8	−40.0 ± 1.4	−18 ± 5
$M + (HL) \rightleftarrows M(HL)$		5.3 ± 0.8	−30.2 ± 4.5	−49.7 ± 1.3	−20 ± 5
$M(HL) + (HL) \rightleftarrows M(HL)_2$		3.6 ± 1.0	−20.4 ± 6.0	−74.2 ± 3.8	−54 ± 7
(*) Obtained by potentiometry					

2.2.4. Results

Figure 2.14 shows the UV-vis absorption spectra collected during the spectrophotometric study. Experimental data (Volume of titrant added and absorbance of the solution at different wavelengths) were processed with the program *Hyperquad 2006* [78] which allows to calculate the molar absorbance and the formation constants of the species in solution on the basis of any assumed speciation model (see Appendix D.3 on page 126 for details concerning the calculation). In this case, according with the indications of previous measurements, we assumed a speciation model consistent with the formation of four successive mononuclear complexes ($[Cu(PTA)_n]^+$, n = 1–4). For each of these species, Hyperquad calculated the corresponding molar absorbance and formation constant (Table 2.2). Figure 2.15 shows the good agreement between the values of absorbance obtained experimentally and those calculated by the program.

Experimental data obtained by the microcalorimetric titrations (Q_{obs}, heat of reaction

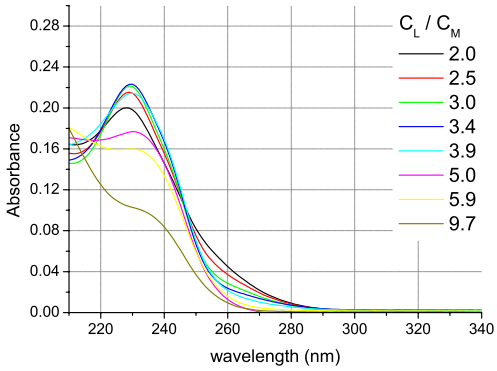

SET 1. $C_L \approx 2.2$ mM; $C_L/C_M = 0.5 - 9.7$; path length = 0.0104 cm.

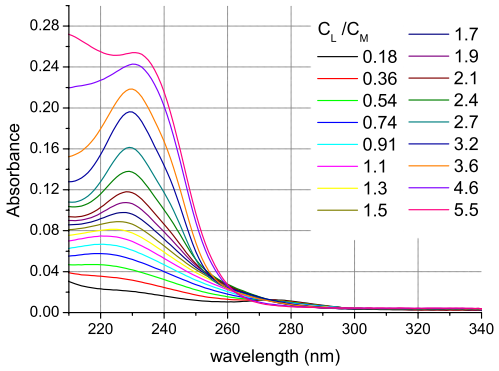

SET 2. $C_L \approx 0.6$ mM; $C_L/C_M = 0.2 - 5.5$; path length = 0.0104 cm.

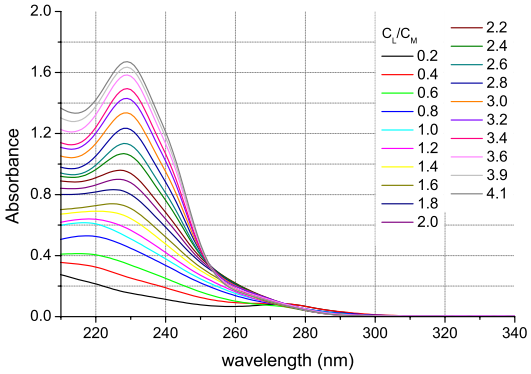

SET 3. $C_L \approx 0.05$ mM; $C_L/C_M = 0.2 - 4.1$; path length = 0.100 cm.

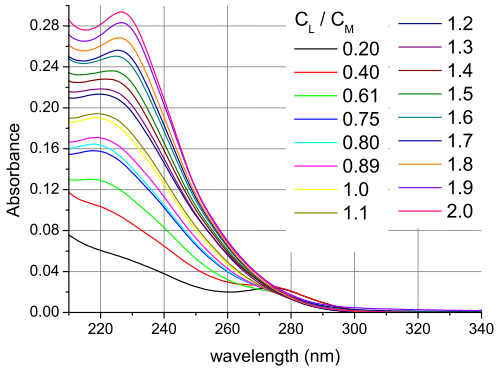

SET 4. $C_L \approx 0.017$ mM; $C_L/C_M = 0.2 - 2.0$; path length = 0.100 cm.

Figure 2.14.: UV-Vis spectra of the Cu(I)–PTA complexes (batch spectrophotometric titrations, analytical data in Table A.2 on page 102); M = Cu^+, L = PTA.

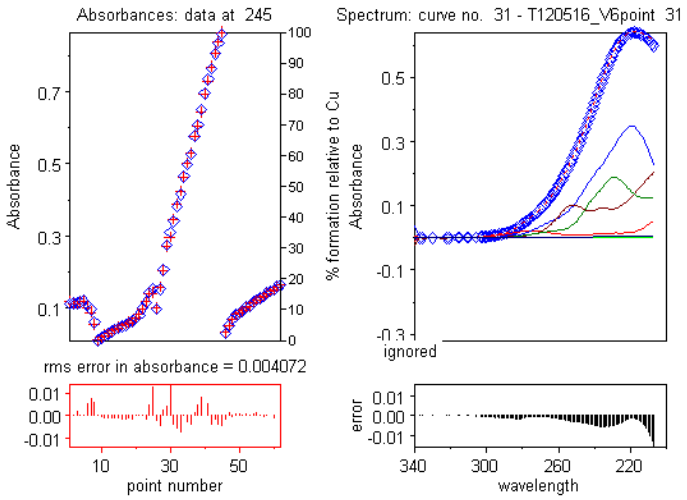

Figure 2.15.: fitting of spectrophotometric data by *Hyperquad* minimization. Figure on the left shows the absorbance of the solutions of a set at a given wavelength (245 nm in the figure). Experimental absorbance values in blue, calculated values in red. Figure on the right shows the observed and calculated absorption spectrum for one of the experimental set (Table A.2 on page 102). The calculated molar absorbances of PTA and of the four Cu(I)–PTA complexes is shown.

mJ, and V_{add}, added volume, μL) were processed with the minimization program *Letagrop Kalle* [86, 104]. The refinement algorithm minimizes the differences between observed and calculated reaction heats, $Q_{obs} - Q_{calc}$, on the basis of the enthalpies and formation constants of any assumed speciation model (see Appendix D.4 for details). The data collected in the first series of titrations were used to obtain ΔH and β_n for the unprotonated complexes; the processing of the experimental data of the second series allowed calculation of ΔH and β_n of the protonated species, $[Cu(HPTA)_n]^{n+1}$.

The, already obtained, formation enthalpies and stability constants of the unprotonated complexes were assumed as known parameters (and therefore constant) in the minimization procedure for the calculation of ΔH and β_n of the protonated species. Figure 2.16 shows that the result of the minimization procedures is very good: as a matter of fact, the values of ΔH and β_n we obtained, allowed to reproduce the experimental data very well.

Noteworthy, the values of the formation constants of the complexes $[Cu(PTA)_n]^+$ obtained independently with the microcalorimetric and spectrophotometric study are in good agreement each other (see Table 2.2).

Figure 2.17 shows the experimental data-fit for the titrations of solutions of Cu(I) with different initial acidities. The agreement between the experimental and calculated values is

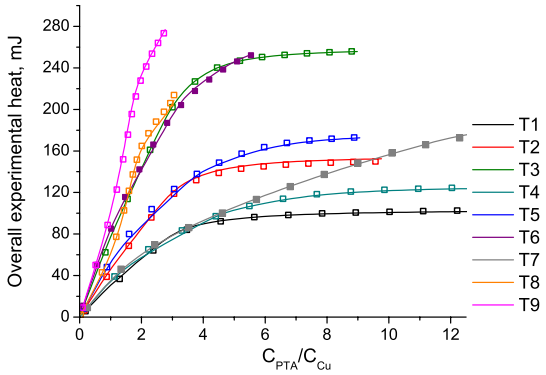

Figure 2.16.: *Overall experimental heat* (mJ) *vs* C_{PTA}/C_{Cu} (ligand to metal molar ratio) for the titrations T1–T9 (analytical data in Table A.1, page 101). Squares, experimental values; lines calculated with the values of ΔH and β_n given in Table 2.2. For sake of clarity, some of the experimental points have been omitted.

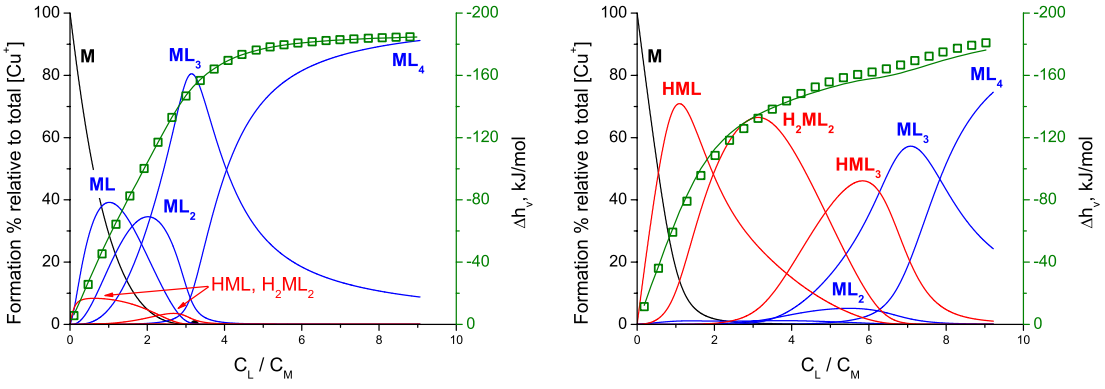

(a) **(b)**

Figure 2.17.: Examples of microcalorimetric titrations: overall formation enthalpy per mole of metal (Δh_v, kJ/mol) vs C_L/C_M. Squares, experimental values; lines calculated with the values of ΔH and β_n given in Table 2.2. Left axes show the variation of the relative percent abundances of the complex species, calculated on the basis of the speciation model given by minimization with Letagrop. **(a)** Titration carried out at neutral or slightly basic pH; the prevalent complex species in these conditions are the complexes $[Cu(PTA)_n]^+$ containing the neutral phosphine (blue curves). **(b)** Titration carried out at acidic pH ($\approx 3-4$); the prevalent species in this case are the protonated complexes (red curves).

especially good. Figures 2.17(a) and 2.17(b) show, in addition, the changes of the solution compositions for two titrations carried out in regions of neutral and acidic pH, respectively.

The almost straight increment of Δh_v in the first part of the titration and the marked inflection at a $C_L/C_L \approx 4$ in Figure 2.17(a) show, and are a consequence, of the formation of four strong deprotonated $[Cu(PTA)_n]^+$ complexes, the last of which has a molar formation enthalpy close to 190 kJ/mol. The data in Figure 2.17(b) show the effect of the formation of protonated complexes on the heat of reaction (Δh_v). The speciation curves in the figure show that the complexes with the protonated phosphine become prevalent in solution when the pH is lower than 4.

The histograms in Figure 2.18 show the values of the thermodynamic functions for the stepwise formation of the first two complexes of Cu(I) with the protonated and deprotonated phosphine, respectively (MHL and ML in Figure 2.18). In both cases the spontaneity of the process is due to the enthalpic factor, while the entropy change, negative, opposes the complex formation, as expected for the general *soft-soft* metal-ligand interaction scheme. At this point of the discussion it is important to remark that: a) Cu(I) in 1 M NaCl exists as $[CuCl_2]^-$ ($\approx 67\%$) and $[CuCl_3]^{2-}$ ($\approx 33\%$). As a consequence, the formation constants of the complexes (and the corresponding thermodynamic functions) reflect the substitution reactions of chloride in the solvatation sphere of the metal according to the reactions (2.16):

$$\begin{aligned} [CuCl_{2,3}]^{(1,2)-} + L &\rightleftarrows [CuLCl_{(2,3)-n}]^{((1,2)+n)-} + nCl^- \\ [CuCl_{(2,3)-n}]^{((1,2)+n)-} + L &\rightleftarrows [CuLCl_{(2,3)-n-m}]^{((1,2)+n+m)-} + mCl^- \\ [CuLCl_{(2,3)-n}]^{((1,2)+n)-} + L &\rightleftarrows [CuL_2Cl_{(2,3)-n}]^{((1,2)+n+m)-} + mCl^- \end{aligned} \tag{2.16}$$

where n and m may be different; b) that the ligand has a considerable steric hindrance and therefore, on the complex formation, it undergoes a significant decrease of its degrees of freedom. In addition it removes from the solvatation sphere of the metal ion n and m chloride ions which are characterized by a higher solvatation, and thus they may exert a higher ordering effect on the solution than the phosphine. The entropy decrease for the formation of the first two complexes of Cu(I) (ML and ML_2 in Figure 2.18), indicates that, despite the number of species in solution does not change[1], or even increases[2],

[1] if m and n are equal to 1.
[2] if n and m are greater than 1.

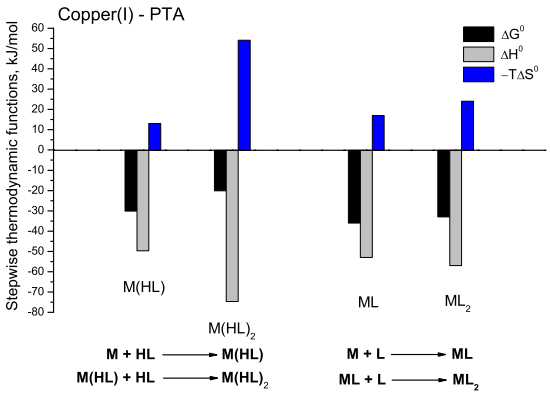

Figure 2.18.: stepwise thermodynamic functions of the first two Cu(I)–PTA complexes with the protonated and the neutral form of the phosphine, respectively. In the Figure: M = Cu^+, L = PTA.

the decrease in entropy that occurs when the ligand enters into the solvation sphere of the metal is certainly larger than the translational entropy gained by chlorides released on complexation. The small difference between the changes of entropy (less negative for the formation of ML) and enthalpy (more favorable for the formation of ML_2) could be interpreted assuming that n is greater than m, thus leading to an increased energetic cost for the removal of chlorides from the first complex, and consequently a more favorable $T\Delta S$.

Anyway, the system is too complicate to draw any definitive conclusion just on the basis of the results of the thermodynamic study. To get additional information on this point we have recently undertaken a theoretical DFT study, in order to relate the complex-formation thermodynamic quantities with the energies of formation of complexes with different stoichiometry calculated by DFT. Results of this study are on the next section.

The stability of the complex M(HL), lower than that of ML, can be justified considering that the ligand in M(HL) is positively charged. Although this charge does not consistently influence the donor properties of the phosphorous atom bound to Cu(I) (the stability of the two complexes is not much different), it may however weaken the interaction M–HL, due to the electrostatic repulsion between the metal and the ligand, positively charged. Moreover, the very negative values of $T\Delta S$ and ΔH for the formation of $M(HL)_2$ may indicate that the formation of this complex occurs with a quantitative removal of chloride from the coordination sphere of Cu(I), leading to the formation of a complex with a high net positive charge, therefore promoting a greater solvation, the reaction exothermicity and,

consequently, the remarkable entropy decrease. Also in this case, however, it would be very useful to confirm our hypotheses with the results of the DFT calculations.

2.2.5. Theoretical DFT calculations on Cu(I)–Cl–PTA complexes

Methods. The minimum energy structures of the complexes $[Cu(PTA)_nCl_m(H_2O)_y]^{1-m}$ (n, m, y ≤ 4, n + m + y = 4) were calculated by means of theoretical methods, carried out using the *Density Functional Theory* (DFT) [105, 106]. This kind of approach proved to be useful in the calculation of the spectroscopic, structural and energetic properties of metal complexes, providing accuracy similar to that of post Hartree-Fock *ab-initio* calculations, which are nevertheless characterized by a greater computational cost.

DFT routines are generally classified on the basis of the different approximations used for the calculation of exchange and correlation terms of the energy of the system. The exchange-correlation functional used in the present work was the well-known B3LYP [107, 108]. This routine was chosen, given its good performance in the calculation of the properties of metal complexes [105, 106].

The set of functions used as basis, for the description of the atomic orbitals (and of the electronic density) are a linear combination of Gaussian-shape curves, namely 6–311++G(2d,p) [109, 110]. The term "6–311" concerns the number of primitive Gaussians used for the description of the core and the valence orbitals, while the letters *d* and *p* indicate that more functions have been added, to take into account of the effects of polarization. The "+" symbol indicates the addition of functions that are "diffused" in the space. This basis set was applied to all the elements except for Cu(I). In order to improve the calculation speed, a number of electrons of the copper core have been actually replaced by an effective potential (*Effective Core Potential*, ECP), which represent their effect on the outer electrons.

Implicitly, it is assumed that the chemical environment does not influence the core electrons, because of the strong nuclear attraction. An ECP (*Stuttgart-Dresden pseudopotential*) [111], implemented right in the calculation software (*Gaussian09*) [112] was chosen in the case of copper.

The structures were optimized in the vacuum until a minimum energy configuration was attained (corresponding to an energy gradient below a fixed cut-off value). The Hessian of

the energy and of the vibrational frequencies was calculated in order to verify the nature of minimum of the steady state obtained, and the absence of one or more imaginary frequencies was checked.

2.2.6. Results.

The structures of $[Cu(PTA)_nCl_m(H_2O)_y]^{1-m}$ (n, m, y $\leq$ 4, n + m + y = 4, see Figure 2.19) complexes, listed in Table 2.3, were optimized. Results of the calculations indicate that both $[CuCl_2]^-$ and $[CuCl_3]^{2-}$ complexes are stable species. A linear coordination in $[CuCl_2]^-$ and a trigonal coordination in $[CuCl_3]^{2-}$ have been predicted, in agreement with the results of a XAS study in solution by Brugger [15]. The optimization of the structure of the complex $[CuCl_4]^{3-}$ leads to the dissociation of two chloride anions from Cu(I), with the subsequent formation of the stable $[CuCl_2]^-$ species. This suggestion is in agreement with the results of a molecular dynamics literature study by Sherman [98], which indicates the formation of up to three stable chlorocomplexes $[CuCl_m]^{1-m}$ (m = 1–3) in aqueous solution, whereas a fourth complex is rather unstable. This last suggestion is also corroborated by a thermodynamic study in aqueous solution carried out by Sharma and Millero [92].

DFT calculations also suggest that water molecules are generally weakly bonded to Cu(I). The linear complex $[CuCl(H_2O)]$ is the only stable species predicted, while in the case of $[CuCl_m(H_2O)]^{1-m}$ (m = 2, 3), Cu(I) dissociates the water molecule (see Table 2.3).

The optimized structures of the stable species are reported in Figure 2.19. Calculations indicate that dicoordinated copper(I) complexes are characterized by a linear geometry, whereas trigonal and tetrahedral arrangements are found in all the tri- and tetra-coordinated species respectively.

Table 2.4 shows the comparison between the calculated metal-ligand bond length in $[CuCl_m]^{1-m}$ and $[Cu(PTA)_nCl_m]$ (n = 1–4; m = 1–3; n + m = 1–4) and the corresponding literature values. The Cu–Cl distance found in the linear $[CuCl_2]^-$ complex is 2.156 Å, in agreement with the value of 2.13 Å reported in a previous work [113]. The calculated Cu–Cl distance in the trigonal $[CuCl_3]^{2-}$ complex is 2.384 Å, significantly larger than that reported by Brugger (2.235 Å) [15]. The average Cu–P bond length in the PTA complexes with a linear geometry is about 2.18 – 2.19 Å, whereas longer distances of about 2.27 – 2.31

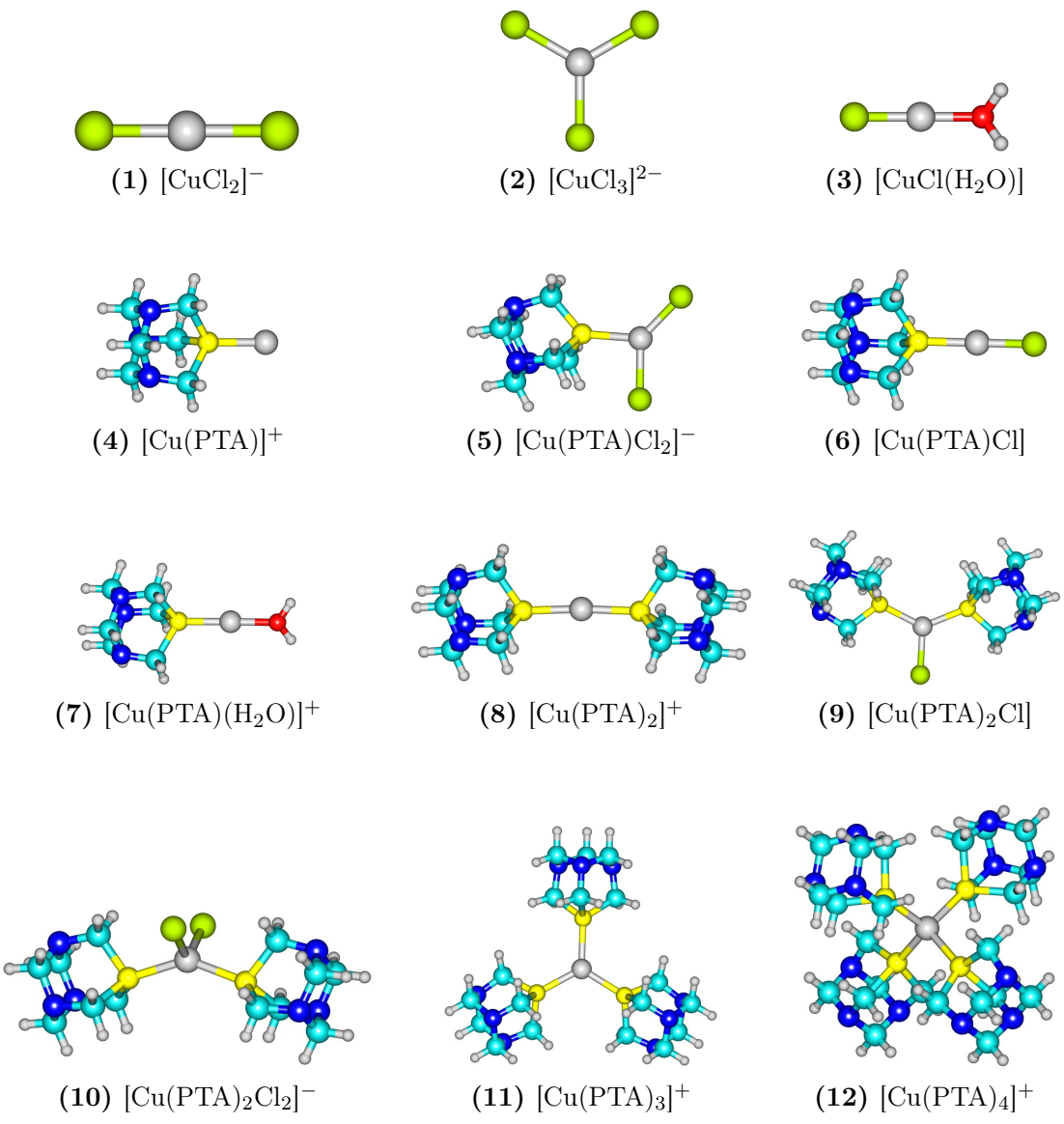

Figure 2.19.: structures of the Cu^+–H_2O–Cl^-–PTA complexes optimized by DTF calculations.

Table 2.3.: starting structures and final structures (optimized by DFT calculations) of the Cu(I) complexes.

Cu coordinative geometry in the starting complex	Symmetry	Starting complex	Final structure/s	Cu coordinative geometry in the final complex
tetrahedral	C_{2v}	$[CuCl_4]^{3-}$	$[CuCl_2]^- + 2Cl^-$	linear
trigonal	D_{3h}	$[CuCl_3]^{2-}$	$[CuCl_3]^{2-}$	trigonal
tetrahedral	C_s	$[CuCl_3(H_2O)]^{2-}$	$[CuCl_3]^{2-} + H_2O$	trigonal
tetrahedral	C_s	$[CuCl_2(H_2O)]^-$	$[CuCl_2]^- + H_2O$	linear
trigonal	C_s	$[CuCl(H_2O)_2]$	$[CuCl(H_2O)] + H_2O$	linear
linear	C_{3v}	$[Cu(PTA)]^+$	$[Cu(PTA)]^+$	linear
linear	C_s	[Cu(PTA)Cl]	[Cu(PTA)Cl]	linear
trigonal	C_s	$[Cu(PTA)Cl_2]^-$	$[Cu(PTA)Cl_2]^-$	trigonal
linear	C_1	$[Cu(PTA)(H_2O)]^+$	$[Cu(PTA)(H_2O)]^+$	linear
trigonal	C_1	$[Cu(PTA)(H_2O)Cl]$	$[Cu(PTA)(OH)Cl]^- + H^+$	trigonal
trigonal	C_1	$[Cu(PTA)(H_2O)_2]^+$	$[Cu(PTA)(H_2O)]^+ + H_2O$	linear
trigonal	C_2	$[Cu(PTA)_2]^+$	$[Cu(PTA)_2]^+$	linear
trigonal	C_s	$[Cu(PTA)_2Cl]$	$[Cu(PTA)_2Cl]$	trigonal
tetrahedral	C_1	$[Cu(PTA)_2Cl_2]^-$	$[Cu(PTA)_2Cl_2]^-$	tetrahedral
tetrahedral	C_1	$[Cu(PTA)_2(H_2O)Cl]$	*in progress*	
tetrahedral	C_1	$[Cu(PTA)_2(H_2O)_2]^+$	*in progress*	
trigonal	C_s	$[Cu(PTA)_3]^+$	$[Cu(PTA)_3]^+$	trigonal
tetrahedral	C_s	$[Cu(PTA)_4]^+$	$[Cu(PTA)_4]^+$	tetrahedral

Å have been found in the complexes with a trigonal arrangement. A Cu–P bond length of 2.364 Å was found in the tetrahedral $[Cu(PTA)_4]^+$ complex. In a previous work, Kirillov et al [114] obtained a crystal structure of the solid $[Cu(PTA)_4]NO_3$ complex (see Figure 2.20) and reported an average Cu–P bond length of about 2.28 – 2.29 Å. The calculated metal-ligand bond lengths of $[CuCl_3]^{2-}$ and $[Cu(PTA)_4]^+$ are significantly larger than those expected on the basis of the experimental literature data. This suggests that the interactions of Cu(I) with the concerned ligands in these complexes should be somewhat underestimated.

In order to compare the relative stability of the different Cu^+–Cl^-–PTA complexes, and ascertain the best stoichiometry of the equilibrium species, the free energies concerning the stability of the species **(1)** – **(12)** in Figure 2.19 were calculated. A first calculation was carried out in-vacuum, then a successive was performed to take into account the solvent effect. In this case, the solvent was implemented as a polarizable continuum medium, which surrounds the solutes (*Polarizable Continuum Model*, PCM) [115]. The reactions concerning the complex formations and the corresponding ΔG° are reported in Table 2.5.

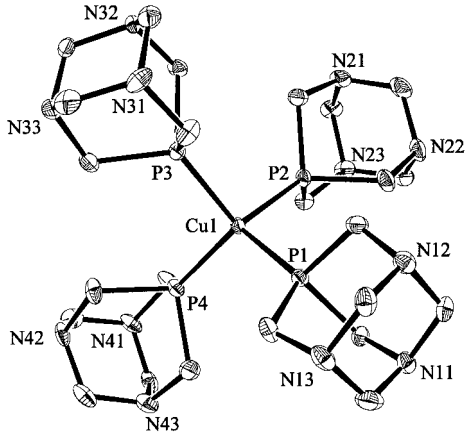

Figure 2.20.: crystal structure of $[Cu(PTA)_4]^+$ obtained by Kirillov et. al [114].

Table 2.4.: Cu–Cl, Cu–O and Cu–P bond lengths (Å).

Species	geometry	r (Cu–Cl) Å	r (Cu–P) Å	Literature value Å
$[CuCl_2]^-$	linear	2.156	-	2.13 [113]
$[CuCl_3]^{2-}$	trigonal	2.384	-	2.235 [15]
$[Cu(H_2O)Cl]$	linear	2.085	-	
$[Cu(PTA)]^+$	linear	-	2.189	–
[Cu(PTA)Cl]	linear	2.115	2.177	–
$[Cu(PTA)(H_2O)]^+$	linear	-	2.184	–
$[Cu(PTA)Cl_2]^-$	trigonal	2.335/2.236	2.279	–
$[Cu(PTA)_2]^+$	linear	2.244	-	–
[Cu(PTA)2Cl]	trigonal	2.237	2.267	–
$[Cu(PTA)_2Cl_2]^-$	tetrahedral	2.436	2.268	–
$[Cu(PTA)_3]^+$	trigonal	-	2.311	–
$[Cu(PTA)_4]^+$	tetrahedral	-	2.364	2.28/2.29 (Fig. 2.20) [114]

Reaction (1), in the table shows that the complex $[CuCl_3]^{2-}$ is weaker than $[CuCl_2]^-$, both in vacuum and in solution, since its formation occurs with a marked positive free energy. The positive ΔG° (PCM) for reaction (1) shows that the linear $[CuCl_2]^-$ complex is the prevalent species in chloride solutions; in addition, its relatively small value suggests a possible equilibrium between $[CuCl_2]^-$ and $[CuCl_3]^{2-}$. This findings are in agreement with the experimental data of literature previously discussed. Reactions (4) – (10) indicate that all Cu(I)–PTA complexes result to be unstable in vacuum, with respect to $[CuCl_2]^-$. However, calculations with PCM lead to an entirely different result: the negative ΔG° indicate in this case, that the formation of the successive Cu(I)–PTA species is a favored process. This suggestion nicely fit the strong evidences from our thermodynamic study on the particular stability of Cu(I)–PTA complexes.

The ΔG° (PCM) of reaction (11), close to zero, shows that complexes $[Cu(PTA)Cl_m]^{1-m}$ (m = 1, 2) have similar stability, and therefore it suggests that possibly formation of 1:1 Cu:PTA complex occurs in solution with the simultaneous formation of the linear $[Cu(PTA)Cl]_{(aq)}$ and the trigonal $[Cu(PTA)Cl_2]^-$ complexes.

The positive ΔG° (PCM) for reaction (13) shows that the tetrahedral $[Cu(PTA)_2Cl_2]^-$ complex should spontaneously dissociate one chloride to give $[Cu(PTA)_2Cl]_{(aq)}$. In addition, reaction (12) shows that $[Cu(PTA)_2Cl]_{(aq)}$ is more stable than the linear $[Cu(PTA)_2]^+$. It turns out that, among the three $[Cu(PTA)_2Cl_m]^{1-m}$ complexes (m = 0–2), the trigonal $[Cu(PTA)_2Cl]_{(aq)}$ results to be the more stable.

All the above findings indicate that the reactions leading to the formation of the first two Cu(I)–PTA complexes occur without a quantitative displacement of chloride anions from copper.

Free energies for reaction (14) and (15) indicate that formation of $[Cu(PTA)_3]^+$, occurs with a quantitative removal of chloride from the metal center. In particular, the slightly positive value of ΔG° (PCM) for reaction (14) suggests that the formation of $[Cu(PTA)_3]^+$ from $[Cu(PTA)_2Cl]_{(aq)}$ is somewhat unfavored, possibly, since it occurs through removal of a tightly bound Cl^-.

The results obtained by this DFT study agree with our thermodynamic findings (see section 2.2.3), according to which the formation of the first two PTA complexes occurs with

Table 2.5.: Free energy reaction values, calculated in vacuum and in a *continuum polarizable medium* (PCM).

	Reaction	ΔG° gas phase (kJ/mol)	ΔG° (PCM) (kJ/mol)
(1)	$[CuCl_2]^- + Cl^- \rightleftarrows [CuCl_3]^{2-}$	296	10.5
(2)	$[CuCl_2]^- + H_2O \rightleftarrows [Cu(H_2O)Cl] + Cl^-$	187	53.6
(3)	$[CuCl_2]^- + PTA + H_2O \rightleftarrows [Cu(H_2O)PTA]^+ + 2Cl^-$	672	114
(4)	$[CuCl_2]^- + PTA \rightleftarrows [Cu(PTA)Cl] + Cl^-$	115	– 15.5
(5)	$[CuCl_2]^- + PTA \rightleftarrows [Cu(PTA)Cl_2]^-$	32.6	– 14.6
(6)	$[CuCl_2]^- + 2PTA \rightleftarrows [Cu(PTA)_2]^+ + 2Cl^-$	110	– 6.7
(7)	$[CuCl_2]^- + 2PTA \rightleftarrows [Cu(PTA)_2Cl] + Cl^-$	120	– 36.4
(8)	$[CuCl_2]^- + 2PTA \rightleftarrows [Cu(PTA)_2Cl_2]^-$	40.2	– 27.6
(9)	$[CuCl_2]^- + 3PTA \rightleftarrows [Cu(PTA)_3]^+ + 2Cl^-$	95.4	– 35.1
(10)	$[CuCl_2]^- + 4PTA \rightleftarrows [Cu(PTA)_4]^+ + 2Cl^-$	101	– 55.2
(11)	$[Cu(PTA)Cl] + Cl^- \rightleftarrows [Cu(PTA)Cl_2]^-$	– 82.0	0.9
(12)	$[Cu(PTA)_2]^+ + Cl^- \rightleftarrows [Cu(PTA)_2Cl]$	10.5	– 30
(13)	$[Cu(PTA)_2Cl] + Cl^- \rightleftarrows [Cu(PTA)_2Cl_2]^-$	– 79.9	8.8
(14)	$[Cu(PTA)_2Cl] + PTA \rightleftarrows [Cu(PTA)_3]^+ + Cl^-$	– 24.7	1.3
(15)	$[Cu(PTA)_2Cl_2]^- + PTA \rightleftarrows [Cu(PTA)_3]^+ + 2Cl^-$	55.2	– 7.5
(16)	$[Cu(PTA)_3]^+ + PTA \rightleftarrows [Cu(PTA)_4]^+$	5.9	– 20.1

similar and high exothermicities ($\Delta H_1 \approx \Delta H_2 \approx -55$ kJ/mol), whereas formation of the third and fourth copper-PTA complexes are markedly less exothermic ($\Delta H_3 \approx \Delta H_4 \approx -38$ kJ/mol) (see Table 2.2 on page 46).

The markedly less favorable enthalpy for the third coordination step agrees with the calculated slightly positive ΔG° for reaction (14) in Table 2.5, which involves the displacement of a chloride from the coordination sphere of the metal center.

2.3. Formation of Ag(I)–PTA complexes

The values of the formation constants of complexes Ag(I)–PTA were obtained by means of a series of potentiometric titrations. Experiments were carried out in an aqueous solution, in $NaNO_3$ 0.1 M at 25 °C. Since Ag(I), unlike Cu(I), is stable in aqueous solution, the background electrolyte is not required to play a stabilizing effect, although it is required for reliable thermodynamic equilibrium data (see appendix C on page 113). The study

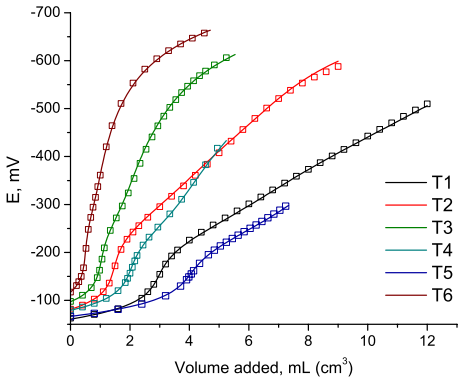

Figure 2.21.: potentials, E (mV) *vs* V_{add} (mL) for titrations T1–T6. Squares, experimental values; lines, calculated with stability constants and analytical data on Table A.3, p. 103. For clarity, some experimental points are omitted.

was divided into three parts, in order to obtain separately: a) the protonation constant of the phosphine; b) the formation constants of the silver complexes with the protonated phosphine $[H_mAg(PTA)_n]^{m+1}$, c) the formation constants of the silver complexes with the neutral ligand, $[Ag(PTA)_n]^+$. The experimental data from potentiometric titrations (V_{added}, mL and E, mV) were processed with the *Hyperquad 2006* minimization suite.

Study of the protonation of the ligand in $NaNO_3$ 0.1 M was carried out by adding known volumes of a standard solution of HNO_3 to solutions containing known concentrations of PTA. The changes in pH during titrations were measured with a glass electrode. The formation of silver(I) complexes was followed with a silver electrode, to determine the concentration of free cation in the solutions. To follow the formation of the acidic complexes $[H_mAg(PTA)_n]^{m+1}$, the solutions of Ag(I) containing an excess of mineral acid (HNO_3) were titrated with acidic solutions of the phosphine. Speciation of complexes $[Ag(PTA)_n]^+$ with the unprotonated ligand was studied with the same approach, in solutions without any excess of mineral acid.

Processing of experimental data with *Hyperquad 2006* yielded the number, composition and formation constants of the complexes in solution (see Table 2.6). Figure 2.21 shows the experimental data (E, mV vs V_{added}, mL) and the corresponding values calculated by *Hyperquad*. The fit between experimental and calculated values is very good.

The enthalpies of formation of Ag(I)–PTA complexes were determined by means a series

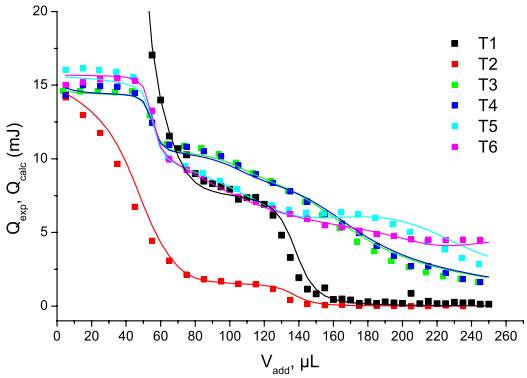

Figure 2.22.: stepwise reaction heats (mJ vs V_{added}, µL.) for titrations T1–T6. Squares, experimental values (Q_{exp}); lines, calculated (Q_{calc}) with stability constants and analytical data in table A.4, p. 103.

of microcalorimetric titrations. Measurements were carried out in the same experimental conditions as the potentiometric studies. The stepwise experimental reaction heats (Q_{exp}, mJ) were processed with *Letagrop*, to obtain the values of the reaction enthalpies (see Table 2.6 on p. 61). In this minimization process, the stability constants obtained by minimization of potentiometric data were assumed as known parameters.

Figure 2.22 shows the data-fit for the calorimetric titrations. Also in this case, the match between the experimental and calculated values is good.

2.3.1. Results

The speciation model for the formation of Ag(I)–PTA complexes which allows the best-fit of the experimental data is consistent with that previously obtained for the analogous Cu(I)–PTA complexes. Also in this case, the model is consistent with the presence of four mononuclear successive complexes, with formula $[Ag(PTA)_n]^+$ (n = 1–4), forming when the solution pH is close to neutrality or slightly basic, and three complexes containing the acidic phosphine, with general formula $[H_mAg(PTA)_n]^{m+1}$ (n = 1–3, m = 1, 2). Complexes $[Ag(PTA)_n]^+$ do form according to an exothermic process and negative entropy, as in the case of the corresponding complexes of copper. The stepwise formation constants indicate that their stability decreases as the number of phosphine ligands increases. The same predictable trend is observed for the stepwise stabilities of the $[H_mAg(PTA)_n]^{m+1}$ complexes.

Table 2.6.: Formation (stability) constants and corresponding thermodynamic functions for Ag(I)–PTA and Ag(I)–(HPTA) complexes in $NaNO_3$ 0.1 M, T = 25 °C. In the Table: M = Ag^+, L = PTA, H = H^+. Ionic charges omitted for convenience.

species	$\log\beta \pm 3\sigma$	$\Delta G \pm 3\sigma$	$\Delta H \pm 3\sigma$	$T\Delta S \pm 3\sigma$
		kJ/mol	kJ/mol	kJ/mol
HL	5.72 ± 0.01	-32.65 ± 0.06	-15.6 ± 0.3	17.1 ± 0.3
ML	8.19 ± 0.01	-46.75 ± 0.06	-56.3 ± 0.5	-9.6 ± 0.5
ML_2	13.67 ± 0.02	-78.0 ± 0.1	-97.7 ± 0.7	-19.7 ± 0.7
ML_3	17.67 ± 0.02	-100.9 ± 0.1	-135.6 ± 0.9	-34.7 ± 0.7
ML_4	20.35 ± 0.12	-116.2 ± 0.7	-177.3 ± 1.8	-61.1 ± 1.9
HML	12.02 ± 0.01	-68.62 ± 0.06	-61.6 ± 1.3	7.0 ± 1.3
H_2ML_2	21.14 ± 0.02	-120.7 ± 0.1	-112.4 ± 4.3	8.3 ± 4.3
HML_2	17.72 ± 0.04	-101.2 ± 0.2	-104.8 ± 5.8	-3.6 ± 5.8
H_2ML_3	26.40 ± 0.09	-150.7 ± 0.5	-135.4 ± 8.2	15 ± 8
reaction	$\log K \pm 3\sigma$	$\Delta G^{step} \pm 3\sigma$	$\Delta H^{step} \pm 3\sigma$	$T\Delta S^{step} \pm 3\sigma$
		kJ/mol	kJ/mol	kJ/mol
$H + L \rightleftarrows HL$	5.72 ± 0.01	-32.65 ± 0.06	-15.6 ± 0.3	17.1 ± 0.3
$M + L \rightleftarrows ML$	8.19 ± 0.01	-46.75 ± 0.06	-56.3 ± 0.5	-9.6 ± 0.5
$ML + L \rightleftarrows ML_2$	5.48 ± 0.02	-31.3 ± 0.1	-41.4 ± 0.9	-10.1 ± 0.9
$ML_2 + L \rightleftarrows ML_3$	4.00 ± 0.03	-22.9 ± 0.1	-37.6 ± 1.1	-14.7 ± 1.1
$ML_3 + L \rightleftarrows ML_4$	2.68 ± 0.12	-15.3 ± 2.0	-41.7 ± 2.0	-26 ± 3
$M + (HL) \rightleftarrows M(HL)$	6.30 ± 0.01	-35.96 ± 0.08	-46.0 ± 1.3	-10.0 ± 1.3
$M(HL) + (HL) \rightleftarrows M(HL)_2$	3.40 ± 0.02	-19.4 ± 0.1	-35.2 ± 4.5	-16 ± 5

A fourth acidic complex with formula $[Ag(PTA)(HPTA)_2]^{3+}$ was suggested by *Hyperquad 2006* treatment of potentiometric data, although, the value of the stepwise stability constant of this complex is very small and its possible presence in solution is limited to very acidic conditions (pH < 3).

The stability constants of the silver–PTA complexes were used to calculate (*HySS 2009* program) [116] some speciation diagrams which provide the relative percentage distribution of the silver complexes as a function of the ligand to metal molar ratio. In particular, Figure 2.23(a) shows the diagram of a solution with a total Ag^+ concentration close to that of the ESI-MS experiments and biological *in vitro* trials (see Introduction). Speciation plots show that the dicoordinate $[Ag(PTA)_2]^+$ complex is the prevailing species in solution, when the concentration of silver is 10^{-5} M, molar ratio Ag to PTA is 1:4 (equal to that achieved when the solid complex is dissolved in aqueous solution) and the solution pH is close to 7.3. Figure 2.23(b) shows the speciation plot when the total silver concentration in solution is 10^{-2} M, near that used in NMR experiments. In this case, the speciation plots shows that the prevalent species in solution is the tetracoordinate $[Ag(PTA)_4]^+$, partially dissociated as $[Ag(PTA)_3]^+$, and the negligible presence of the dicoordinated complex. The plots in the figure indicate that, in general and regardless of silver concentration, the presence in solution of protonated species is certainly negligible at physiological pH (pH = 7.32). Instead, these species appear in solution at about pH = 5 (Figure 2.24(a)) and become prevalent at pH < 4 (Figure 2.24(b)).

For information on the above equilibria, some $^{31}P\{^1H\}$–NMR spectra of $\backsim 10^{-2}$ M solutions of complex $[Ag(PTA)_4]^+$ were collected. However, the experiments provided few indications, since the spectra only showed a single broad peak of ^{31}P, shifted to higher fields than the corresponding signal of the free phosphine. Such a spectrum certainly reflects coordination of the phosphine to the metal center, although the exchange kinetics between the free and coordinated ligands is too rapid to obtain any valuable information.

Interesting information regarding the nature of the complexes in solution came from the trend of the values of $\log K_{step}$ of complexes $[Ag(PTA)_n]^+$ in solution, concerning the reactions shown in Tables 2.7 and 2.6 on page 61.

The values of $\log K_n$ show that the difference between the formation constants of the first

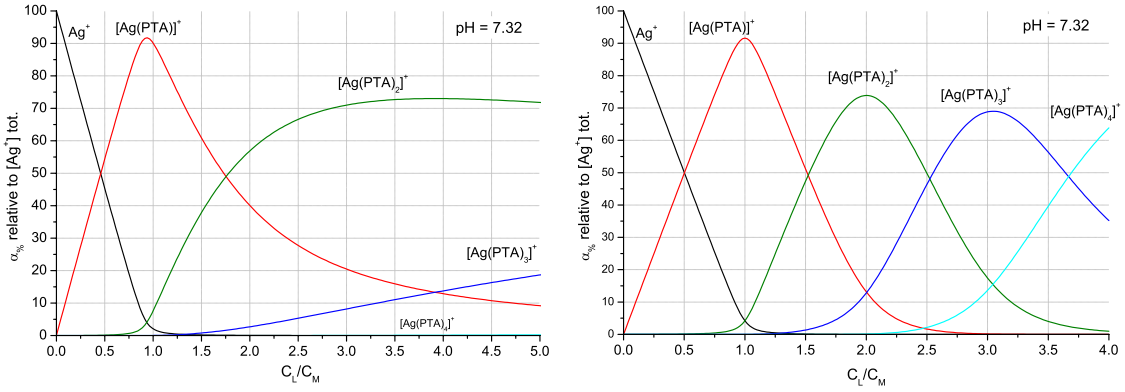

(a) **(b)**

Figure 2.23.: Ag^+ speciation plots: percentage distribution of Ag^+–PTA complexes, relative to $[Ag^+]_{tot}$ as function of PTA/silver molar ratio, C_L/C_M; pH = 7.32. **(a)** $[Ag^+]_{tot} = 10^{-5}$ M; **(b)** $[Ag^+]_{tot} = 10^{-2}$ M.

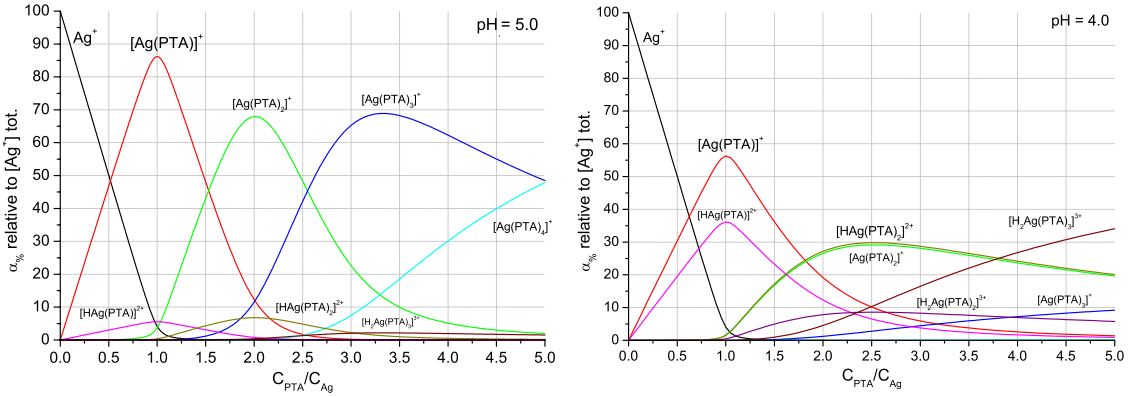

(a) **(b)**

Figure 2.24.: Ag^+ speciation plots: percentage distribution of Ag^+–PTA complexes, relative to $[Ag^+]_{tot}$ as function of PTA/silver molar ratio, C_L/C_M and $[Ag^+]_{tot} = 10^{-2}$ M. **(a)** pH = 5.0; **(b)** pH = 4.0.

Table 2.7.: stepwise formation constants of Ag(I)–PTA complexes . M = Ag^+, L = PTA (ionic charges omitted for convenience).

reaction	$\log K_{n,\,step}$	$\Delta \log K_n$
$M + L \rightleftarrows ML$	8.19	
		2.7
$ML + L \rightleftarrows ML_2$	5.48	
		1.5
$ML_2 + L \rightleftarrows ML_3$	4.00	
		1.3
$ML_3 + L \rightleftarrows ML_4$	2.68	

two complexes is larger by more than one order of magnitude, compared with the difference between the formation constants of the successive species, which varies very little. These trends in K_n, characterized by discontinuities in the decrease of the formation constants of the successive complexes, are often the result of variations in coordinative geometries at the metal center during the formation of the species. In the case of Cu(I)–PTA complexes, as previously discussed, the formation of the Cu–P bonds was accompanied by displacement of chloride anions from the coordination sphere of the metal: thus, the thermodynamic functions related to the formation of the phosphino complexes which we calculated reflect presence of chloride ions in some of them. The formation of Ag(I)–PTA complexes obviously does not involve such mechanisms, and the relative difficulty concerning the formation of the second complex may be related with the particular nature of the silver aquoion in solution. A recent EXAFS study in solution showed that the structure of the aquoion complex of Ag(I) is characterized by coordinative geometry intermediate between linear and tetrahedral [117]. In particular, the results of the study indicate that Ag(I) coordinates up to two water molecules, with a significant covalent contribution, leading to a complex with linear structure. Ag(I) is affected by the electrostatic interaction of two other weakly bonded water molecules, which significantly alter its structure to that similar to a distorted tetrahedron.

Thermodynamic parameters for the stepwise formations of Ag(I)–PTA complexes, shown in Table 2.6 on page 61, clearly show the origin of their enthalpic stability. All the enthalpy values are negative (they favor the formation of the complexes), whereas the entropies of reaction, also negative, act in the opposite direction. This observation matches the

considerations made for the similar Cu(I)–PTA complex. The values of $\Delta H_{j,step}$ also show that $\Delta H_{1,step}$ is very different, and more favorable, than the other three: $\Delta H_{1,step} = -56.3$ kJ/mol, as opposed to $\Delta H_{j,step} \approx 40$ kJ/mol for j = 2–4. The entropic term is always unfavorable to the course of the reaction, especially in the last stage of complexation.

According to the indications concerning the structure of Ag(I) aquoion, the first coordination of the phosphine to the metal center may be interpreted as reflecting displacement of one, or both, of the more labile water molecules from the coordination sphere of Ag(I). The values of $\Delta H_{j,step}$ and $T\Delta S_{j,step}$ for the coordination of the second and third phosphines to the metal would indicate substitution reactions involving similar mechanisms, whereas the value of $T\Delta S_{4,step}$, much lower than the previous, may be the consequence of a change in the coordinative structure at the metal center, from trigonal to tetrahedral. This may also account for $\Delta H_{4,step}$, more favorable, since the transition from trigonal to tetrahedral coordination should not involve displacement of water molecules from the solvation sphere of the metal.

2.3.2. Comparisons between Cu(I) and Ag(I) complexes of PTA

As already noted, the formation of complexes Cu(I)–PTA in 1 M NaCl takes place through a series of substitution reactions of chloride ions from the coordination sphere of Cu(I) by PTA, whereas formation of Ag(I) complexes, in 0.1 M $NaNO_3$, is due to the ability of the ligand to displace water molecules from the solvation sphere of the metal. Taking into account the chloride competition (see Table 2.1 on page 32) the "true" formation constants between the free Cu(I) ion and PTA would be higher by approximately two orders of magnitude than the values reported in Table 2.2, p. 46.

The histogram and diagram of Figures 2.25 and 2.26 (data in Table 2.8) compare the values of the stepwise thermodynamic functions for the formation of the four mononuclear complexes of Cu(I) and Ag(I) with PTA. Both figures show the difference between the thermodynamic functions characterizing the formation of complexes of Cu(I) and Ag(I). In particular, the formation of the first two species occurs with $-\Delta G_{1,Cu} < -\Delta G_{1,Ag}$ and $-\Delta G_{2,Cu} \approx -\Delta G_{2,Ag}$ whereas the values of $-\Delta G_{3,Cu}$ and $-\Delta G_{4,Cu}$ are higher than those for Ag(I) complexes.

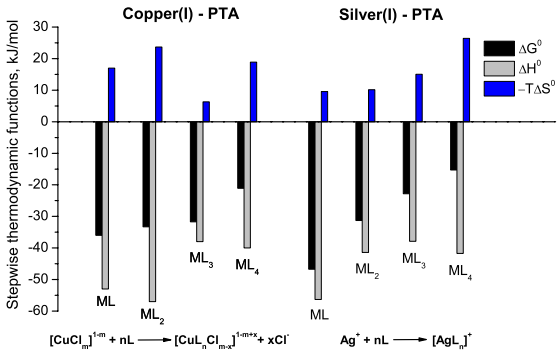

Figure 2.25.: stepwise thermodynamic functions for the formation of four successive complexes $[M(PTA)_n]^+$ (M = Ag(I), Cu(I); L = PTA; n = 1–4).

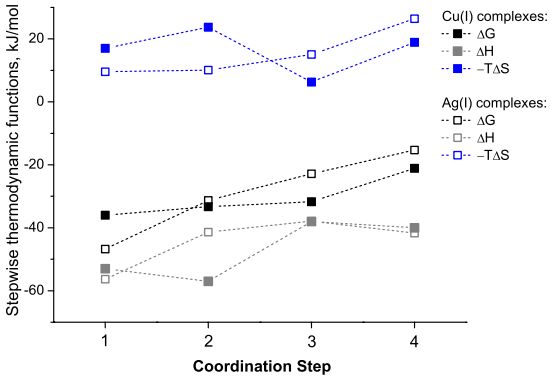

Figure 2.26.: trends of stepwise thermodynamic functions for the formation of four successive complexes $[M(PTA)_n]^+$ (M = Ag(I), Cu(I); L = PTA; n = 1–4).

Table 2.8.: comparison between the stepwise formation constants of the $[M(PTA)_n]^+$ complexes (M = Cu^+, Ag^+, L = PTA). Ionic charges omitted for convenience.

Reaction	logK ± 3σ		$\Delta G^{step} \pm 3\sigma$ kJ/mol		$\Delta H^{step} \pm 3\sigma$ kJ/mol		$T\Delta S^{step} \pm 3\sigma$ kJ/mol	
M =	Cu^+	Ag^+	Cu^+	Ag^+	Cu^+	Ag^+	Cu^+	Ag^+
$M + L \rightleftarrows ML$	6.3 ± 0.6	8.19 ± 0.01	-36 ± 3	-46.75 ± 0.06	-53 ± 2	-56.3 ± 0.5	-17 ± 4	-9.6 ± 0.5
$ML + L \rightleftarrows ML_2$	5.8 ± 0.7	5.48 ± 0.02	-33 ± 4	-31.3 ± 0.1	-57 ± 5	-41.4 ± 0.9	-24 ± 7	-10.1 ± 0.9
$ML_2 + L \rightleftarrows ML_3$	5.6 ± 0.7	4.00 ± 0.03	-32 ± 4	-22.9 ± 0.1	-38 ± 5	-38±1	-6 ± 7	-15 ± 1
$ML_3 + L \rightleftarrows ML_4$	3.7 ± 0.8	2.7 ± 0.1	-21 ± 5	-15 ± 2	-40 ± 1	-42 ± 2	-19 ± 5	-26 ± 3

The histogram shows also that the first two Cu(I) complexes form with very high reaction enthalpies ($-\Delta H_{1,step} < -\Delta H_{2,step}$), favorable to complexation, and negative entropies, unfavorable ($-T\Delta S_1 < -T\Delta S_2$). Instead, the formation of the corresponding Ag(I) complexes occurs with $-\Delta H_{1,step} > -\Delta H_{2,step}$ and $-T_{\Delta S1,step} \approx -T\Delta S_{2,step}$. As a result of the compensation between the enthalpic and entropic contributions, the decrease in free energy for the formation of the first Cu(I) complex is lower than that of the first Ag(I) complex, whereas the values of $-\Delta G_2$ for the formation of the complexes ML_2 are similar.

The formations of the third and fourth complex of Cu(I) and Ag(I) show an opposite trend: the enthalpy values are similar for both complexes ($-\Delta H_{3,step} \leq -\Delta H_{4,step}$), whereas the entropies of formation of silver complexes are more unfavorable than those of copper. It follows that the stability of $[Cu(PTA)_3]^+$ and $[Cu(PTA)_4]^+$ is higher than that of $[Ag(PTA)_3]^+$ and $[Ag(PTA)_4]^+$.

Figure 2.25 shows that the stability of the complexes of the two metals with PTA decreases as the number of ligands coordinated to them increases. However, whereas this decrease is quite regular for Ag(I) complexes, the stability trend for the copper complexes is almost constant for the first three species, whereas the formation of the fourth complex occurs with a significant decrease in $-\Delta G_4$.

In addition, the stability order of the copper and silver complexes is: $K_{1,Cu} < K_{1,Ag}$; $K_{2,Cu} \approx K_{2,Ag}$; $K_{1,Cu}$ and $K_{3,Cu} > K_{1,Ag}$ and $K_{3,Ag}$. This apparently anomalous trend in the stabilities of the first two Cu(I) complexes may reflects the energy demand required to remove the chloride ions from the coordination sphere of the metal. This would lead to an increase of charged and more solvated species in solution which exert a greater ordering effect.

2.4. Formation of Cu(II), Ag(I), Cu(I) complexes with the amino acid methionine in aqueous solution

The natural amino acid methionine, HMet, is a chemical species which gives two acid-base equilibria in aqueous solution, according to the scheme in Figure 2.27.

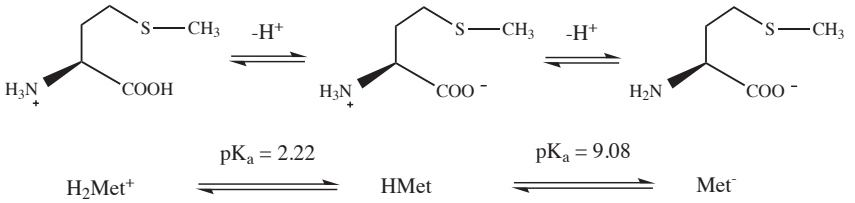

Figure 2.27.: successive protonation equilibria of amino acid methionine.

In order to study: a) the protonation reactions of the aminic and carboxylic acid functions of HMet; b) the formation of methionine complexes with Cu(II), c) the formation of methionine complexes with Cu(I) and Ag(I), three sets of microcalorimetric titrations were carried out.

2.4.1. Protonation of methionine in aqueous solution

Methionine (*Aldrich*, pur. $> 99\%$) was purified by recrystallization from water. The resulting product is the neutral species (HMet), present in solution as a zwitterion.

Study of the protonation of the amine and carboxyl functions of HMet consisted of a series of microcalorimetric titrations in aqueous solution and an ionic medium of NaCl 1.0 M at 25°C. During these titrations, solutions of methionine with known concentrations (2.5–10.5 mM) were titrated with solutions of strong mineral acid (ca. 0.5 M) or base (ca. 0.1 M) (analytical data in Table A.5, p. 103). The values of the two protonation constants of the ligand and the related enthalpies were simultaneously obtained by minimizing the enthalpy data (Q_{obs}, mJ vs. V_{added}, µL) with the program *Letagrop* (results in Table 2.12 p. 78). Figure 2.28 shows the good match between the experimental data (dotted line) and those calculated (solid line). Figure 2.28(a) shows the total heat measured as a function of the volume of titrant; Figure 2.28(b) shows the Δh_v value (overall formation enthalpy of protonated species per mole of H^+ added) as a function of the average number of protons coordinated to methionine (N_{bar}).

It is interesting to note that the log K values obtained as a result of minimization of the microcalorimetric data clearly match those obtained in previous potentiometric studies [118]. Comparison of the values determined in this study and those in the literature are listed in Table 2.9.

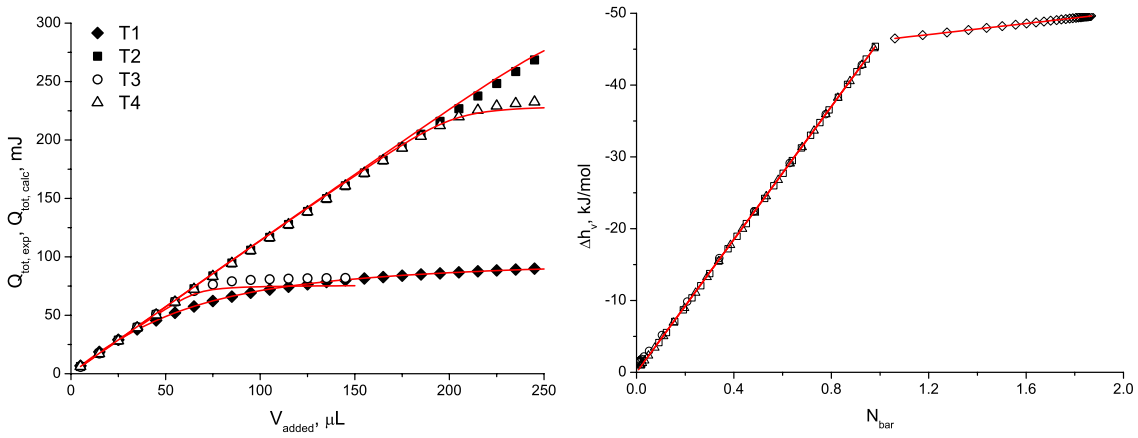

(a) **(b)**

Figure 2.28.: (a) Q_{tot}, mJ vs V_{add}, µL; (b) Δh_v vs N_{bar}; ♦ T1, ■ T2, ○ T3, △ T4 (see Table A.5, p. 103).

Likewise, the values of the protonation enthalpies fit those estimated in one of the previous works [96] through the Van't Hoff relation, and with those obtained by Grigorova [119] by means of a calorimetric study of the solvatation heats of methionine in water.

Table 2.9.: comparison between the values of the protonation constants and protonation enthalpies of methionine and determined in this study (see Table 2.12) with those in the literature.

reaction	$H^+ + Met^- \rightleftarrows HMet$		$H^+ + HMet \rightleftarrows [H_2Met]^+$	
	$\log K_1$	ΔH_1, kJ/mol	$\log K_2$	ΔH_2, kJ/mol
Pettit, 1981 [118] 25°C, 0.10 M (KNO_3)	9.06	–	2.14	–
Sharma, 2003 [96] 25°C, 0.10 M (NaCl)	9.15	–44.7 (*)	2.25	–2.8 (*)
Grigorova, 2010 [119] 25°C, (water)	9.22	–44.3	1.97	–7.2
This work 25°C, 1.0 M (NaCl)	**9.08**	**–46.3**	**2.20**	**–3.8**
(*) 0.25 M (NaCl)				

These results represent another clear indication of the reliability and accuracy of the results which can be achieved when the microcalorimetric approach is applied to complex formation equilibria in solution. In addition, the excellent match between the thermodynamic quantities of the protonation reactions of methionine obtained here and those in the

literature is an example of the flexibility of the technique, since the protonation equilibria of the amino acid have values which differ by several orders of magnitude.

2.4.2. Formation of Cu(II) complexes with methionine

This study was carried out because, in view of the ease with which Cu(I) can be oxidized to Cu(II) by atmospheric oxygen, we were interested in evaluating what kind of side-reactions would occur between methionine and Cu(II), in the following study HMet/Cu(I).

The anhydrous $CuCl_2$ salt used to prepare Cu(II) solutions, subsequently employed for thermodynamic studies, was prepared by recrystallization from water of the dihydrate salt (Aldrich> 99%), followed by dehydration under vacuum at 120 °C for 24 hours, according to published procedure [120].

Preliminary titrations were first carried out, to verify that Cu(II) does not interact at all with HMet in acidic environment. During these experiments, an acidic (pH = 2–3) HMet solution was added to dilute solutions of $CuCl_2$ (0.10–1.0 mM) with an excess of mineral acid (approximately 1.0 mM). During these experiments no heat changes were observed, indicating that, in these regions of pH, Hmet, which is the dominant species in solution, has no affinity for Cu(II). Since the amino group of methionine is protonated in acidic solution, the result was expected according to many data in the literature [121–123], which report that methionine can only bind Cu(II) via its amino group. For instance, Lenz and Martell [121], by a series of potentiometric measurements, showed that methionine forms two successive mononuclear complexes, $[Cu(Met)]^+$ and $[Cu(Met)_2]_{(aq)}$, quite strong ($\log K_1$ = 7.87, $\log K_2$ = 6.85), but not strong enough to be formed at acidic pH. More recently, Tewari [123], by means of electrophoretic techniques, obtained logK values lower than those of Lenz and Martell ($\log K_1$ = 6.40, $\log K_2$ = 4.50) (see Table 2.10).

A successive series of microcalorimetric titrations was then carried out in order to study the formation of copper(II)–methionine complexes in slightly basic conditions. In this study we measured the heat changes in the calorimeter cell when known volumes of a buffer solution HMet/Met^- (pH = 8–9) were added to diluted solutions of $CuCl_2$ (0.10–1.0 mM). All experiments were carried out in NaCl 1.0 M at 25 °C (analytical data in Table A.6 on page 104).

Table 2.10.: comparisons between formation constants and enthalpies of complexes $[Cu(Met)]+$, $[Cu(Met)_2]_{(aq)}$ obtained in this study, with those in literature.

reaction	$Cu^{2+} + Met^- \rightleftarrows [Cu(Met)]^+$		$[Cu(Met)]^+ + Met^- \rightleftarrows [Cu(Met)_2]_{(aq)}$	
	$\log K_1$	ΔH_1, kJ/mol	$\log K_2$	ΔH_2, kJ/mol
Lenz, 1964 25°C, 0.10 M (KNO_3)	7.87	–	6.85	–
Tewari, 2007 25°C, 0.10 M (KNO_3)	6.40	–	4.50	–
This work 25°C, 1.0 M (NaCl)	**8.42**	**–26.3**	**5.78**	**–31.9**

In this case too, the thermodynamic functions for the complex formation (β_j and ΔH_j) were obtained by processing only the experimental data from microcalorimetric titrations by *Letagrop*. In this way, we obtained the formation constants and related ΔH of two successive copper(II)–methionine complexes. The values of the formation constants of these complexes ($\log K_1 = 8.42$, $\log K_2 = 5.78$) do not confirm any of the previous results even if they are closer to those reported by Lenz and Martell (see comparisons in Table 2.10). It is of interest to point out that the protonation constants of methionine we have obtained with the microcalorimetric study match those in the literature. So, we are confident that also the stability data reported herein are a better estimate of the formation constants of the Cu(II) complexes. The values of formation enthalpies, which have never been measured before, match those expected according to the interaction of an amino group with a divalent metal ion [124]. The complex formation is favored by an exothermic process, which generally accompanies also the formation of complexes between Cu(II) and other amines.

In conclusion, by these studies we determined the optimal pH conditions to carry out successive speciation experiments between Cu(I) and methionine ($pH < 7$) and avoid, at the same time, any interference due to the possible formation of complexes of Met^- with Cu(II) in the case of unwanted oxidation of Cu(I). In addition, with this study we obtained accurate data on the thermodynamic formation functions (ΔG_j, ΔH_j, $T\Delta S_j$) of complexes of Cu(II) with methionine. Some of these data (the reaction enthalpies) were not previously available in the scientific literature, although they are useful for a more comprehensive overview about the affinity of this amino acid toward *soft* divalent cations, such as Cu(II), in aqueous solution.

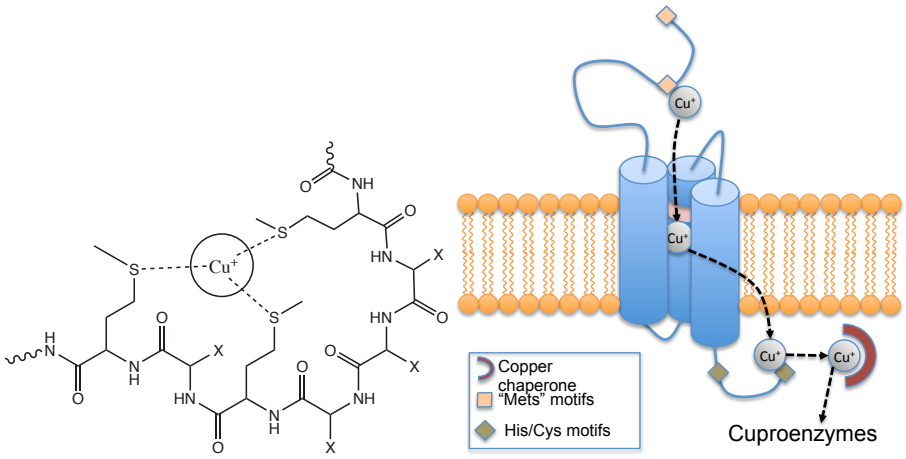

Figure 2.29.: proposed binding model [21] for the formation of adducts of Cu(I) with Mets sequences of Ctr transport protein.

2.4.3. Formation of Cu(I) complexes with methionine

As it was shown, the complex formation between Cu(II) and methionine is pH-dependent, on the contrary, Cu(I) binds methionine through a pH-independent process where the thioether sulfur, which does not undergo acid-base reactions in solution, is involved [23, 24].

In general, studies of the formation of complexes between Cu(I) with biological substrates, even with simple amino acids, are very rare in the literature, probably because of the considerable experimental difficulties related to the intrinsic instability of Cu(I) in water. Rubino et al. recently quantified [21, 22], by means of ESI mass spectrometry and circular dichroism UV-vis absorption techniques, the interaction between Cu(I) or Ag(I) and some "Mets" peptide sequences like "MXXM" and "MXMXXM" (M = methionine residue, X = several amino acid residues). As previously discussed (see Introduction), these sequences are the main coordination site for Cu(I) in membrane proteins hCtr1, used for specific intracellular intake of copper. Results showed that these peptide sequences have good affinity toward Cu(I) and coordinate the metal through the thioether groups of methionine residues, with stability constant values in the range of $10^5 - 10^6$ $mol^{-1}dm^3$. The study also shows that the affinity of Cu(I) toward these substrates increases with the number of methionines in the chain, up to a maximum of three residues. This observation suggests that Cu(I) can coordinate no more than two or three thioether groups of the same peptide sequence, as shown in Figure 2.29.

The study of the complexation of Cu(I) by methionine was carried out to gain information about the stability of complexes Cu(I)–HMet in conditions similar to those in biological systems, and also to provide reliable data about possible side-reactions. At the same time, we studied the interaction of Ag(I) with methionine, to compare the relative affinities of the two monovalent cations toward the amino acid.

The formation of Cu(I)–Hmet complexes was studied by microcalorimetry, according to the method already used for the studies of Cu(I)–PTA complexes. Also in this case, experiments were carried out in aqueous solution, in the presence of a constant ionic medium of NaCl 1.0 M, at 25°C. Experimental data (Q_{react}, mJ *vs* V_{add}, mL), were processed by *Letagrop*.

In a first set of experiments, solutions of methionine of known concentration or buffer solutions HMet/Met^- were titrated with solutions of Cu(I) (for analytical data, see Table A.7 on page 104). During a subsequent series of titrations, concentrated methionine solutions (0.100 M) were added to solutions of Cu(I) (1.0 – 5.0 mM). The initial acidity of the metal solution was maintained at pH $\approx$ 3 by adding known volumes of standard HCl to the calorimeter cell. In these experimental conditions, the only species in solution is HMet, which, as previously shown, is unable to bind Cu(II) but able to coordinate Cu(I), through its thioether group.

Also in this case data processing was carried out by *Letagrop*. Various speciation models were examined and tested during the minimization process, since the maximum number of ligands which the metal can coordinate was uncertain from the literature data. The best data fit was consistent with the formation of two successive complexes, $[Cu(HMet)]^+$ and $[Cu(HMet)_2]^+$. Diagrams in Figure 2.30 show the excellent match between the experimental values and those calculated on the basis of the formation constants and enthalpies of reaction, obtained by minimization (see Table 2.12 on page 78).

The stepwise formation constants in Table 2.11 show that Cu(I)–methionine complexes are markedly weaker than Cu(I)–PTA ones. The *soft* thioether group is known to be relatively weak-coordinating toward a number of transition metal ions, especially those with a *hard* character (see Appendix B). In addition, HMet does not compete as effectively as PTA toward the chloride of the ionic medium (1.0 M). The formation constants determined

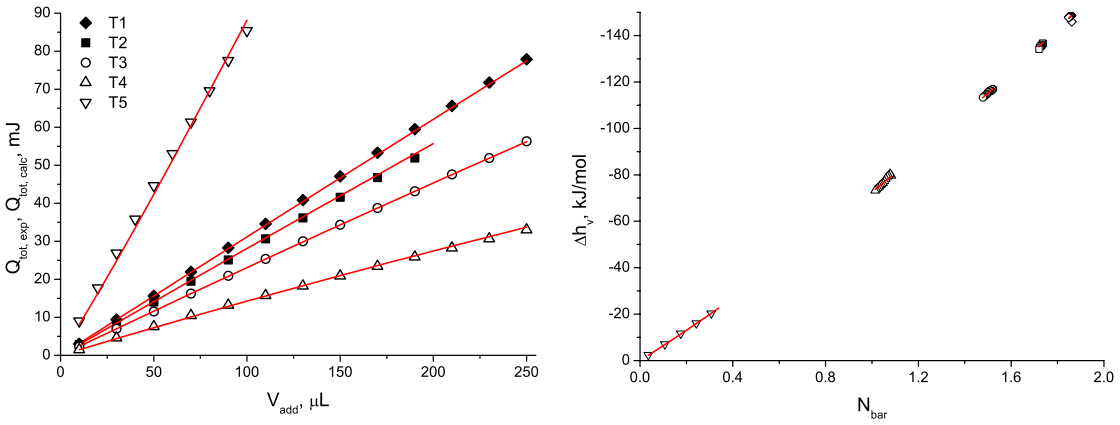

(a) **(b)**

Figure 2.30.: (a) Q_{tot}, mJ vs V_{add}, µL; (b) Δh_v vs N_{bar}; ♦ T1, ■ T2, ○ T3, △ T4, ▽ T5 (see Table A.7, p. 104, T6 not reported for sake of clarity).

with this study are significantly lower than those reported by Rubino [21] for the formation of adducts between Cu(I) and "Mets" peptide sequences. The individual contributions of Cl^- and HMet toward stabilization of complexes Cu(I)–HMet in NaCl 1.0 M cannot be assessed only on the basis of thermodynamic results. Consequently, neither the competition reactions between chlorides and methionine toward coordination of copper(I) nor the number of chlorides the complexes contain can be ascertained. According to the trends of the stepwise formation functions of the two species $[Cu(HMet)_j]^+$ (j = 1, 2, see Table 2.11), only a qualitative hypothesis about the stoichiometry of these complexes in solution can be proposed. Thermodynamic data show that, whereas the formation enthalpy of both complexes is exothermic, as expected in the case of *soft-soft* interactions, the entropy change is only slightly negative for the first formation step and significantly negative for the second one. The marked difference in entropic terms and the higher exothermicity for the formation of the second adduct are compatible with the displacement from Cu(I) in the first coordination step of two and one chloride anions, respectively, as shown in reaction scheme (2.17).

$$\begin{aligned} [CuCl_3]^{2-} + HMet &\rightleftarrows [CuCl(Met)]_{(aq)} + 2Cl^- \\ [CuCl_2]^{-} + HMet &\rightleftarrows [CuCl(HMet)]_{(aq)} + Cl^- \\ [CuCl(Met)]_{(aq)} + HMet &\rightleftarrows [Cu(HMet)_2]_{(aq)} + Cl^- \end{aligned} \tag{2.17}$$

Here too, a theoretical DFT study is planned to compare the calculated energies involved in these processes, together with the observed stabilities of the Cu(I)–Cl–HMet adducts in solution.

Table 2.11.: stepwise formation constants and related thermodynamic functions of $[Cu(HMet)]^+$, $[Cu(HMet)_2]^+$ complexes (see Table 2.12). HL = HMet. Ionic charges omitted for convenience

reaction	$\log K \pm 3\sigma$	$\Delta G_{step} \pm 3\sigma$ kJ/mol	$\Delta H_{step} \pm 3\sigma$ kJ/mol	$T\Delta S_{step} \pm 3\sigma$ kJ/mol
$Cu^{(I)} + (HL) \rightleftarrows Cu^{(I)}(HL)$	2.52 ± 0.65	-14.4 ± 3.7	-16.8 ± 7.9	-2 ± 9
$Cu^{(I)}(HL) + (HL) \rightleftarrows Cu^{(I)}(HL)_2$	2.0 ± 1.0	-11.5 ± 5.9	-53 ± 12	-41 ± 13
$Cu^{(I)} + 2(HL) \rightleftarrows Cu^{(I)}(HL)_2$	4.54 ± 0.79	-25.9 ± 4.5	-69.8 ± 9.0	-44 ± 10

2.4.4. Formation of Ag(I) complexes with methionine

In order to study the system Ag(I)–PTA, a series of microcalorimetric titrations was performed. Experiments were carried out in $NaNO_3$ 0.100 M at a constant temperature of 25 °C. Titrations were carried out over a wide range of acidities (pH = 3.0 – 9.8). To study the formation of silver complexes with HMet or Met^-, the heat changes were collected, measured when known volumes of methionine or HMet/Met^- buffer solutions were added to solutions of Ag(I) (1.0 – 4.0 mM) in the presence of different excess of mineral acid (0.02 – 10.0 mM) (analytical data in Table A.8 on page 104). The results of the minimizations of the sum of the squares of the difference between experimental and calculated heat changes with *Letagrop* are consistent with the formation of two complexes in acidic or nearly neutral pH conditions ($[Ag(HMet)]^+$ and$[Ag(HMet)_2]^+$) and a third species, $[Ag(Met)]_{(aq)}$, forming at basic pHs (8 – 9.8). The formation constants of these species agree with those previously obtained by Pettit in KNO_3 0.1 M [118] by means of potentiometric measurements (seeTable 2.12).

Also in this case, the fit between experimental and calculated data testifies the good representation of the solution equilibria obtained by using the microcalorimetric technique

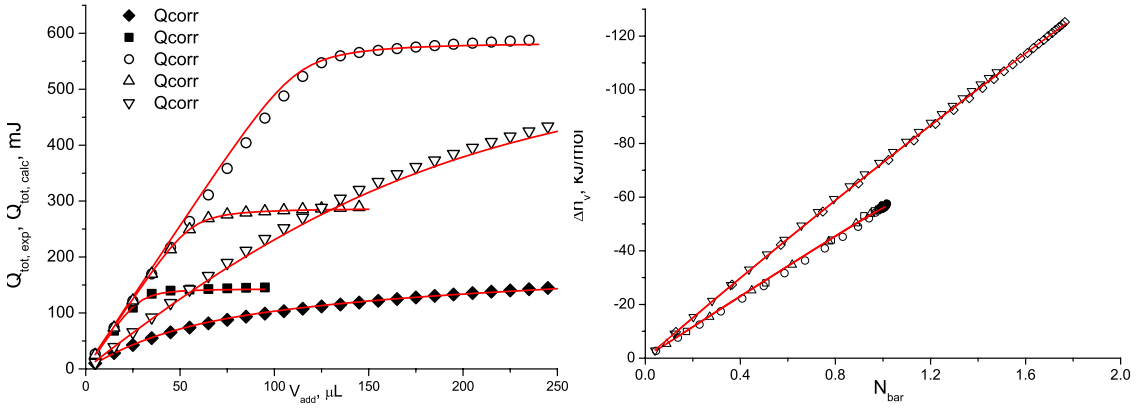

(a) (b)

Figure 2.31.: (a) Q_{tot}, mJ vs V_{add}, µL; (b) Δh_v vs N_{bar}; ♦ T1, ■ T2, ○ T3, △ T4, ▽ T5 (see Table A.8, p. A.8, T6, T7 not reported for sake of clarity).

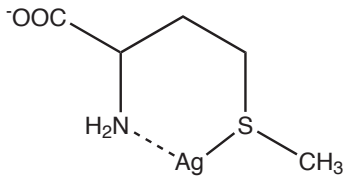

Figure 2.32.: Ag(I)–methionine adduct formed in basic pH conditions (pH > 9).

to calculate simultaneously the enthalpies and the stability constants of the species in solution (see Figure 2.31). The formations of $[Ag(HMet)]^+$ and $[Ag(HMet)_2]^+$ are enthalpy driven processes. The entropic factors, $T\Delta Sj$, do not give any particular contribution to the stability of the species. Similar trends are typical for *soft-soft* interactions.

The formation constant of $[Ag(Met)]_{(aq)}$ is greater than that of $[Ag(HMet)]^+$: logK = 4.58 and 3.98, respectively. Since the main interaction which stabilizes both complexes is the same, the relatively small difference between the unprotonated and protonated complexes could be ascribed to the formation of a six-term chelate complex trough the coordination of the deprotonated amino group (see Figure 2.32). According to this hypothesis the enthalpy of formation of unprotonated complex is much more negative than that of the protonated one, whereas its formation entropy is much more unfavorable.

The formation constant of $[Ag(HMet)_2]^+$ is greater by about three order of magnitude

than that of $[Cu(HMet)_2]^+$. Then, even if the competition between copper(I) and chloride, characterizing our Cu(I)–HMet study, is taken into account, this result shows that the silver complexes with methionine are stronger than those of Cu(I). This is in agreement with the Rubino's studies [21, 22] which indicate that Mets sequences certainly bind silver(I), and do so preferentially over copper(I).

Table 2.12.: Formation (stability) constants and corresponding thermodynamic functions for the systems H^+/Ag^+/methionine ($NaNO_3$ 0.1 M); Cu^{2+}/methionine and H^+/Cu^+/methionine (NaCl 1.0 M); T = 25 °C. In the Table: L = PTA, H = H^+. Ionic charges omitted for convenience.

species	$\log\beta \pm 3\sigma$	$\Delta G \pm 3\sigma$ kJ/mol	$\Delta H \pm 3\sigma$ kJ/mol	$T\Delta S \pm 3\sigma$ kJ/mol
HL	9.08 ± 0.37	-51.8 ± 2.1	-46.3 ± 0.1	5.5 ± 2.1
H_2L	11.3 ± 0.5	-64.5 ± 2.9	-50.1 ± 0.3	14.4 ± 2.9
AgL	4.58 ± 0.45	-26.1 ± 2.6	-54.6 ± 0.8	-28.5 ± 2.7
HAgL	12.9 ± 0.6	-73.4 ± 3.5	-75.6 ± 2.4	-2 ± 4
H_2AgL_2	25.0 ± 0.4	-143 ± 2	-140 ± 3	3 ± 4
$HCu^{(I)}L$	11.4 ± 0.6	-65.1 ± 3.3	-63.0 ± 7.9	2 ± 9
$H_2Cu^{(I)}L_2$	22.3 ± 0.7	-127 ± 4	-162 ± 9	-34.9 ± 9.7
$Cu^{(II)}L$	8.42 ± 0.09	-48.1 ± 0.5	-26.3 ± 0.2	21.8 ± 0.5
$Cu^{(II)}L_2$	14.2 ± 0.6	-81.0 ± 3.4	-58.2 ± 0.6	22.9 ± 3.5
reactions	$\log K \pm 3\sigma$	$\Delta G_{step} \pm 3\sigma$ kJ/mol	$\Delta H_{step} \pm 3\sigma$ kJ/mol	$T\Delta S_{step} \pm 3\sigma$ kJ/mol
$H + L \rightleftarrows HL$	9.08 ± 0.37	-51.8 ± 2.1	-46.3 ± 0.1	5.5 ± 2.1
$(HL) + L \rightleftarrows H_2L$	2.2 ± 0.6	-12.7 ± 3.6	-3.8 ± 0.3	8.9 ± 3.6
$Ag + L \rightleftarrows AgL$	4.59 ± 0.44	-26.2 ± 2.5	-54.6 ± 0.8	-28.4 ± 2.6
$Ag + (HL) \rightleftarrows Ag(HL)$	3.98 ± 0.69	-22.7 ± 3.9	-29.4 ± 2.4	-7 ± 5
$Ag(HL) + (HL) \rightleftarrows Ag(HL)_2$	3.24 ± 0.90	-18.5 ± 5.2	-17.7 ± 4.1	1 ± 7
$Ag + 2(HL) \rightleftarrows Ag(HL)_2$	7.22 ± 0.58	-41.2 ± 3.3	-47.1 ± 3.4	-6 ± 5
$Cu^{(I)} + (HL) \rightleftarrows Cu^{(I)}(HL)$	2.52 ± 0.65	-14.4 ± 3.7	-16.8 ± 7.9	-2 ± 9
$Cu^{(I)}(HL) + (HL) \rightleftarrows Cu^{(I)}(HL)_2$	2.0 ± 1.0	-11.5 ± 5.9	-53 ± 12	-41 ± 13
$Cu^{(I)} + 2(HL) \rightleftarrows Cu^{(I)}(HL)_2$	4.54 ± 0.79	-25.9 ± 4.5	-69.8 ± 9.0	-44 ± 10
$Cu^{(II)} + L \rightleftarrows Cu^{(II)}L$	8.42 ± 0.09	-48.1 ± 0.5	-26.3 ± 0.2	21.8 ± 0.6
$Cu^{(II)}L + L \rightleftarrows Cu^{(II)}L_2$	5.78 ± 0.61	-33.0 ± 3.5	-31.9 ± 0.6	1 ± 4

CHAPTER 3

Relationship between ESI behavior, stability and cytotoxic activity of M(I) phosphino complexes

Mass Spectrometry (MS) is a powerful analytical technique, useful as test bench to obtain information on the biological activity of target compounds. Since MS allows to examine the speciation of analytes in solution, it make also possible to investigate the stability of active compounds, predict their behavior in the environment of interest, and obtain structure-reactivity relationships for new molecules with potential pharmacological applications. For example, electron ionization and metastable-ion studies provide evidence of correlations between the mutagenic properties of a series of aryl and heteroaryl triazenes and mass spectrometric data [125, 126]. Similarly, a linear relationship between the energetics of C(O)–O bond cleavage of some carbamic acid O-aryl esters and their fatty acid amide hydrolase (FAAH) inhibition activity has been proven by electrospray-ionization ion-trap mass spectrometry [127–129].

Interestingly, MS studies on compounds with potential applications in medicine can usually be carried out in solutions where the concentration of the pro-drug the ionic medium and pH conditions are close to those of biological trials.

In view of our interest in evaluating Cu(I)–PTA complex stability in solution, a series of MS experiments on dilute solutions of the complex $[Cu(PTA)_4][PF_6]$ were carried out. The results of these experiments have recently been published [130]. They provide useful comparisons with those from thermodynamic studies on the formation of Cu(I)–PTA complexes,

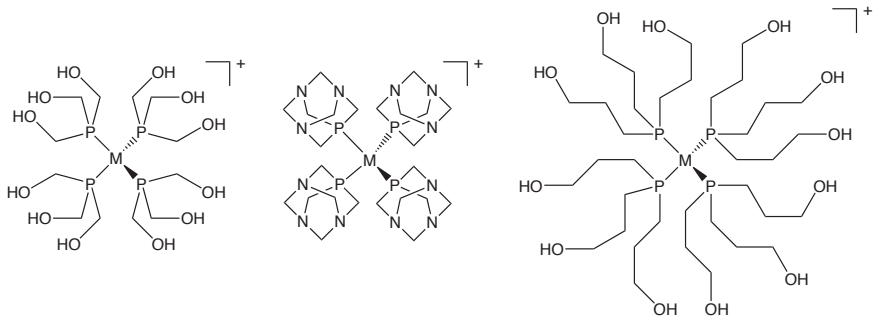

Figure 3.1.: structures of the coinage metal-phosphine complexes which stability in solution have been studied by ESI-MS and cytotoxicity *in vitro* tested (M = Cu^+, Ag^+, Au^+).

and give deeper insights into the correlation between the stability of the complexes and their behavior in biological tests. A previous study [72] demonstrated an inverse correlation between the stability of these copper phosphino complexes and their *in vitro* biological activity. Results of this study showed that solid complexes $[Cu(PTA)_4][X]$ ($[X] = [BF_4]^-$, $[PF_6]^-$), once dissolved in aqueous solutions at micromolar concentrations (near those employed in biological trials) are partially dissociated to lower stoichiometry species $[Cu(PTA)_3]^+$ and $[Cu(PTA)_2]^+$. The inverse relationship between the thermodynamic stability in solution and biological activity of these complexes suggested that the dissociation of one or more phosphine ligands from the metal center is the process underlying the biological activity of these compounds.

A new series of ESI-MS studies has also been extended to $[Ag(PTA)_4]^+$, $[Au(PTA)_4]^+$ and $[Cu(thp)_4]^+$ complexes (Figure 3.1). In the next sections a comparison between the stabilities of the different complexes found in ESI-MS conditions and in thermodynamic studies will be discussed.

The last section of this chapter reports the results of *in vitro* cytotoxicity assays of these compounds.

3.1. Experimental

Samples. Phosphino copper(I) complexes $[Cu(thp)_4][PF_6]$ and $[Cu(PTA)_4][PF_6]$ were prepared according to published procedures [12, 73]. $[Ag(PTA)_4][PF_6]$ and $[Au(PTA)_4][PF_6]$

were synthesized as reported elsewhere [74].

MS measurements. Mass spectra were obtained with a *LCQ Fleet Thermo-Scientific* mass spectrometer equipped with an ESI ion trap operating in the positive ion mode. All compounds were solubilized in *milliQ* water, giving stock solutions of about 10^{-2} M. These were subsequently diluted to about 10^{-5} M solutions in *milliQ* water, methanol or acetonitrile, and directly infused into the ESI source by syringe at a flow rate of 8 μl/min. Ions were produced with a spray voltage of 4 kV and entrance capillary temperature of 280°C. Other instrumental parameters were adjusted for each solution to optimize the signal-to-noise ratio. Tandem mass spectrometric (MS/MS) experiments were performed by resonant excitation of the ion of interest through a supplementary r.f. voltage in the range 10-35% of its maximum value (5 V peak-to peak). The isolation width was set at 1 mass unit for the gold complex and 4 for copper and silver complexes.

3.1.1. Results and discussion

In a previous mass spectrometry study, focused on $[Cu(thp)_4]^+$ and $[Cu(PTA)_4]^+$, it was established that such complexes undergo dissociation in ESI(+) conditions, with the formation of coordinative unsaturated $[Cu(P)_3]^+$ and $[Cu(P)_2]^+$ species (P = thp, PTA). That study was performed in water, in order to simulate physiological conditions. Dissociations were accomplished with the production of water adducts for both complexes, indicating that the solvent probably plays a role in the decomposition of the original species and/or the rearrangement of collisionally generated fragments inside the ion trap.

To clarify the function of the solvent, metal complexes $[M(PTA)_4]^+$ were dissolved in three solvents suitable for MS studies: water, methanol, and acetonitrile. The ESI(+) spectra of solutions of complex $[Cu(PTA)_4]^+$ in the three solvents are shown in Figure 3.2. Almost overlapping behavior was observed for metal-based adducts in the water and methanol solutions, showing the most abundant ion at m/z 377, corresponding to the bis-substituted $[Cu(PTA)_2]^+$ species. Less abundant ions at m/z 534 and m/z 158 were attributable to the tris-substituted $[Cu(PTA)_3]^+$ species and the protonated form of the phosphine ligand $(HPTA)^+$. Instead, the spectrum in acetonitrile showed a quite different

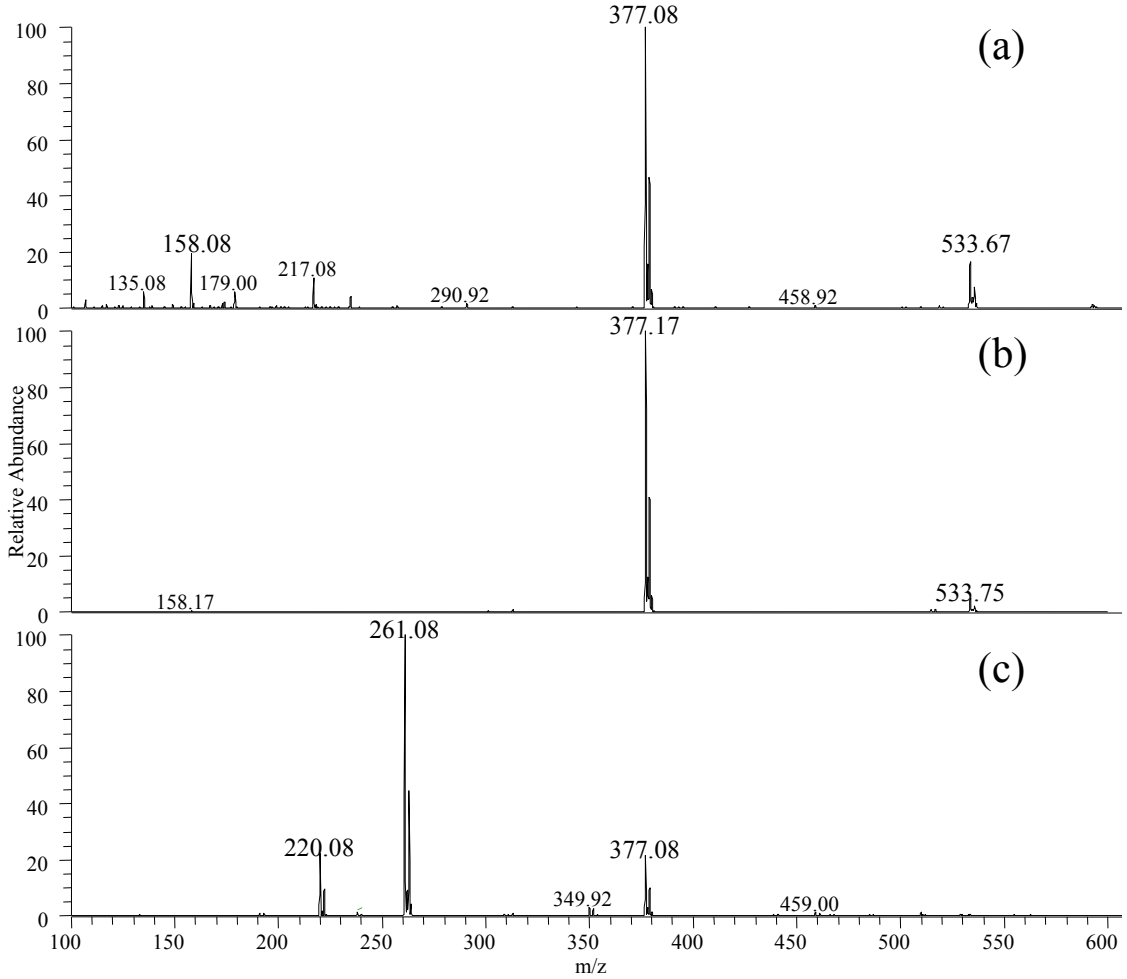

Figure 3.2.: ESI(+) spectrum of $[Cu(PTA)_4]^+$ in water (a), methanol (b), and acetonitrile (c)

profile, with a base peak at m/z 261 attributable to solvent adduct $[Cu(PTA)\cdot(MeCN)]^+$ and low abundant ions at m/z 377 and 220, corresponding to bis-substituted $[Cu(PTA)_2]^+$ and mono-substituted $[Cu(PTA)]^+$ species, respectively.

Also in the case of $[Cu(thp)_4]^+$ solvent-dependent behavior was detected in the in acetonitrile solution, adduct $[Cu(thp)\cdot(MeCN)]^+$ (m/z 228) being the base peak in the ESI(+) spectrum (Figure 3.3). Low abundant ions at m/z 435 and 311 corresponded to coordinative unsaturated $[Cu(thp)_3]^+$ and $[Cu(thp)_2]^+$ species, respectively, and that at m/z 145 corresponded to the bis-solvent adduct $[Cu(MeCN)_2]^+$, never previously detected.

The $[Ag(PTA)_4]^+$ spectra in the three solvents were instead dominated by the ion at m/z 421, corresponding to the bis-substituted $[Ag(PTA)_2]^+$ species. Only in the acetonitrile

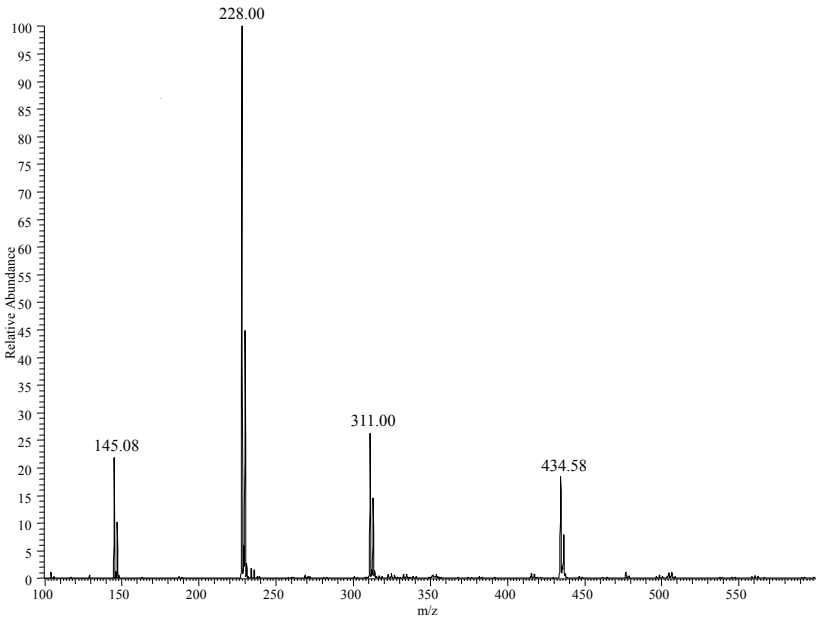

Figure 3.3.: ESI(+) spectrum of $[Cu(thp)_4]^+$ in acetonitrile.

solution were some other low abundant ions observed, at m/z 305 and 158, corresponding to solvent adduct $[Ag(PTA)\cdot(MeCN)]^+$ species and the protonated form of PTA, respectively. Another peak including two silver ions at m/z 556, attributable to the rearranged adduct $[Ag(PTA)_2\cdot AgCN]^+$, was also detected.

Irrespective of the solvent used, the $[Au(PTA)_4]^+$ spectra were invariably dominated by the ion at m/z 511, corresponding to $[Au(PTA)_2]^+$ species, without any additional fragment.

The combined analysis of the full spectra of solutions of $[M(PTA)_4]^+$ complexes in the three solvents provided the following evidences: 1) complexes dissolved in water or methanol showed very similar behavior, but methanol ensured better a signal-to-noise ratio and better sensitivity (signal twice as high); 2) methanol did not interfere with rearrangements, whereas water only participated in some rearrangements with copper, although to a limited extent; 3) decomposition of $[Cu(PTA)_4]^+$ was strongly promoted by acetonitrile, giving primarily solvated species when acetonitrile was used, whereas, in similar experimental conditions, $[Ag(PTA)_4]^+$ was mildly affected and $[Au(PTA)_4]^+$ not affected at all by acetonitrile as solvent. The formation of acetonitrile adducts of copper in ESI(+)

conditions was also validated in the case of $[Cu(thp)_4]^+$. The strong affinity of copper for acetonitrile is confirmed by the number of coordination compounds of copper(I) containing acetonitrile molecules found in MS conditions, especially in dimeric complexes [131]. Since ESI-MS analyses of diluted solutions of $[M(PTA)_4]^+$ complexes in water and in methanol are very similar (reflecting similar solution behavior) and using methanol ensured better signal-to-noise ratios and enhanced sensitivity, methanol was selected for the following studies with the above class of complexes.

Although $[Cu(PTA)_4]^+$ represents the correct formulation of the complex in the solid state, as confirmed by several X-ray structures, and also in the solution state at elevated concentration (^{31}P and ^{63}Cu NMR at ca. 10^{-2} M), ESI(+) measurements did not show such a tetra-coordinated complex but always $[Cu(PTA)_2]^+$ as the base peak of the spectrum. Therefore, the formation of coordinative unsaturated species in dilute solutions is an intrinsic property of this class of "$Cu(P)_4$"-type compounds, as proposed in our previous MS study. It is consequently reasonable to presume that similar dissociation occurs in the case of heavier silver and gold complexes, the base peaks in the ESI(+) spectra being those corresponding to $[Ag(PTA)_2]^+$ and $[Au(PTA)_2]^+$.

The fragmentation profiles observed in the spectra of water and methanol solutions of $[Cu(PTA)_4]^+$, $[Ag(PTA)_4]^+$ match the speciation models obtained from our thermodynamic studies. In particular, Figure 3.4 shows the relative percentage abundance of complexes $[M(PTA)_n]^+$ (M = Cu(I) in (a), and Ag(I) in (b)), in aqueous solutions in which the total concentration of complex $[M(PTA)_4][PF_6]$ was about $10^{-5} - 10^{-6}$ M, near that found during these ESI-MS experiments.

The above percentages, calculated according to the stability constants of the complexes (Table 2.2, page 46 and Table 2.6, page 61), clearly show that, in high dilution conditions, the prevalent complex species is generally the bis-substituted complex $[M(PTA)_2]^+$, according to the MS evidence. In particular, Figure 3.4 shows that the dicoordinated $[Ag(PTA)_2]^+$ complex is largely prevalent in these conditions. This is a direct consequence of the higher value of the stepwise formation constant of the complex $[Ag(PTA)_2]^+$ with respect to those of the two following species $[Ag(PTA)_3]^+$ and $[Ag(PTA)_4]^+$. This observation also explain why the mass spectra of solutions of phosphine complexes of Ag(I) only show the presence

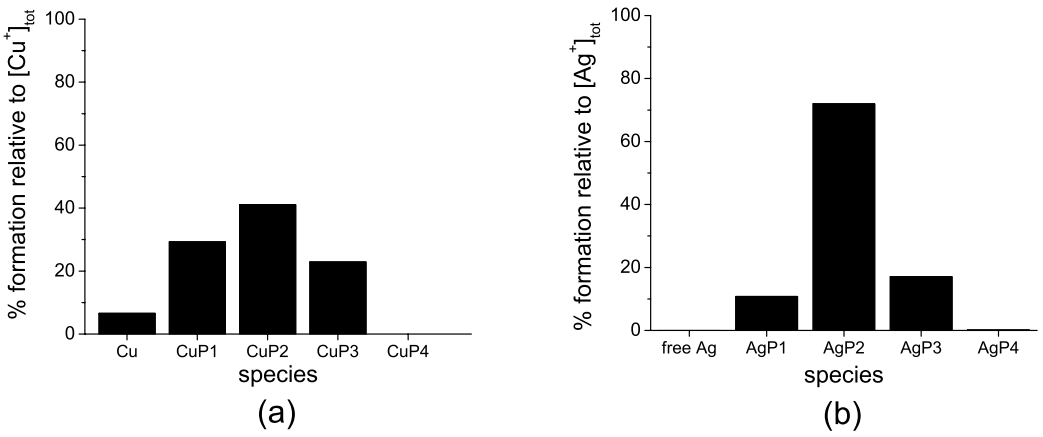

Figure 3.4.: percentage relative abundance of $[M(PTA)_n]^+$ complexes (M = Cu(I), Ag(I), n = 1 − 4, $C_{M,\,total} = 10^{-5} - 10^{-6}$ M) calculated on the basis of their formation constants obtained by thermodynamic studies (chapter 2). In the figure: P = PTA, ionic charges omitted for convenience.

of complex $[Ag(PTA)_2]^+$.

3.2. *In vitro* cytotoxicity assays of phosphino complexes

In vitro cytotoxic activity of phosphino complexes copper(I), silver(I) and gold(I) of PTA and the two other phosphines, thp and thpp, have recently been evaluated for their cytotoxic activity toward a panel of seven human tumor cell lines [74], containing samples of ovarian (2008 and C13), cervical (HeLa), lung (A549), colon (HCT-15), breast (MCF-7) cancers and melanoma (A375). Cytotoxicity was evaluated by MTT tests after 48 h of treatment with increasing concentrations of the tested compounds. For comparison purposes, the cytotoxicity of cisplatin, which is still the most frequently used anticancer metallodrug, was evaluated in the same experimental conditions. IC_{50} values, calculated from dose-survival curves, are listed in Table 3.1. It should be noted that a previous study proved that phosphines thp, thpp and PTA, when not coordinated to a metal center, show no cytotoxic activity against all tested cancer cell lines (data not shown in table) [12, 73].

Among the tested compounds, metal-thp species generally showed better cytotoxic activity compared with metal-PTA and metal-thpp ones, and copper derivatives were always found to be the most efficacious. Figure 3.5 compares the various *in vitro* cytotoxicities of these

Table 3.1.: *In vitro* cytotoxic activity of $[M(P)_4]^+$ compounds (M = Cu^+, Ag^+, Au^+, P = PTA, thp, thpp). [74]

Compound	IC_{50} (μM) ± S.D.							
	A549	MCF-7	A375	HCT-15	HeLa	2008	C13	RF
$[Cu(thp)_4][PF_6]$	9.11 ± 2.71	11.08 ± 0.52	4.58 ± 2.41	2.00 ± 0.03	8.21 ± 1.50	1.48 ± 0.21	2.88 ± 1.07	1.9
$[Ag(thp)_4][PF_6]$	18.22 ± 2.11	17.75 ± 2.71	32.12 ± 1.22	21.32 ± 1.34	12.32 ± 1.24	20.15 ± 1.72	36.65 ± 2.24	1.8
$[Au(thp)_4][PF_6]$	17.4 ± 1.76	18.32 ± 1.98	23.99 ± 1.67	13.21 ± 2.11	18.43 ± 1.21	16.21 ± 1.43	30.22 ± 1.41	1.8
$[Cu(PTA)_4][PF_6]$	7.31 ± 0.87	21.51 ± 1.31	12.76 ± 0.70	15.3 ± 1.5	7.42 ± 0.65	13.81 ± 1.16	10.67 ± 1.31	0.8
$[Ag(PTA)_4][PF_6]$	24.43 ± 1.55	26.44 ± 1.99	21.11 ± 2.01	13.52 ± 1.13	21.65 ± 2.33	11.23 ± 1.65	13.52 ± 1.13	0.8
$[Au(PTA)_4][PF_6]$	50.32 ± 1.53	50.72 ± 2.41	44.63 ± 1.71	32.23 ± 1.62	53.43 ± 1.99	29.52 ± 1.92	38.33 ± 1.97	1.2
$[Cu(thpp)_4][PF_6]$	18.4 ± 3.24	27.31 ± 1.53	31.26 ± 1.65	8.65 ± 3.11	17.96 ± 2.78	20.41 ± 1.43	39.43 ± 2.64	1.9
$[Ag(thpp)_4][PF_6]$	55.64 ± 1.76	77.41 ± 1.56	74.51 ± 1.23	42.93 ± 2.41	55.57 ± 2.65	64.52 ± 1.87	90.30 ± 2.32	1.4
$[Au(thpp)_4][PF_6]$	79.53 ± 1.56	92.34 ± 1.87	73.57 ± 2.54	67.89 ± 1.97	79.34 ± 2.84	87.32 ± 1.27	99.34 ± 1.54	1.1
Cisplatin	29.21 ± 1.92	19.04 ± 1.51	20.33 ± 1.33	25.34 ± 1.31	10.50 ± 1.51	12.96 ± 1.72	89.18 ± 4.50	7.02

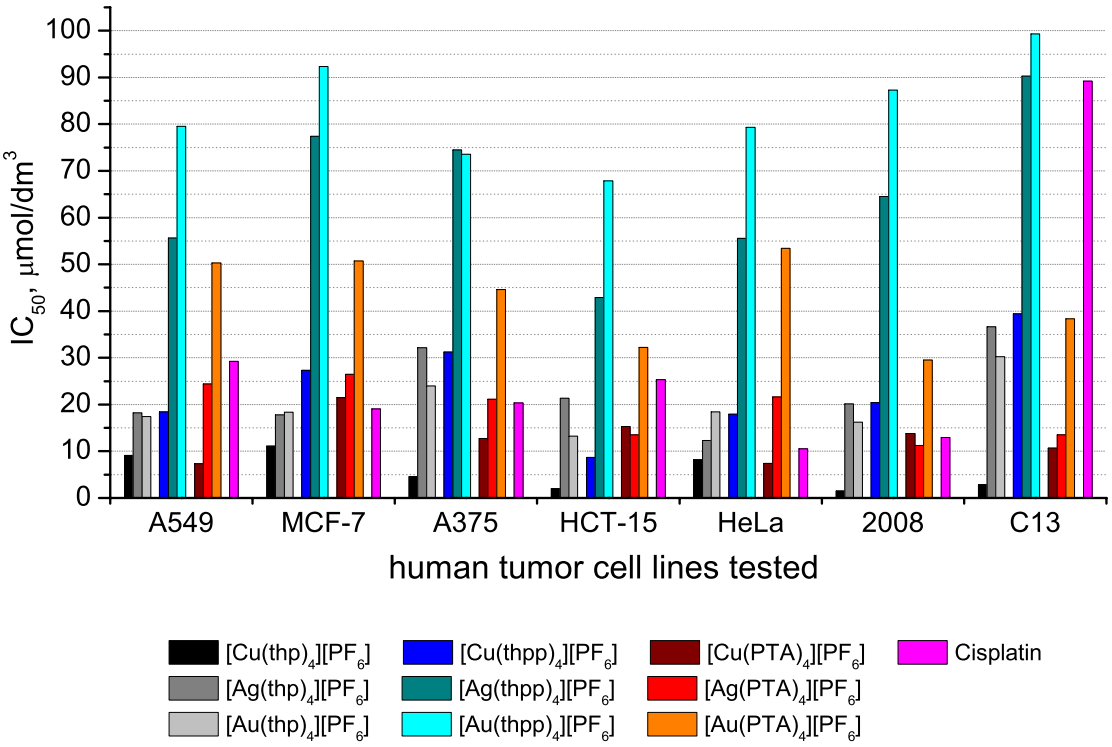

Figure 3.5.: *In vitro* cytotoxic activity of $[M(P)_4]^+$ compounds (M = Cu^+, Ag^+, Au^+, P = PTA, thp, thpp, see Table 3.1). [74]

metallodrugs. In detail, $[Ag(thp)_4][PF_6]$ and $[Au(thp)_4][PF_6]$ showed similar cytotoxicity, about four times lower than that of $[Cu(thp)_4][PF_6]$, with IC_{50} ($\mu mol/dm^3$) average values of 5.64 (1.48–11.08), 22.64 (12.32–36.65) and 19.68 (13.21–30.22) for copper–, silver– and gold–thp complexes, respectively. The cytotoxic potency was roughly three to four times lower from thp- to the bulkier thpp-complexes, with average IC_{50} ($\mu mol/dm^3$) values of 23.34 (8.65–39.43), 65.84 (42.93–90.30) and 82.76 (67.89–99.34) for Cu(I)-, Ag(I)- and Au(I)-thpp complexes, respectively. Intermediate average IC_{50} values were shown by Cu(I)– and Au(I)–PTA derivatives (13.19 and 42.74 $\mu mol/dm^3$, respectively); $[Ag(PTA)_4][PF_6]$ exhibited cytotoxic efficacy (mean IC_{50} of 18.84 $\mu mol/dm^3$) slightly better than that of the silver-thp analog. A549 and HCT-15 tumor cell lines were generally more sensitive to all tested compounds, with six out of nine metal(I) complexes having better cytotoxic activity than that of cisplatin. As A549 non-small cell lung and HCT-15 colon cancer cells have low cisplatin sensitivity, these results indicate the ability of $[M(P)_4]^+$-type species to overcome intrinsic cisplatin resistance, and agree with previous observations proposing a mechanism of action different from platinum complexes for some of them.

Conclusions

In the last few decades, many metal-based compounds have been developed in order to find potential anti tumor drugs. In this context, some new $[M(PTA)_4][X]$ complexes (M = Cu(I), Ag(I), Au(I), PTA = 1,3,5-7-triaza phosphadamantane, X = $[PF_6]^-$, $[BF_4]^-$) have recently been prepared and tested *in vitro* as anti-proliferative agents, showing promising results. The cytotoxic activity of these compounds seems to be related to the ability of copper to bind important biological substrates after dissociation of one ore more phosphines, and this dissociation processes have been ascribed to the high dilution of the compounds during the biological tests. The possibility of studying the in-solution stability of these compounds in conditions similar to those of biological testing is therefore attractive, in order to determine which species exist during *in vitro* trials, and to which of them biological activity should be ascribed.

We therefore carried out a series of thermodynamic studies in order to define the formation equilibria of Cu(I) and Ag(I) with PTA in aqueous solution. In these studies we used microcalorimetric, potentiometric and spectrophotometric techniques and experiments were carefully designed to provide accurate determinations of the thermodynamic functions concerning the formation of the four successive complexes of the metal ions, $[M(PTA)_j]^+$, j = 1–4, M = Cu(I), Ag(I).

In order to gain information about the coordinative geometry and stability of the copper complexes, a theoretical DFT study by in-vacuum calculation was performed, and the structures of several Cu(I)–PTA complexes were optimized. Results provide the most stable coordinative geometry of each of the Cu(I)–PTA complexes. The calculation of the free energies of all the species which had proved to be stable at the end of the optimization process, was carried out both by in-vacuum and polarizable continuum solvent. The results

of DTF calculations correlate well and corroborate the complex formation sequence obtained by the thermodynamic study.

Speciations of the systems, calculated according to the thermodynamic studies, indicate that both silver and copper complexes, characterized as tetracoordinated species in solid and solution at relatively high concentrations ($> 10^{-2}$ M), when diluted to about micromolar concentrations typical of biological testing, are partially dissociated to lower stoichiometry species. In particular, at the biological testing conditions the calculated speciations show that dicoordinated $[M(PTA)_2]^+$ complex of both metals is the prevailing species in solution. This indication is nicely supported by the results of MS studies in aqueous solution, which gave information about the $[M(PTA)_4][PF_6]$ complex dissociation processes and the prevalent species in solution at micro-molar concentrations.

These novel phosphine compounds showed remarkable *in vitro* cytotoxicity, especially against A549 and HCT-15 human tumor cell lines, with IC_{50} values near or lower than those of cisplatin as reference. The copper derivatives generally showed higher cytotoxicity than the silver ones. In addition, all these compounds exhibited marked cytotoxicity against the C13 cisplatin-resistant cell line, with IC_{50} values lower by about one order of magnitude than those of cisplatin. These results are definitely encouraging and indicate that this novel class of compounds may have future promising applications in clinical use.

All the experimental results of thermodynamic studies, ESI-MS experiments and cytotoxicity assays strongly indicate that the dissociation equilibria of complexes $[M(PTA)_4]^+$ in solution are the crucial processes underlying their cytotoxic activity. More generally, these studies show that the toxicity of a metal compound is intrinsically linked to its stability in solution. The well-known concept of the relationship between the "structure and activity" (SAR) of a metal compound with potential clinical use should thus be extended, to take into account its stability in solution (SSAR). Although the solid state structure of a metal coordination compound is known, it is always necessary to consider that in solution, especially at high dilutions typical of the biological applications, it may dissociate leading to marked changes in its stoichiometry, coordinative geometry and hence chemical properties. Therefore, studies on the formation equilibria of the metal-based drugs, like those reported in this thesis, are certainly valuable, since they may provide essential information about

their potential as a drug for clinical use.

During this thesis project, a series of experimental methods, suitable for study Cu(I) equilibrium systems in aqueous solution, were also developed. In particular, microcalorimetry proved to be an affordable approach to studies on these systems, which are severely hampered by Cu(I) instability in aqueous environment. Using this technique, for example, the formation of two successive complexes between Cu(I) and the amino acid methionine was studied. Results of this study provide useful information about the number of possible adducts formed by the monovalent metal, which may help to explain some results concerning the binding sites of copper transport proteins. All the experimental methods and procedures may be used in the future, to study many other chemical processes underlying interactions between Cu(I) and other biological substrates, for crucial information about the mechanisms of intracellular copper uptake and its trafficking.

Bibliography

[1] Abu-Surrah, A. S.; Kettunen, M. *Curr. Med. Chem.* **2006**, *13*, 1337.

[2] Devarajan, P.; Tarabishi, R.; Mishra, J.; Ma, Q.; Kourvetaris, A.; Vougiouka, M.; Boulikas, T. *Oncol. Rep.* **2004**, *11*, 559.

[3] Barnes, K. R.; Lippard, S. J. *Met. Ions. Biol. Syst.* **2004**, *42*, 143.

[4] Dempke, W.; Voigt, W.; Grothey, A.; Hill, B. T.; Schmoll, H. J. *Anti-Cancer Drugs* **2000**, *11*, 225.

[5] Galanski, M.; Jakupec, M. A.; Keppler, B. K. *Curr. Med. Chem.* **2005**, *12*, 2075.

[6] Ott, I.; Gust, R. *Pharm. unserer Zeit* **2006**, *35(2)*, 124–33.

[7] Cohen, S. M.; Lippard, S. J. *Prog. Nucleic Acids Res. Mol. Biol.* **2001**, *67*, 93–130.

[8] Hall, M. D.; Hambley, T. W. *Coord. Chem. Rev.* **2002**, *232*, 49.

[9] Zhang, C. X.; Lippard, S. J. *Curr. Opin. Chem. Biol.* **2003**, *7*, 481.

[10] Shaw, C. F. *Chem. Rev.* **1999**, *99*, 2589.

[11] Simon, T.; Kunishima, D. H.; Vibert, G. J.; Lorber, A. *Cancer Res.* **1981**, *41*, 94.

[12] Porchia, M.; Benetollo, F.; Refosco, F.; Tisato, F.; Marzano, C.; Gandin, V. *J. Inorg. Biochem.* **2009**, *103*, 1644.

[13] Berners-Price, S. J.; Sant, M. E.; Christopherson, R. I.; Kuchel, P. W. *Magn. Reson. Med.* **1991**, *18*, 142.

[14] Popova, T. V.; Aksenova, N. V. *Russ. J. Coord. Chem.* **2003**, *29*, 743.

[15] Brugger, J.; Etschmann, B.; Liu, W.; Testemale, D.; Hazemann, J. L.; Emerich, H.; van Beek, W.; Proux, O. *Geochim. Cosmochim. Acta* **2007**, *71*, 4920.

[16] Cotton, F. A.; Wilkinson, G.; Murillo, C. A.; Bochmann, M. In *Advanced Inorganic Chemistry, 6th ed.*; Wiley-Interscience„ Ed.; 1999.

[17] Medeiros, D. M.; Jennings, D. *J. Bioenerg. Biomembr.* **2002**, *34*, 389.

[18] Yang, L.; Huang, Z.; Li, F. *J. Pept. Sci.* **2012**, *18*, 449.

[19] Voskoboinik, I.; Camakaris, J. *J. Bioenerg. Biomembr.* **2002**, *34*, 363.

[20] Lutsenko, S.; Efremov, R. G.; Tsivkovskii, R.; Walker, J. M. *J. Bioenerg. Biomembr.* **2002**, *34*, 351.

[21] Rubino, J. T.; Riggs-Gelasco, P.; Franz, K. J. *J. Biol. Inorg. Chem.* **2010**, *15*, 1033.

[22] Rubino, J. T.; Chenkin, M. P.; Keller, M.; Riggs-Gelasco, P.; Franz, K. J. *Metallomics* **2011**, *3*, 61.

[23] Puig, S.; Thiele, D. J. *Curr. Opin. Chem. Biol.* **2002**, *6*, 171.

[24] Puig, S.; Lee, J.; Lau, M.; Thiele, D. J. *J. Biol. Chem.* **2002**, *277*, 26021.

[25] De Feo, C. J.; Aller, S. G.; Siluvai, G. S.; Blackburn, N. J.; Unger, V. M. *Proc. Natl. Acad. Sci. USA* **2009**, *106*, 4237.

[26] Cobine, P. A.; Ojeda, L. D.; Rigby, K. M.; Winge, D. R. *J. Biol. Chem.* **2004**, *279*, 14447.

[27] Cobine, P. A.; Pierrel, F.; Winge, D. R. *Biochim. Biophys. Acta Mol. Cell. Res.* **2006**, *1763*, 759.

[28] Kim, H.-s.; Ahner, B. A. *Anal. Chim. Acta* **2006**, *575*, 223.

[29] Nose, Y.; Rees, E. M.; Thiele, D. J. *Trends. Biochem. Sci.* **2006**, *31*.

[30] Rorabacher, D. B. *Chem. Rev.* **2004**, *104*.

[31] Georgatsou, E.; Mavrogiannis, L. A.; Fragiadakis, G. S.; Alexandraki, D. *J. Biol. Chem.* **1997**, *272*.

[32] Prohaska, J. R.; Gybina, A. A. *J. Nutr.* **2004**, *134*.

[33] Xue, Y.; Davis, A. V.; Balakrishnan, G.; Stasser, J. P.; Staehlin, B. M.; Focia, P.; Spiro, T. G.; Penner-Hahn, J. E.; O'Halloran, T. V. *Nat. Chem. Biol.* **2008**, *4*, 107.

[34] Davis, A. V.; O'Halloran, T. V. *Nat. Chem. Biol.* **2008**, *4*, 148.

[35] Pufahl, R. A.; Singer, C. P.; Peariso, K. L.; Lin, S. J.; Schmidt, P. J.; Fahrni, C. J.; Cizewski Culotta, V.; Penner-Hahn, J. E.; O'Halloran, T. V. *Science* **1997**, *278*, 853.

[36] Balatri, E.; Banci, L.; Bertini, I.; Cantini, F.; Ciofi-Baffoni, S. *Structure* **2003**, *11*, 1431.

[37] Brewer, G. J. *J. Am. Coll. Nutr.* **2009**, *3*, 238.

[38] Brewer, G. J. *Curr. Opin. Chem. Biol.* **2003**, *7*, 207.

[39] Gitlin, J. D. *Gastroenterology* **2003**, *125*, 1868.

[40] Petrukhin, K.; Fischer, S. G.; Pirastu, M.; Tanzi, R. E.; Chernov, I.; Devoto, M.; Brzustowicz, L. M.; Cayanis, E.; Vitale, E. *Nat. Genet.* **1993**, *5*, 338.

[41] Roberts, E. A.; Schilsky, M. L. *Hepathol.* **2008**, *47*, 2089.

[42] Roberts, E. A.; Schilsky, M. L. *Hepathol.* **2003**, *37*, 1475.

[43] Tisato, F.; Marzano, C.; Porchia, M.; Pellei, M.; Santini, C. *Med. Res. Rev.* **2010**, *30*, 708.

[44] Lowndes, S. A.; Adams, A.; Timms, A.; Fisher, N.; Smythe, J.; Watt, S. M.; Joel, S.; Donate, F.; Hayward, C.; Reich, S. *Clin. Cancer Res.* **2008**, *14*, 7526.

[45] Tang, J.; Donsante, A.; Desai, V.; Patronas, N.; Kaler, S. G. *Mol. Genet. Metab.* **2008**, *3*, 174.

[46] Di Donato, M.; Sarkar, B. *Biochim. Biophys. Acta* **1997**, *1360*, 3.

[47] Sarkar, B. *Chem. Rev.* **1999**, *99*, 2535.

[48] Garnica, A.; Chan, W. Y.; Rennert, O. *J. Pediatr.* **1994**, 336.

[49] Basun, H.; Forssell, L. G.; Wetterberg, L.; Winblad, B. *J. Neural Transm.* **1991**, *3*, 231.

[50] Iakovidis, I.; Delimaris, I.; Piperakis, S. M. *Mol. Biol. Int* **2011**, 1.

[51] Haeffner, F.; Smith, D. G.; Barnham, K. J.; Bush, A. I. *J. Inorg. Biochem.* **2005**, *99*, 2403.

[52] Hureau, C.; Faller, P. *Biochimie* **2009**, *91*, 1212.

[53] Deraeve, C.; Boldron, C.; Maraval, A.; Mazarguil, H.; Gornitzka, H.; Vendier, L.; Pitie, M.; Meunier, B. *Chem. Eur. J.* **2008**, *14*, 682.

[54] Deraeve, C.; Pitie, M.; Mazarguil, H.; Meunier, B. *New. J. Chem.* **2007**, *31*, 193.

[55] Gupte, A.; Mumper, R. J. *Cancer Treat. Rev.* **2009**, *35*, 32.

[56] Elo, H. *Zeit. Naturforsch.* **2004**, *59*, 609.

[57] Dou, Q. P.; Smith, D. M.; Daniel, K. G.; Kazi, A. *Prog. Cell Cycle Res.* **2003**, *5*, 441.

[58] Marques, A. J.; Palanimurugan, R.; Matias, A. C.; Ramos, P. C.; Dohmen, R. J. *Chem. Rev.* **2009**, *109*, 1509.

[59] Daniel, K.; Gupta, P.; Harbach, R.; Guida, W.; Dou, Q. *Biochem. Pharmacol.* **2004**, *67*, 1139.

[60] Hindo, S. S.; Frezza, M.; Tomco, D.; Heeg, M. J.; Hryhorczuk, L.; McGarvey, B. R.; Dou, Q. P.; Verani, C. N. *Eur. J. Med. Chem.* **2009**, *44*, 4353.

[61] Zhang, Z.; Bi, C.; Schmitt, S. M.; Fan, Y.; Dong, L.; Zuo, J.; Dou, Q. P. *J. Biol. Inorg. Chem.* **2012**, *17*, 1257.

[62] Handsley, M. M.; Edwards, D. R. *Int. J. Cancer* **2005**, *115*, 849.

[63] Sen, C. K.; Khanna, S.; Venojarvi, M.; Trikha, P.; Ellison, E. C.; Hunt, T. K.; Roy, S. *Am. J. Physiol.* **2002**, *282*, H1821.

[64] Nasulewicz, A.; Mazur, A.; Opolski, A. *J. Trace Elem. Med. Biol.* **2004**, *18*, 1.

[65] Moriguchi, M.; Nakajima, T.; Kimura, H.; Watanabe, T.; Takashima, H.; Mitsumoto, Y.; Katagishi, T.; Okanoue, T.; Kagawa, K. *Int. J. Cancer* **2002**, *102*, 445.

[66] Shrivastava, H. Y.; Kanthimathi, M.; Nair, B. U. *Biochim. Biophys. Acta* **2002**, *2*, 149.

[67] Murugkar, A.; Unnikrishnan, B.; Padhye, S.; Bhonde, R.; Teat, S. J.; Triantafillou, E.; Sinn, E. Hormone anchored metal complexes. 1. Synthesis, structure, spectroscopy and in vitro antitumor activity of testosterone acetate thiosemicarbazone and its metal complexes. 1999.

[68] Marin-Hernandez, A.; Gracia-Mora, I.; Ruiz-Ramirez, L.; Moreno-Sanchez, R. *Biochem. Pharmacol.* **2003**, *65*, 1979.

[69] Chaviara, A. T.; Christidis, P. C.; Papageorgiou, A.; Chrysogelou, E.; Hadjipavlou-Litina, D. J.; Bolos, C. A. *J. Inorg. Biochem.* **2005**, *99*, 2102.

[70] Berners-Price, S. J.; Mirabelli, C. K.; Johnson, R. K.; Mattern, M. R.; McCabe, F. L.; Faucette, L. F.; Sung, C. M.; Mong, S. M.; Sadler, P. J.; Crooke, S. T. *Cancer Res.* **1986**, *46*, 5486.

[71] Berners-Price, S. J.; Sadler, P. J. *Bioinorg. Chem.* **1988**, *70*, 27.

[72] Tisato, F.; Refosco, F.; Porchia, M.; Tegoni, M.; Gandin, V.; Marzano, C.; Pellei, M.; Papini, G.; Lucato, L.; Seraglia, R.; Traldi, P. *Rapid Commun. Mass Spectrom.* **2010**, *24*, 1610.

[73] Marzano, C.; Gandin, V.; Pellei, M.; Colavito, D.; Papini, G.; Lobbia, G. G.; Del Giudice, E.; Porchia, M.; Tisato, F.; Santini, C. *J. Med. Chem.* **2008**, *51*, 798.

[74] Santini, C.; Pellei, M.; Papini, G.; Morresi, B.; Galassi, R.; Ricci, S.; Tisato, F.; Porchia, M.; Rigobello, M. P.; Gandin, V.; Marzano, C. *J. Inorg. Biochem.* **2011**, *105*, 232.

[75] Endrizzi, F.; Di Bernardo, P.; Zanonato, P.; Tisato, F.; Porchia, M.; Isse, A. A. *Dalton Trans.* **2012**, *in press*.

[76] Rossotti, F. J. C.; Rossotti, H. *The determination of stability constants*; McGraw-Hill book company, Inc.: New York (US), 1961.

[77] Sabatini, A.; Vacca, A.; Gans, P. *Coord. Chem. Rev.* **1992**, *120*, 389.

[78] Gans, P.; Sabatini, A.; Vacca, A. *Talanta* **1996**, *43*, 1739.

[79] Hartley, F. R.; Burgess, C.; Alcock, R. M. In *Solution Equilibria*; sons Inc., J. W. ., Ed.; Ellis Horwood Limited: Baffins Lane, Chichester, West Sussex PO19 1UD, England, 1980.

[80] Di Bernardo, P.; Zanonato, P.; Rao, L.; Bismondo, A.; Endrizzi, F. *Dalton Trans.* **2011**, *40*, 9101.

[81] Rao, L. *Chem. Soc. Rev.* **2007**, *36*, 881.

[82] Dyrssen, D.; Ingri, N.; Sillen, L. G. *Acta Chem. Scand.* **1961**, *15*, 694.

[83] Ingri, N.; Sillen, L. G. *Acta Chem. Scand.* **1962**, *16*, 173.

[84] Ingri, N.; Sillen, L. G. *Arkiv Kem.* **1964**, *23*, 97.

[85] Ingri, N.; Sillen, L. G. *Arkiv Kem.* **1964**, *23*, 97.

[86] Arnek, R. *Arkiv Kem.* **1970**, *32*, 81.

[87] Ahrland, S.; Rawsthorne, J. *Acta Chem. Scand.* **1970**, *24*, 157.

[88] Hikita, H.; Ishikawa, H.; Esaka, N. *Nippon Kagaku Kaishi* **1973**, 13.

[89] Sugasaka, K.; Fujii, A. *Bull. Chem. Soc. Jpn.* **1976**, *49*, 82.

[90] Davis, D. D.; Stevenson, K. L.; Davis, C. R. *J. Am. Chem. Soc.* **1978**, *100*, 5344.

[91] Fritz, J. J. *J. Phys. Chem.* **1980**, *84*, 2241.

[92] Sharma, V. K.; Millero, F. J. *J. Solution Chem.* **1990**, *19*, 375.

[93] Ciavatta, L.; Iuliano, M. *Ann. Chim.* **1998**, *88*, 71.

[94] Xiao, Z.; Gammons, C. H.; Williams-Jones, A. E. *Geochim. Cosmochim. Acta* **1998**, *62*, 2949.

[95] Liu, W.; Brugger, J.; McPhail, D. C.; Spicca, L. *Geochim. Cosmochim. Acta* **2002**, *66*, 3615.

[96] Sharma, V. K.; Zinger, A.; Millero, F. J.; De Stefano, C. *Biophys. Chem.* **2003**, *105*, 79.

[97] Sharma, V. K.; Millero, F. J.; De Stefano, C.; Crea, P. *Mar. Chem.* **2007**, *106*, 463.

[98] Sherman, D. M. *Geochim. Cosmochim. Acta* **2007**, *71*, 714.

[99] Pitzer, K. S. *J. Phys Chem.* **1973**, *77*, 268.

[100] Pitzer, K. S.; Mayorga, G. *J. Phys. Chem.* **1973**, *77*, 2300.

[101] Sharma, V. K.; Millero, F. J. *Mar. Chem.* **1988**, *25*, 141.

[102] Daigle, J., Donald; Pepperman, J., A. B.; Vail, L., Sidney *J. Heterocycl. Chem.* **1974**, *11*, 407.

[103] Daigle, D. J. *Inorg. Synth.* **1998**, *32*, 40.

[104] Brauner, P.; Sillen, L. G.; Whiteker, R. *Arkiv Kem.* **1969**, *31*, 365.

[105] Sholl, D.; Steckel, J. A. *Density Functional Theory: A Practical Introduction*; Wiley-Interscience: Hoboken NJ, 2009.

[106] Koch, W.; Holthausen, M. C. *A Chemist's Guide to Density Functional Theory*; Wiley-VCH: Weinheim, 2001.

[107] Becke, A. D. *J. Chem. Phys.* **1993**, *98*, 1372.

[108] Lee, C. T.; Yang, W. T.; Parr, R. G. *Phys. Rev. B* **1988**, *37*, 785.

[109] Krishnan, R.; Binkley, J. S.; Seeger, R.; Pople, J. A. *J. Chem. Phys.* **1980**, *72*, 650.

[110] McLean, A. D.; Chandler, G. S. *J. Chem. Phys.* **1980**, *72*, 5639.

[111] Dolg, M.; Wedig, U.; Stoll, H.; Preuss, H. *J. Chem. Phys.* **1987**, *86*, 866.

[112] Frisch, M. J.; Trucks, G. W.; Schlegel, H. B.; et.al, *Gaussian 09, Revision A.02. Gaussian 09, Revision A.02, Gaussian, Inc.*; 2009.

[113] Fulton, J. L.; Hoffmann, M. M.; Darab, J. G. *Chem. Phys. Letters* **2000**, *330*, 300.

[114] Kirillov, A. M.; Smolenski, P.; Fatima, M.; Guedes da Silva, C.; Pombeiro, A. J. L. *Eur. J. Inorg. Chem.* **2007**, 2686.

[115] Tomasi, J.; Mennucci, B.; Cammi, R. *Chem. Rev.* **2005**, *105*, 2999.

[116] Alderighi, L.; Gans, P.; Ienco, A.; Peters, D.; Sabatini, A.; Vacca, A. *Coord. Chem. Rev.* **1999**, *184*, 311.

[117] Persson, I.; Nilsson, K. B. *Inorg. Chem.* **2006**, *45*, 7428.

[118] Pettit, L. D.; Siddiqui, K. F.; Kozlowski, H.; Kowalik, T. *Inorg. Chim. Acta* **1981**, *55*, 87.

[119] Grigorova, E. V.; Bondarev, L. P.; Kornienko, T. S. *Russ. J. Gen. Chem.* **2010**, *80*, 2450.

[120] Armarego, W. L. F.; Chai, C. In *Purification of laboratory chemicals*; Butterworth-Heinemann,, Ed.; 2012.

[121] Lenz, G. R.; Martell, A. E. *Biochem.* **1964**, *3*, 745.

[122] Israeli, M.; Pettit, L. *J. Inorg. Nucl. Chem.* **1975**, *37*, 999.

[123] Tewari, B. B. *Z. Neorg. Kim.* **2007**, *52*, 878.

[124] Martell, A. E.; Smith, R. M. In *Critical Stability Constants*; Corp., P. P., Ed.; Plenum Press: 233 Spring Street, New York, NY 10013, 1982.

[125] Tarzia, G.; Diamantini, G.; Tontini, A.; Favretto, D.; Traldi, P. *Rapid Commun. Mass Spectrom.* **1996**, *10*, 1156.

[126] Tarzia, G.; Diamantini, G.; Tontini, A.; Bedini, A.; Favretto, D.; Traldi, P. *Rapid Commun. Mass Spectrom.* **1997**, *11*, 1365.

[127] Basso, E.; Duranti, A.; Mor, M.; Piomelli, D.; Tontini, A.; Tarzia, G.; Traldi, P. *J. Mass. Spectrom.* **2004**, *39*, 1450.

[128] Valitutti, G.; Duranti, A.; Lodola, A.; Mor, M.; Piersanti, G.; Piomelli, D.; Rivara, S.; Tontini, A.; Tarzia, G.; Traldi, P. *J. Mass. Spectrom.* **2007**, *42*, 1624.

[129] Valitutti, G.; Duranti, A.; Mor, M.; Piersanti, G.; Piomelli, D.; Rivara, S.; Tontini, A.; Tarzia, G.; Traldi, P. *J. Mass. Spectrom.* **2009**, *44*, 561.

[130] Tisato, F.; Porchia, M.; Refosco, F.; Endrizzi, F.; Di Bernardo, P. **2012**, *in corso di pubblicazione*.

[131] Sanghamitra, N. J.; Phatak, P.; Das, S.; Samuelson, A. G.; Somasundaram, K. *J. Med. Chem.* **2005**, *48*, 977.

[132] Schwarzenbach, G. Interpretation of solution stabilities of metal complexes. 1977.

[133] Irving, H. M.; Williams, R. J. P. *J. Chem. Soc.* **1953**, 3192.

[134] Griffith, J. S. *The Theory of Transition–Metal Ions*; Cambridge University Press: Cambridge CB2 8RU, UK, 2009.

[135] Debye, P.; Hückel, E. *Phys. Z.* **1923**, *24*, 185.

[136] Debye, P.; Hückel, E. *Phys. Z.* **1923**, *24*, 305.

[137] Bronsted, J. N. *J. Am. Chem. Soc.* **1922**, *44*, 877.

[138] Guggenheim, E. A.; Turgeon, J. C. *T. Faraday Soc.* **1955**, *51*, 747.

[139] Scatchard, G. *Chem. Rev.* **1936**, *19*, 309.

[140] Ciavatta, L. *Ann. Chim.* **1980**, *70*, 551.

[141] Anstiss, R. G.; Pitzer, K. S. *J. Soln. Chem.* **1991**, *20*, 849.

[142] Chen, C. C.; Evans, L. B. *AIChe J.* **1986**, *32*, 444.

[143] Mock, B.; Evans, L. B.; Chen, C. C. *AIChe J.* **1986**, *32*, 1655.

[144] Gans, P. *Data fitting in the chemical sciences by the method of Least Squares*; Wiley: Baffins Lane, Chichester, West Sussex PO19 1UD, England, 1992.

APPENDIX A

Analytical details of the experiments

Table A.1.: analytical detail of the microcalorimetric titrations on the system Cu(I) – PTA (see section 2.2.3 on page 43).

Tit n.	$C^0_{Cu^+}$ mM	$C^0_{H^+}$ mM	C^0_{PTA} mM	$C^{titrant}_{Cu^+}$ mM	$C^{titrant}_{H^+}$ mM	$C^{titrant}_{PTA}$ mM	V^0 mL
1	0.199	0.020	–	–	–	49.8	2.763
2	0.302	0.030	–	–	–	49.8	2.728
3	0.502	0.050	–	–	–	49.8	2.737
4	0.200	0.499	–	–	–	30.0	2.756
5	0.296	0.494	–	–	–	30.0	2.787
6	0.462	0.478	–	–	–	30.0	2.876
7	0.204	2.044	–	–	–	30.0	2.689
8	0.293	1.846	–	–	–	30.0	2.775
9	0.491	1.947	–	–	–	49.8	2.750
10	–	–	0.504	11.0	–	–	2.760
11	–	–	0.989	11.0	–	–	2.748
12	–	–	2.00	11.0	–	–	2.735
13	–	–	10.8	11.0	–	–	2.760
14	–	0.501	0.500	10.3	1.00	–	2.752
15	–	5.01	10.05	10.3	1.03	–	2.752

Table A.2.: analytical details of the spectrophotometric batch titrations of the system Cu(I)–PTA (see section 2.2.3 on page 43); spectra in Figure 2.14 on page 47.

SET 1						SET 2					
point n.	C_M^0	C_L^0	C_L/C_M	V	path length	point n.	C_M^0	C_L^0	C_L/C_M	V	path length
	mM	mM		mL	cm		mM	mM		mL	cm
1	4.546	2.251	0.50	2.988	0.0104	1	0.607	0.106	0.18	3.045	0.0104
2	2.259	2.222	0.98	2.985	0.0104	2	0.612	0.218	0.36	3.020	0.0104
3	1.494	2.248	1.50	2.988	0.0104	3	0.607	0.329	0.54	3.024	0.0104
4	1.120	2.236	2.00	2.986	0.0104	4	0.606	0.448	0.74	3.013	0.0104
5	0.894	2.249	2.52	2.991	0.0104	5	0.616	0.561	0.91	3.020	0.0104
6	0.759	2.236	2.95	2.999	0.0104	6	0.624	0.673	1.08	3.015	0.0104
7	0.651	2.229	3.43	3.009	0.0104	7	0.615	0.787	1.28	3.007	0.0104
8	0.572	2.234	3.91	3.002	0.0104	8	0.613	0.900	1.47	3.013	0.0104
9	0.449	2.231	4.96	3.012	0.0104	9	0.610	1.022	1.68	3.011	0.0104
10	0.381	2.242	5.88	3.001	0.0104	10	0.603	1.124	1.86	3.027	0.0104
11	0.231	2.238	9.69	3.002	0.0104	11	0.607	1.252	2.06	3.028	0.0104
12	0.000	2.226	–	3.004	0.0104	12	0.608	1.440	2.37	3.022	0.0104
SET 3						13	0.607	1.659	2.73	3.007	0.0104
point n.	C_M^0	C_L^0	C_L/C_M	V	path length	14	0.614	1.949	3.17	3.009	0.0104
						15	0.611	2.206	3.61	3.025	0.0104
	mM	mM		mL	cm	16	0.607	2.784	4.59	2.991	0.0104
1	0.050	0.010	0.19	2.980	1.000	17	0.606	3.346	5.52	2.995	0.0104
2	0.050	0.020	0.39	2.989	1.000	18	0.611	–	–	3.006	0.0104
3	0.049	0.028	0.57	3.042	1.000	SET 4					
4	0.050	0.042	0.84	3.005	1.000	point n.	C_M^0	C_L^0	C_L/C_M	V	path length
5	0.048	0.049	1.01	3.110	1.000						
6	0.050	0.060	1.21	3.014	1.000		mM	mM		mL	cm
7	0.050	0.070	1.40	2.994	1.000	1	0.017	0.003	0.20	9.088	1.000
8	0.050	0.079	1.59	3.018	1.000	2	0.016	0.007	0.40	9.084	1.000
9	0.050	0.090	1.79	2.982	1.000	3	0.017	0.010	0.61	9.054	1.000
10	0.050	0.100	2.00	3.007	1.000	4	0.017	0.013	0.75	8.981	1.000
11	0.050	0.108	2.15	3.000	1.000	5	0.017	0.013	0.80	9.049	1.000
12	0.050	0.120	2.39	2.993	1.000	6	0.017	0.015	0.89	8.990	1.000
13	0.050	0.127	2.57	3.009	1.000	7	0.017	0.017	1.01	9.001	1.000
14	0.050	0.137	2.75	3.008	1.000	8	0.017	0.018	1.07	9.001	1.000
15	0.050	0.150	3.01	3.005	1.000	9	0.017	0.021	1.22	9.037	1.000
16	0.049	0.159	3.22	3.004	1.000	10	0.017	0.022	1.29	8.992	1.000
17	0.049	0.170	3.44	3.007	1.000	11	0.017	0.024	1.39	8.978	1.000
18	0.050	0.180	3.63	2.989	1.000	12	0.017	0.025	1.49	9.010	1.000
19	0.049	0.191	3.88	2.987	1.000	13	0.017	0.027	1.65	9.149	1.000
20	0.049	0.200	4.06	3.006	1.000	14	0.017	0.029	1.69	9.040	1.000
						15	0.017	0.030	1.79	9.027	1.000
						16	0.017	0.032	1.87	8.044	1.000
						17	0.017	0.034	1.98	5.285	1.000

Table A.3.: analytical detail of the potentiometric titrations on the system Ag(I) – PTA (see section 2.3 on page 58).

Tit n.	$C^0_{Ag^+}$ mM	$C^0_{H^+}$ mM	$C^{titrant}_{H^+}$ mM	$C^{titrant}_{PTA}$ mM	V^0 mL
1	1.811	0.992	1.006	10.23	16.73
2	0.952	1.003	1.006	10.23	15.71
3	0.485	–	–	9.98	21.14
4	1.007	–	–	9.98	20.06
5	2.010	–	–	9.98	19.94
6	0.255	–	–	9.98	19.98

Table A.4.: analytical detail of the microcalorimetric titrations on the system Ag(I) – PTA (see section 2.3 on page 58).

Tit n.	$C^0_{Ag^+}$ mM	$C^0_{H^+}$ mM	$C^0_{PTA^+}$ mM	$C^{titrant}_{Ag^+}$ mM	$C^{titrant}_{PTA}$ mM	V^0 mL
1	–	–	5.052	100.2	–	2.709
2	–	–	1.011	20.00	–	2.691
3	0.9909	0.05046	–	–	51.12	2.726
4	1.000	0.942	–	–	51.12	2.702
5	1.001	0.986	–	–	51.12	2.704
6	0.9899	2.998	–	–	51.12	2.710

Table A.5.: analytical detail of the microcalorimetric titrations for the protonation of methionine (section 2.4.1 on p. 68).

Tit n.	C^0_{HMet} mM	$C^{tit}_{H^+}$ mM	$C^{tit}_{OH^-}$ mM	V^0 mL
T1	9.72	517	–	2.733
T2	9.72	–	101	2.728
T3	2.48	–	101	2.703
T4	7.51	–	101	2.717

Table A.6.: analytical detail of the microcalorimetric titrations on the system Cu(II)/methionine (section 2.4.2 on page 70)

Tit. n.	$C^0_{H^+}$	$C^0_{Cu^{2+}}$	$C^{tit}_{H^+}$	$C^{tit}_{Met^-}$	V^0
	mM	mM	mM	mM	mM
T1	0.0125	0.122	0.822	13.1	2.749
T2	0.0256	0.256	1.65	26.4	2.750
T3	0.050	0.504	3.30	52.8	2.749
T4	0.100	1.023	3.30	52.8	2.749

Table A.7.: analytical detail of the microcalorimetric titrations on the system Cu(I)/methionine (see section 2.4.3 on p. 72)

Tit. n.	$C^0_{H^+}$	$C^0_{Cu^+}$	$C^0_{Met^-}$	$C^{tit}_{H^+}$	$C^{tit}_{Cu^+}$	$C^{tit}_{Met^-}$, mM	V^0
	mM	mM	mM	mM	mM	mM	mL
T1	99.9	–	99.9	–	4.98	–	2.720
T2	50.3	–	50.3	–	4.98	–	2.708
T3	24.9	–	24.9	–	4.98	–	2.692
T4	9.80	–	9.80	–	4.98	–	2.694
T5	0.960	4.51	–	99.9	–	99.9	2.723
T6	0.970	2.52	–	99.9	–	99.9	2.718

Table A.8.: analytical detail of the microcalorimetric titrations on the system Ag(I)/methionine (see section 2.4.4, p. 75)

Tit. n.	$C^0_{H^+}$	$C^0_{Ag^+}$	$C^{tit}_{H^+}$	$C^{tit}_{Met^-}$	V^0
	mM	mM	mM	mM	mL
T1	10.02	0.970	110.2	10.03	2.683
T2	0.01	1.01	10.50	100.2	2.694
T3	0.04	4.03	10.50	100.2	2.690
T4	0.02	2.00	10.50	100.2	2.687
T5	9.85	4.05	110.2	100.3	2.722
T6	10.09	1.96	110.2	100.3	2.574
T7	0.04	4.00	99.46	99.46	2.703

APPENDIX B

The solution chemistry of *soft* transition metal complexes

From "Interpretation of solution stabilities of metal complexes"

by Gerold Shwarzenbach [132]

B.1. *Hard* and *soft* complexes

Transition metal cations are characterized by very diverse coordination chemistry, which depends on the electronic configuration of the d valence shell of the metal, its oxidation state and its ionic radius. Given this, different transition metal cations have very distinct affinities toward ligands. Depending upon the ligands, we can distinguish between two types of behavior (or characters), which we shall call hard and soft.

The hard character. d^0-cations show an extreme hard character: in aqueous solutions they interact only with fluoride and oxygen donors to any appreciable extent. Many of the d^0-cation fluoride complexes have poor water solubility, but quite often they can be dissolved by addition of an excess of the ligand, which drives the formation of high stoichiometry, negative-charged, complexes, as in the case of the hexafluoro aluminate:

$$\mathrm{Al^{3+}} + 3\mathrm{F^-} \rightarrow \mathrm{AlF_{3\,(s)}}$$
$$\mathrm{AlF_3} + 3\mathrm{F^-} \rightarrow [\mathrm{AlF_6}]^{3-}$$

On the other hand d^0-cation have no tendency to form complexes with the heavier

halides: for example the $[Al(H_2O)_6]Cl_3$ salt crystallizes from concentrated hydrochloric acid solutions.

The most important ligands for d^0-cation are the oxygen donors, including the hydroxide ion, oxalate, citrate, tartrate and EDTA. In particular OH^-, in a similar way to F^-, can form with Al^{3+} a hexahydroxo complex:

$$Al^{3+} + 3OH^- \rightarrow Al(OH)_{3\,(s)}$$
$$Al(OH)_3 + 3F^- \rightarrow [Al(OH)_6]^{3-}$$

As far as the intensity of the interaction is concerned, it is generally observed that the stability of the complexes rises rapidly with the charge of the d0-cation and falls as its radius becomes larger:

$$K(I) \ll Ca(II) \ll Sc(III) \ll Ti(IV)$$
$$Al(III) \gg Sc(III) \gg Y(III) > La(III)$$

This regularity suggests that the coordination of the d^0-center is primarily due to Coulombic forces. This explains why the favored ligands are those that bring the negative charge on the ligand close to the metal center, such as fluoride and oxygen donors. Cyanide and sulfide anions, even if charged, are rather not coordinating species for hard cations in aqueous solutions. This is partly due to their remarkable basicity, so that these ligands add a proton from water leading the formation of coordinating hydroxide ions in solutions.

The *soft* character. The low charged d^{10} centers Cu(I), Ag(I) and Au(I) are the best examples of metal cations with a soft character. These monovalent cations form complexes with heavy halides, much stronger than those formed by hard metal centers, and fluoride in general is poorly coordinated ($F^- \ll Cl^- < Br^- < I^-$). Sulfur donor more than oxygen ones, ammonia and amines are able to compete with the more polar H_2O even in aqueous solution (that means an environment with a very large excess of water). As discussed in the present work, phosphino complexes are an important class of soft ligands for Cu(I), Ag(I), Au(I).

The formation of this type of complexes cannot be explained in terms of electrostatic

forces, as in the case of the hard complexes: charges and ionic radii are certainly not decisive factors causing the stability of these adducts. Among these three prototypes of soft metals, Au(I), which is the largest, forms the most stable complexes, and with the halide anions, the one having the greatest radius, I^-, is preferred. Furthermore, the complex stability with selective ligands is reduced when the charge on the metallic center is increased in a series of isoelectronic d^{10} cations (e.g. Ag(I) > Cd(II)). All of these facts demonstrate the formation of covalent bonds. The deciding factors for complex stability seem to be the ionization potential of the metal ion (the more noble is the metal, more stable are its complexes) and the electronegativity of the ligand (complex stability increases with decreasing electronegativity of the ligand itself).

General and selective ligands. Fluorides and oxygen donors show to be suitable coordinating ligands for both hard and *soft* *d*-valence metal cation, so they are generally referred as "general ligands". The other types are rather named as "selective ligands" and the more so, the lower their negative charge, their polarity and the lower their electronegativity of the ligand donor atom. The distinction between hard and soft characters is related to the difference between an electrovalent and a covalent behavior. The lower the charge and the grater the radius of the metal cation, the less marked is its *hard* character.

Transition metal cations nd^q ($0 < q < 10$). The transition metal cations of the third period, from $3d^1$ to $3d^5$ have a remarkable hard character. Therefore, their tendency to coordinate selective ligands is small. Weak complexes with Cl^-, Br^- and I^- can be obtained only in concentrated solutions of the corresponding hydrogen halide. Ammonia, sulfide and cyanide usually act as a base and precipitate the corresponding hydroxide salt. The behavior of a complete series of the divalent $3d^5$ to $3d^{10}$ cations can be described using the the rule of Irving-Williams [133]:

$$\mathrm{Mn(II)} < \mathrm{Fe(II)} < \mathrm{Co(II)} < \mathrm{Ni(II)} < \mathrm{Cu(II)} > \mathrm{Zn(II)} \tag{B.1}$$

The stability of these complexes generally increases from Mn(II) up to Cu(II) and falls off again by passing on to Zn(II). However, zinc is not considered a transition metal [134],

Table B.1.: stability constants of some complexes of $3d^5$ to $3d^{10}$ cations with some oxygen and nitrogen donors ligands.

		$\log K_1$					
ligand	donor	Mn(II)	Fe(II)	Co(II)	Ni(II)	Cu(II)	Zn(II)
oxalate	O, O	3.9	4.5	4.8	5.2	6.2	4.9
glycinate	O, O	3.2	3.9	4.6	5.7	8.2	5.2
ethylene diamine	N, N	2.8	4.3	5.9	7.6	10.8	5.9

due to its d^{10} valence shell electronic configuration present in all of its oxidation states. There are but a few exceptions to Irving rule. They include some complexes of multidentate ligands which do not fit the coordination geometry favored by Cu(II) (as discussed in the introduction, Cu(II) prefers to form tetracoordinate complexes with a square-planar arrangement) so that the stability of the $3d^9$ ions such as Cu(II) falls too low in comparison to what is expected according to the (B.1). Furthermore, the substitution of H_2O in the aquoion, is in some instances accompanied by a rearrangement of the valence electrons, for example that with cyanide as in these two cases:

$$[Fe(H_2O)_6]^{2+}\,(\text{high spin}) \rightarrow [Fe(CN)_6]^{4-}\,(\text{low spin})$$
$$[Ni(H_2O)_6]^{2+}\,(\text{octahedral, paramagnetic}) \rightarrow [Ni(CN)_4]^{2-}\,(\text{sq. planar, diamagnetic})$$

Which causes these two complexes to become more stable than predicted by the (B.1).

The reason for the general validity of the Irving-Williams rule is not difficult to understand: the radii of the cations decrease slightly from Mn(II) to Cu(II), whereas Zn(II) is larger again. Furthermore, the ionization potentials of the metals considered increase from Mn to Cu, but as well known Zn is less noble than Cu. Therefore, both the coordination due to electrostatic forces (which depends upon charge and radii) as well as the covalency of the bonds formed (depending on electronegativities) change as predicted by the relationship (B.1). The values of the stability constants reported in table B.1 and plotted in Figure B.1 make it clear that the change in ionization potentials is much more important than the differences in radii. With fluoride and oxygen donors the maximum at Cu(II), shown in the figure, is much less pronounced than with nitrogen donors.

We give an insight to these facts by stating that all the $3d^q$ cation have a dominant hard character, but that more and more the soft character becomes mixed in as q increases, the

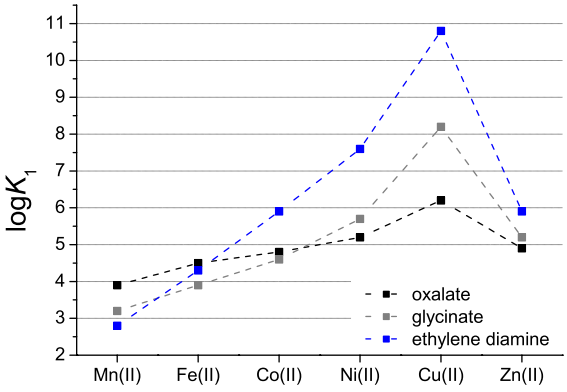

Figure B.1.: trends of the stability constants of some complexes of $3d^5$ to $3d^{10}$ cations with some oxygen and nitrogen donors ligands.

maximum being at q = 9, because the d^9 Cu(II) is the most noble of the $3d^q$ cations series. However this behavior is not exhibited with the heavy halide anions, and their complexes are surprisingly weak and formed only in concentrated solutions of hydrogenhalides, with stability constants with values generally lower than 1.

In contrast with the $3d^q$ case, the metal cations of the further periods, $4d^q$ and $5d^q$ are characterized by a marked soft character, dominant for q > 5. Whereas aquoion complexes of the third period transition cations can be easily obtained, those of the fourth and fifth ones are more difficult to be obtained or even unknown. Conversely, complexes with heavy halides of $4d^q$ and $5d^q$ cations are known. We can summarize that the coordination behavior of the transition metal cations nd^q as follow: 1) The third period transition metal cations show a marked hard character, and a soft character increasing up to $3d^9$. 2) The soft character of a transition metal center increases more with n than with q: fourth and fifth transition cations show a soft behavior, finally becoming dominant in the nd^5–nd^{10} (n = 4,5) configurations.

B.2. Enthalpy and entropy of formation of hard and soft complexes

The free Gibbs energy, ΔG^0, accounts for the spontaneity of a reaction. It is expressed by the well-known Gibbs-Helmholtz equation, $\Delta G^0 = \Delta H^0 - T\Delta S^0$. The formation of hard

and soft complexes differ strikingly from one another with respect to the relative importance of ΔH^0 and $T\Delta S^0$ terms in the equation.

Hard complexes associations are characterized by $T\Delta S^\circ$ values positive and dominant, while ΔH° contributes little or nothing to the stability.

Soft complexes associations are characterized by ΔH° values negative (exothermic) and dominant, and $T\Delta S^\circ$ contributes little or nothing to the stability.

As previously explained, *hard* complexes are characterized by coordinative metal–ligand bonds with a poor or negligible character of covalency. Therefore the formation of hard complexes is a process driven by long-range Coulombic attractive forces, between the anionic ligand and the metal center, usually bringing a high positive charge. A positive value of the formation entropic term, $T\Delta S^0$, takes into account this type of association, in which are involved reactants having opposite charges. Anyway, the complex formation with anionic ligands is more or less concerned whether the metallic center reveals a soft or hard character. This phenomenon has nothing to do with the nature of the bonds broken or newly formed (be them electrovalent or covalent) during the reaction. It must therefore related with the neutralization of the opposite charges following the formation of the complex and be caused by structural changes occurring within the solvent. In fact, many polar solvent molecules can be oriented by the field of forces created by ionic charges and then set free when these charges are neutralized in the course of the reaction. This increases the disorder in solution, which means an increment of the degree of freedom of the solvent particles present, and therefore raises the entropy of the system.

Uncharged ligands, which are less polar than water, can only be coordinated in aqueous solution if covalent bonds are formed. In this case the complex formation is due to the establishment of short-range forces, which take into account of the exothermicity of the reaction. A negative enthalpy value (a pronounced exothermicity of reaction) is the driving force of the association process. In general, the entropy variation exerts a negative, but most often a negligible, contribution to the stabilization of the complex formed.

Nevertheless, entropy is much more negative for reactions of soft metal cations with phosphines and thioethers, such as in the case of the formation of complexes of Cu(I),

Ag(I) with PTA and methionine, widely discussed in this work. In fact, these type of ligands are the most selective ones known. In particular phosphines in general show a high affinity toward soft cations, and are much less polar than the corresponding amine obtainable by formal substitution of the phosphorous with a nitrogen atom. In the course of a reaction with pronounced soft cations, strongly polar water molecules in the coordination sphere of the metal are substituted by a less polar and less solvated phosphine or thioether. The coordinative bond has a strong covalent character, which accounts for the reaction exothermicity. Moreover the water molecules, weakly bonded to the metal cation, once dissociated following the formation of the complex, result to be highly solvated by the solvent, bringing to a decrease of the freedom degrees of the particles in solution, which means a remarkable entropy decrease too.

APPENDIX C

Effect of the ionic medium on the solution equilibria

The *thermodynamic stability constant* of an equilibrium system is expressed as a funtion of the *activities* of the reagents. The equilibrium constants of this thesis work are conversely *stoichiometric stability constants*, which are functions of the concentration of the species at the equilibrium, obtained in a constant ionic medium by means of a high concentration of an inert background electrolyte. In these conditions, the activity coefficients are constant, and, using a correct model it is possible to convert the experimental stability constants to the real thermodynamic ones.

Three models are mainly used to describe the ionic medium dependence of equilibrium constants: 1) The Debye–Hückel Law, in which the activity coefficients of reactants and products depend only on the ionic charge and the ionic strength. 2) The Specific ion Interaction Theory (SIT), an extension of the Debye–Hückel, which accounts for the medium specific properties, by introducing ion pairing between the medium ions and the species involved in the equilibrium reactions. 3) The Pitzer models, which are a further extensions of the SIT, used to evaluate the activity coefficients of the species in highly concentrated ionic media.

C.1. The Debye–Hückel limiting Law.

The *Debye–Hückel limiting Law* [135, 136], eqn. (C.1) was the first empiric model, developed in order to provide the calculation of the activity coefficients, γ_J of the species

present in solution at the equilibrium.

$$\ln \gamma_{\mathrm{J}} = -z_j^2 \frac{A\sqrt{I}}{1+\sqrt{I}} \tag{C.1}$$

The fundamental assumption of the law is that an ion in solution is mainly surrounded by particles with opposite charge. This approximation is true for solutions with a low ionic strength ($I \lesssim 0.01$ mol/dm^3) and low contentrations of soluted to be studied: in these conditions, as implied by the (C.1) the activity coefficient of a ionic species depends only on the charge of the ion itself and on the ionic strength, regardless the chemical composition of the background electrolyte.

For water solutions, $A = 0.509$. To note, according to this model, the activity coefficients of neutral species in solution do not change as the ionic strength is varied, since for uncharged species, $z_j = 0$ and therefore $\ln \gamma_{\mathrm{J}} = 0$, $\gamma_{\mathrm{J}} = 1$.

C.2. The Specific ion Interaction Theory (SIT)

The Specific ion Interaction Theory (SIT) is a theory developed by Bronsted [137] and further developed by Guggenheim, Scatchard and Ciaviatta [138–140]. SIT is an extension of the Debye–Hückel Law, used to estimate the values of the activity coefficients of species at the chemical equilibrium, at relatively high ionic strengths ($I \lesssim 1.0$ mol/dm^3). In these conditions, deviations from the Debye–Hückel are significative, and the SIT-based model account of them. In particular, first-order deviations due to specific interactions with the background electrolytes are estimated. In the SIT model, the activity coefficients of the species are set to depend both on the concentration of the ionic medium (as in the Debye–Hückel expression), and on the particular chemical nature of the ions of the background electrolyte. The value of the activity coefficient of a species J in the SIT model is calculated by:

$$\ln \gamma_{\mathrm{J}} = -z_j^2 \frac{0.509\sqrt{I}}{1+1.5\sqrt{I}} + \sum_k b_{j,k} c_k \tag{C.2}$$

Where the first term is derived by the Debye expression. The second term is a sum which provide the first-order corrections to the Debye: $b_{j,k}$ is an empirical parameter which

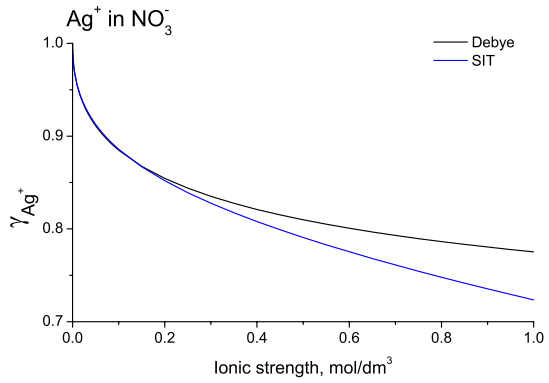

Figure C.1.: dependence of the activity coefficient of Ag^+ with the ionic strength ($NaNO_3$ background electrolyte).

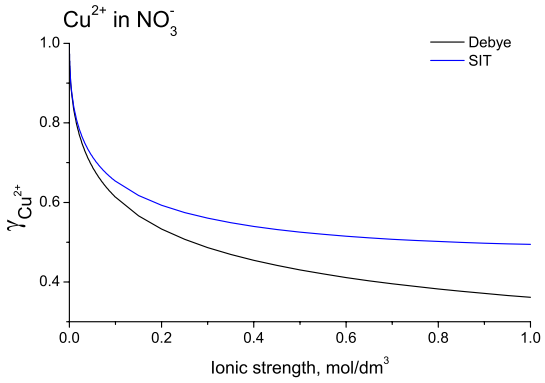

Figure C.2.: dependence of the activity coefficient of Cu^{2+} with the ionic strength ($NaNO_3$ background electrolyte).

accounts for the specific interaction between the ion J with another ion K with opposite charge in solution. The terms in the sum are linearly dependent on the concentration of the interacting ionic species. The diagrams in the Figures C.1 and C.2 show the dependence of the activity coefficients of Ag^+ and Cu^{2+} respectively, as a function of the ionic strength, in solutions with different concentrations of $NaNO_3$ as background electrolyte. A comparison between the calculation made on the basis of the Debye–Hückel law (black line) and with the extended SIT expression (blue line) is reported. Diagrams show that at low ionic strength ($I \leq 0.05$ mol/dm^3) the values of the activity coefficients calculated on the basis of the two models are close each other and therefore the Debye–Hückel provides a reliable determination of the activity coefficients. Marked deviations between the two models are instead observed at higher ionic strength (> 0.15 mol/dm^3 for γ_{Ag^+} and > 0.05 mol/dm^3 for $\gamma_{Cu^{2+}}$.

The activity coefficients of neutral species calculated in the SIT model, are no longer constant with respect to variations of the ionic strength, but depend linearly on I as:

$$\ln \gamma_{\mathrm{J}} = k_{\mathrm{J}} \cdot I \tag{C.3}$$

Where k_{J} is an empiric parameter to be determined.

C.3. The Pitzer models

These models, devised by Pitzer and coworkers [100] allow the calculation of the activity coefficients of the species at the equilibrium, in solutions with multiple electrolytes, and in presence of high concentrations of the ionic medium (up to 6 mol/dm^3).

In very concentrated solutions ($I > 3$ mol/dm^3, i.e. salt brines), the assumption that an ion is mainly surrounded by solvent molecules and background electrolytes with opposite charges is no longer valid. Pitzer models take therefore into account electrostatic interactions between triplets of a cation an two anions or an anion with two cations. If the ionic medium is much more concentrated than the analyte solutes, triple interactions comprising a couple of cations or anions of the same solute are reasonably neglected. At lower ionic medium concentrations (0.100 – 1.0 mol/dm^3) triple interactions can be neglected at all, and the only interaction between couples of ions with opposite charges is taken into account. In these cases, Pitzer models behave likewise those of SIT.

In the model, three empirical parameters, $\beta^{(0)}$, $\beta^{(1)}$ and C^{ϕ} describe the interaction of couples and/or of triplets of ionic species. They need to be determined by the fitting of several experimental data collected during thermodynamic studies, carried out at different ionic medium concentrations. The interaction parameters for the most common electrolytes have been reported by Pitzer and coworkers [141] and are currently available in several handbook and databases (*Aspen Physical Property Methods & Models*).

These models are very complex, and the determination of the parameters reported above is not discussed here. Details are available in the literature [99, 100, 142, 143].

C.3.1. Application in the study of Cu(I)–chloride complexes

The Pitzer models have been used to estimate the activity coefficients of Cu^+, Cl^- and Cu(I) chlorocomplexes in aqueous solution of NaCl 1.0 M, on the basis of the data mainly provided by a literature work by Sharma and coworkers [92] (see section 2.2 on page 31).

The authors evaluated the stability constants of the three successive chlorocomplexes with general formula $[CuCl_m]^{1-m}$ (β_m, with m = 1 – 3), formed in solution at relatively high concentrations of chloride (0.100 – 5.00 M). For these species, they also calculated the

Table C.1.: Pitzer interaction parameters for aqueous Cu(I) solutions in NaCl.

interactions	$\beta^{(0)}$	$\beta^{(1)}$	C^{ϕ}	ref.
Na^+, Cl^-	0.0765	0.2664	0.0013	[100]
Na^+, $[CuCl_2]^-$	0.0837	0.1595	0.0196	[91]
Na^+, $[CuCl_3]^{2-}$	-0.0016	1.8547	0.1142	[91]

Table C.2.: Activity coefficients and overall stability constants β calculated by the Pitzer model (see Figure C.3).

Species		NaCl, 0.1 M		**NaCl, 1.0 M**	
	$\log \beta^0$ [92]	γ	$\log \beta$	γ	$\log \beta$
Cu^+	–	0.777	–	**0.655**	–
$CuCl_{(aq)}$	*3.10*	1.013	2.87	**1.141**	**2.68**
$[CuCl_2]^-$	*5.42*	0.767	5.20	**0.635**	**5.07**
$[CuCl_3]^{2-}$	*4.75*	0.380	4.72	**0.171**	**4.78**

stability constants at $I = 0$, providing for each interaction between couples of ionic species the corresponding three Pitzer parameters, reported on Table C.1. Parameters concerning triple ionic interactions have been not taken into account, since the maximum chloride[1] concentration investigated was 1.0 M. Since $CuCl_{(aq)}$ is a neutral compound, its activity coefficient depends only on the ionic strength, as reported in eqn. (C.3), and no parameters for specific interactions of this species are therefore reported in the Table.

The stability constants of the three chlorocomplexes in NaCl 1.0 M have been calculated from the values of $\log \beta^0$ and γ_J of the different ionic species (Table C.2 and diagram in Figure C.3). The stability constants have been subsequently used to calculate the relative distribution of the chlorocomplexes in a 1.0 M NaCl aqueous solution (see section 2.2 on page 2.2).

[1] Chloride is both a complexing species and the background electrolyte in this case.

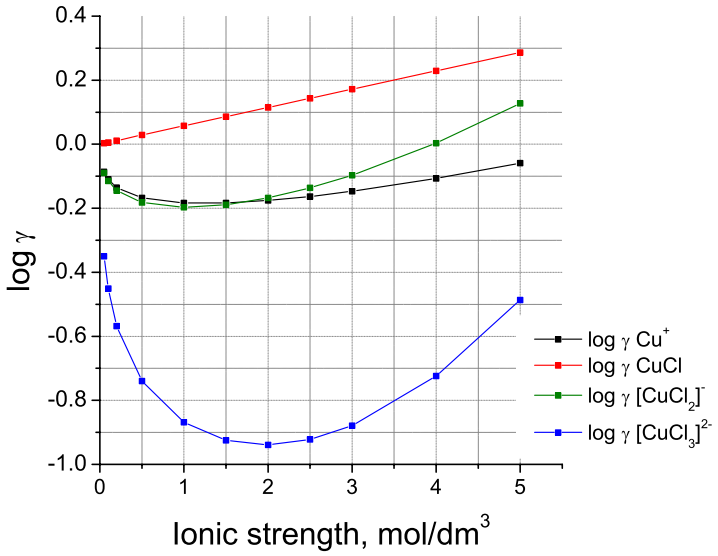

Figure C.3.: $\log\gamma$ ($\log_{10}$ values of the activity coefficients) of the Cu(I)–Cl^- complexes *vs* I (mol/dm^3). Values of γ at $I = 0.1$ and 1.0 M are reported on Table C.2.

APPENDIX D

Numerical methods

D.1. The method of least-squares

The program *Hyperquad*, used for the minimization of the experimental data obtained by potentiometry and spectrophotometry is based on the method of least–squares [77, 78, 144]. This method consists of finding a set of parameters that minimize an *objective function*. It is called *objective* because it is the object of the method to minimize this function. In the case of our experiments, which are made by means of titrations, the objective function depends for instance on the *experimental points*, a set of couples of dependent/independent variables, in which the dependent variable is the property we measure: electrodic potential E (mV) in potentiometric titrations and absorbance spectra, $\{A_{\lambda 1},\ A_{\lambda 2}, \cdots A_{\lambda n}\}$ in spectrophotometric titrations; independent variable is the volume of titrant added (mL).

Nevertheless, the objective function also depends on some parameters, specifically on a set of *group parameters*, which are the analytical concentrations of the titrand species (those in the measure cell) and on the titrant ones (loaded in the burette) and on a set of *common parameters*, which are the values of the formation constants chosen to describe the chemical system. Regarding the group parameters, it is obvious that the accuracy in the determination of the initial concentrations of the species, by means of careful standardizations prior to the experiments is fundamental. Common parameters are related instead to the *model* chosen for describing the chemical system.

Therefore, we begin by defining a model of the chemical system. Suppose that n measures

have been made. Corresponding to each experimental quantity, f_i^{exp}, there is a calculated value, $f_i^{calc}(v_i, p_1, p_2, \ldots, p_m)$, which is a function of the ith independent variable, the volume v_i and on a set of parameters p_m as described above. This functional relationship defines the model. We then define the residuals, r_i, in equation (D.1):

$$r_i = f_i^{exp} - f_i^{calc}(v_i, p_1, \ldots, p_m) \qquad \mathbf{r} = \{r_1, \ldots, r_n\}^T \tag{D.1}$$

Now, the simplest objective function to be minimized is the sum of squared residuals of the n measurements: the term "least squares" derives from this kind of function (D.2):

$$U = \sum_{i=1}^{n} r_i^2 \qquad U = \mathbf{r}^T\mathbf{r} \tag{D.2}$$

The relation on the right in (D.2) is the same operation expressed in the vector/matrix notation, so $\mathbf{r}^T$ is the *transpose* vector of $\mathbf{r}$. However, in defining the objective function in this way we are making two important assumptions: 1) we assume that the calculated values f_i^{calc} as well as the independent variables are not subject to experimental error. The error just affects the measured values f_i^{exp}; 2) we assume that the errors e_i are all equal and not statistically correlated each other. This last assumption is generally good when the program is asked to minimize with respect to few dependent variable or parameters. In general, the design of the experiments should be properly done in order to minimize correlations. Anyway, a chemical system with multiple complexes present at the equilibrium requires, to be described, a simultaneous calculation of several formation constants, β_n, which values obtained at the end of the minimization process allow to determine the relative distribution of the species at the equilibrium. In the simplest case of potentiometric titrations, the calculation involves the minimization of electrodic potential as dependent variable and the refinement of the parameters β_n. However electrodic potentials are related to the concentration of the species by the *Nernst's Law* and therefore a calculated value of the electrodic potential can be obtained directly from the calculated values of the formation constants.

On the other hand, the minimization process of microcalorimetric data involves the simultaneous calculation of both the molar enthalpy of formation and the related value of the constant for each species. This calculus is much more delicate than that of potentiometric data and it is very common to observe a certain correlation between enthalpies and constants.

So, to be more general, we must accept that each observation is not only affected by an error related on its single quantity, expressed by *variance*, but that different observations are also subject to different errors and that the errors of each pair of observations are connected trough a *covariance* term.

Variance is defined as (D.3):

$$\sigma^2 = \frac{\sum_i (f_i^{exp} - f_i^{calc})^2}{n-1} = \frac{\sum_i r_i^2}{n-1} \tag{D.3}$$

where n is the number of measurements; the correlation between pairs of observations f_i^{exp} and f_j^{exp} is estimated instead by the *covariance*, defined as (D.4):

$$\mathrm{COV}(f_i^{exp},\, f_j^{exp}) = \frac{\sum_{k=1,n} (f_{ik}^{exp} - f_i^{calc})(f_{jk}^{exp} - f_j^{calc})}{n-1} \tag{D.4}$$

As suggested above, it is a good experimental practice to design properly the experiments and to handle carefully the results of minimizations in order to try to reduce the covariance to zero. Covariance is related to correlation coefficient ρ_{ij} by (D.5):

$$\mathrm{COV}_{ij} = \sigma_i \sigma_j \rho_{ij} \tag{D.5}$$

A correlation coefficient can only take values between +1 and –1. The more its value is close to zero the less correlation between the pair measurements is estimated. The correlation coefficients of the form ρ_{ii} are equal to 1, since the error on any quantity is completely correlated with itself.

Together, variance and covariance make up the so-called variance-covariance matrix, whose elements are given by (D.6):

$$\mathbf{M} = \begin{pmatrix} \sigma_1^2 & \sigma_1\sigma_2\rho_{12} & \cdots & \sigma_1\sigma_n\rho_{1n} \\ \sigma_2\sigma_1\rho_{21} & \sigma_2^2 & \cdots & \sigma_2\sigma_n\rho_{2n} \\ \vdots & \vdots & \ddots & \vdots \\ \sigma_n\sigma_1\rho_{n1} & \sigma_n\sigma_1\rho_{n1} & \cdots & \sigma_n^2 \end{pmatrix} \tag{D.6}$$

This matrix is symmetrical with respect its diagonal, because obviously $\sigma_i\sigma_j\rho_{ij} = \sigma_j\sigma_i\rho_{ji}$. When no correlation between a pair of measurements f_i^{exp} and f_j^{exp} is observable, the relative covariance matrix element M_{ij} is zero. Instead, variance (diagonal) elements $\mathrm{M}_{ii} = \sigma_i^2$ are always non-zero.

So, we have allocated variance and covariance for a pair of observations as matrix elements in the form M_{hk}; $h = 1,\ n$; $k = 1,\ n$ where n is the number of measurements. We define now $\mathbf{W}$ as the *weight matrix*, which is the inverse of the variance-covariance matrix as follows:

$$\mathbf{WM} = \mathbf{MW} = \mathbf{I};\quad \sum_{h=1,n} \mathrm{W}_{ih}\mathrm{M}_{\mathrm{hk}} = 1\,(i = k);\quad \sum_{h=1,n} \mathrm{W}_{ih}\mathrm{M}_{\mathrm{hk}} = 0\,(i \neq k) \tag{D.7}$$

We can therefore gain a more complete definition of the objective function U as follow:

$$U = \sum_{h=1,\,n}\sum_{k=1,\,n} r_h\mathrm{M}_{hk}r_k \qquad U = \mathbf{r}^T\mathbf{W}\mathbf{r} \tag{D.8}$$

The expressions for the objective functions in equations (D.2) and (D.8) become equivalent if no correlation is present ($\mathrm{M}_{hk} = 0$, $\mathrm{W}_{\mathrm{hk}} = 0$).

The method of least-square is used to calculate that value of the m-vector $\mathbf{p}$ of parameters that minimizes U. The minimum of the objective function can be found by setting its partial derivatives with respect to each parameter to zero:

$$\frac{\partial U}{\partial p_j} = -\sum_h\sum_i \mathrm{W}_{hi}\left(r_h\frac{\partial f_i}{\partial p_j} + r_i\frac{\partial f_h}{\partial p_j}\right) = 0; \qquad \mathbf{g} = -2\mathbf{J}^T\mathbf{W}\mathbf{r} = 0 \tag{D.9}$$

$\mathbf{g}$ is called the *gradient vector* and contains the m elements $\partial U/\partial p_j$. $\mathbf{J}$ is known as the *Jacobian matrix* whose elements are the partial derivatives $\partial f_i/\partial p_j$.

In linear systems, f_i is a linear combination of the parameters: $\mathbf{f} = \mathbf{Jp}$, therefore the residual become $\mathbf{r} = \mathbf{f}^{exp} - \mathbf{Jp}$. If this expression for the residual is substituted into the equation (D.9) we obtain the so-called *normal equations* (D.10):

$$-2\mathbf{J}^T\mathbf{W}(\mathbf{f}^{exp} - \mathbf{Jp}) = 0; \qquad \mathbf{J}^T\mathbf{WJp} = \mathbf{J}^T\mathbf{Wf}^{exp} \tag{D.10}$$

However, in equilibrium systems, the models are non-linear and a numeric method by means of an iterative process of successive approximations must be used. It is first necessary to provide the program a proper speciation model, which is an input instruction containing a description of the system, about how many complexes we expect to be present in solution at the equilibrium, their stoichiometry and the estimated values of the formation constants that will be subsequently minimized by the iterative process. Ideally, as usual when dealing with iterative algorithms, in order to attain a fast and reliable convergence to the best-fit, the starting estimates should be taken close to those for which the gradient vector is zero.

Let the vector of estimates be $\mathbf{p}^0$. Each element of the gradient vector is now expanded as a first-order Taylor series about $\mathbf{p}^0$:

$$g_j = g_j^0 + \sum_{k=1,n} \frac{\partial g_j}{\partial p_k}(p_k - p_k^0); \qquad \mathbf{g} = \mathbf{g}^0 + \mathbf{Hs} \tag{D.11}$$

Since g is zero at the minimum, equation (D.11) can be written as:

$$\mathbf{Hs} = -\mathbf{g}^0 \tag{D.12}$$

and the normal equations as:

$$\mathbf{Hs} = 2\mathbf{J}^T\mathbf{Wr} \tag{D.13}$$

where $\mathbf{s}$ is the *shift vector*. The matrix $\mathbf{H}$ in known as the *Hessian* and its elements are

obtained by differentiating equation (D.9) as follow:

$$\frac{\partial g_j}{\partial p_k} = -\sum_h \sum_i \mathrm{W}_{hi} \left(r_h \frac{\partial^2 f_i}{\partial p_j \partial p_k} + r_i \frac{\partial^2 f_h}{\partial p_j \partial p_k} - \frac{\partial f_h}{\partial p_k} \frac{\partial f_i}{\partial p_j} - \frac{\partial f_i}{\partial p_k} \frac{\partial f_h}{\partial p_j} \right) \tag{D.14}$$

$$C_{jk} = \sum_h \sum_i \mathrm{W}_{hi} \left(r_h \frac{\partial^2 f_i}{\partial p_j \partial p_k} + r_i \frac{\partial^2 f_h}{\partial p_j \partial p_k} \right) \tag{D.15}$$

$$\mathbf{H} = 2\mathbf{J}^T\mathbf{W}\mathbf{J} - 2\mathbf{C} \tag{D.16}$$

On substituting equation (D.16) into the normal equation (D.13) we obtain the relation (D.17), which is the expression of the Newton-Raphson equation:

$$(\mathbf{J}^T\mathbf{W}\mathbf{J}\mathbf{s} - \mathbf{C})\mathbf{s} = \mathbf{J}^T\mathbf{W}\mathbf{r} \tag{D.17}$$

The residual vector $\mathbf{r}$ represents the difference between the observed values f_i^{exp} and the values calculated with the initial parameters estimates f_i^0. Now, by setting the matrix $\mathbf{C}$ equal to zero, as it is in a linear system where $\mathbf{f} = \mathbf{J}\mathbf{p}$, we therefore obtain equation (D.18), the normal equation of the Gauss-Newton method:

$$\mathbf{J}^T\mathbf{W}\mathbf{J}\mathbf{s} = \mathbf{J}^T\mathbf{W}\mathbf{r} \tag{D.18}$$

Solution of this equation yields the shift vector $\mathbf{s}$. Now, if the first-order Taylor series expansion (D.11) is valid, then adding the shift vector $\mathbf{s}$ to the vector of parameter estimates $\mathbf{p}^0$ gives those parameters for whose values the gradient vector $\mathbf{g}$ is zero. If the expansion is a broader approximation, the sum $\mathbf{s} + \mathbf{p}^0$ becomes the new parameter estimates vector for the subsequent iteration. The iterative process continues until an established convergence criterion is satisfied. At that point the objective function has reached its minimum value, U_{min}. Upon convergence, the variance-covariance matrix of the parameters is obtained by error propagation as:

$$\mathbf{M}(p) = \frac{U_{min}}{n-m}(\mathbf{J}^T\mathbf{W}\mathbf{J})^{-1} \tag{D.19}$$

Hence the parameter standard deviations and correlation coefficients are given by:

$$\sigma_i = [\mathrm{M}(p)_{ii}]^{1/2}; \qquad \rho_{ij} = [(\mathrm{M}_{ij}/\mathrm{M}_{ii}\mathrm{M}_{jj})]^{1/2} \tag{D.20}$$

D.2. Calculating the concentrations of the species at the equilibrium

Let be a set of n_r reactant A, B, ... present in a titrand solution. The total concentration T^0_{A} of the reactant A is analytically calculated as:

$$T^0_{\mathrm{A}} = \frac{n^0_{\mathrm{A}} + C^{tit}_{\mathrm{A}} \cdot V_{added}}{V_0 + V_{added}} \tag{D.21}$$

where: n^0_{A} is the initial quantity of A in the titrand solution; C^{tit}_{A} is the concentration of A in the titrant solution. V_0 is the initial volume of the titrand solution.

These reactant form n_k species at the equilibrium, with stoichiometric coefficients a, b, ... as:

$$a\mathrm{A} + b\mathrm{B} + \ldots \rightleftarrows \mathrm{A}_a\mathrm{B}_b \ldots \tag{D.22}$$

The concentration of the generic jth species, $\mathrm{A}_{a_j}\mathrm{B}_{b_j}\ldots$ is given by:

$$C_j = [\mathrm{A}_{a_j}\mathrm{B}_{b_j}\ldots] = \beta_j[\mathrm{A}]^{a_j}[\mathrm{B}]^{b_j}\ldots \tag{D.23}$$

Where β_j is the overall formation constant of the species $A_{a_j}\mathrm{B}_{b_j}\ldots$ For sake of clarity, in this example any charges of the species have been omitted. The total concentration of each reactant in solution is constrained by a condition of mass balance:

$$\begin{aligned} T_{\mathrm{A}} &= [\mathrm{A}] + \textstyle\sum_j a_j C_j \\ T_{\mathrm{B}} &= [\mathrm{B}] + \textstyle\sum_j b_j C_j \\ &\dots \end{aligned} \tag{D.24}$$

If the formation constants of eqn. (D.23) are known, the set of n_r equations (D.24) can be solved for the "free" concentrations [A], [B], ... and therefore the concentration of the species $\mathrm{A}_{a_j}\mathrm{B}_{b_j}\dots$ can be calculated by (D.23).

D.3. The program Hyperquad: the minimization of potentiometric and spectrophotometric data

Hyperquad [77, 78, 144] is a software based on a suite of programs, developed for the minimization of potentiometric and spectrophotometric data in order to obtain the value of the formation constants in complex chemical systems with multiple equilibria. As many other minimization softwares, Hyperquad calculation is based on the lest-squares approach [144]. In Hyperquad, the sum of the squares residuals of the objective function is minimized by means of the Gauss–Newton–Marquardt algorithm.

The core of the calculation is the determination of the free concentrations of the species, which is carried out by solving the non-linear simultaneous equations of mass balance (eqn. D.24) using the Newton-Raphson method. Potentiometric data points (E, mV and V_{added}, mL) are weighted by formula that allows for greater potential errors in the region of an end-point than elsewhere. For absorbance data points a relative weighting scheme is used.

In order to obtain a reliable speciation model for a chemical equilibrium system is in general a good idea to make use of more than one kind of analytical technique, and it would be indeed useful to use the same approach to minimize experimental data from these technique. With this aim, Hyperquad was developed in order to process both potentiometric and spectrophotometric data together. However, working on different kind of data simultaneously, make imperative that a full and rigorous weighting scheme is used. Given this, is possible to apply simple statistical tests for the goodness of the fit, with an expectation value of unity for the sample variance [78].

Calculation. A simple system of three reagents, including a metal M, a ligand L and the proton H, is taken as example to describe the calculation principles of Hyperquad (ion charges are omitted for convenience). In this outline the system is studied by means of potentiometric measurements, using an electrode responding to H, and by spectrophotometry, during which measurements are taken at n_l wavelengths. The speciation model consists in a set of n_k equilibrium constants.

The objective function is given in matrix notation simply as $U = \mathbf{r^T W r}$, as in eqn. (D.8), $\mathbf{r}$ is given by eqn. (D.1), $\mathbf{W}$ is the matrix of weights (eqn. D.7) and the functions calculated in the residuals are the potential values (mV) or the absorbance data (A_{obs}). To minimize the objective function, is used the Gauss–Newton–Marquardt method, which expression derives from eqn. (D.18):

$$(\mathbf{J^T W J} + \lambda \mathbf{D})\Delta\mathbf{p} = \mathbf{J^T W r} \tag{D.25}$$

Where $\mathbf{J}$ is the Jacobian matrix and $\mathbf{\Delta p}$ is the vector of shifts to be applied to the parameters. $\mathbf{D}$ is taken as equal to the diagonal elements of $\mathbf{J^T W J}$ and λ is the Marquardt parameter which may, of course, be zero. For the minimization of potentiometric data, the elements of the Jacobian relative to any unknown parameter x (a stability constant) are obtained from the expression of the Nernst Law:

$$E = E^0 + \frac{RT}{nF}\ln[\mathrm{H}] = E^0 + slope \cdot \ln[\mathrm{H}] \tag{D.26}$$

Where E^0 is the *standard potential* of the electrode and *slope* is equal to RT/nF in the ideal case. We therefore obtain:

$$\frac{\partial E}{\partial x} = \frac{\partial E}{\partial [\mathrm{H}]}\frac{\partial [\mathrm{H}]}{\partial x} = \frac{slope}{[\mathrm{H}]}\frac{\partial [\mathrm{H}]}{\partial x} \tag{D.27}$$

For the spectrophotometric data minimization, the elements are found from the expression of the Lambert-Beer Law:

$$A_\lambda = l \sum_{j=1,n_a} \epsilon_{\lambda_j} C_j \tag{D.28}$$

$$\frac{\partial A_\lambda}{\partial x} = l \sum_j \epsilon_{\lambda_j} \frac{\partial C_j}{\partial x} \tag{D.29}$$

The system is subject to the constraint that the equations of mass balance are satisfied, as in eqn. (D.24). Furthermore, given the expression for the the stability constants in eqn. (D.23) we obtain an equation for the total metal M concentration:

$$T_{\mathrm{M}} = [\mathrm{M}] + \sum_{j=1,n_j} p_j \beta_j [\mathrm{M}]^{p_j} [\mathrm{L}]^{q_j} [\mathrm{H}]^{r_j} = [\mathrm{M}] + \sum_{k=1,n_j} p_j C_j \tag{D.30}$$

Where $p_j \ldots r_j$ are stoichiometric coefficients. Similar expression can be written for L and H. Moreover, the total concentration of M can be obtained as analytical value from the initial amount n_{M} and its eventual concentration in the burette, as reported in eqn. (D.21):

$$T_{\mathrm{M}} = \frac{n^0_{\mathrm{M}} + C^{tit}_{\mathrm{M}} \cdot V_{added}}{V_0 + V_{added}} = [\mathrm{M}] + \sum_{k=1,n_j} p_j C_j \tag{D.31}$$

Again, similar expression can be written for L and H.

Now, the partial derivatives $\partial[\mathrm{M}]/\partial x \ldots$ are obtained by solving the set of simultaneous equations:

$$\begin{pmatrix} [\mathrm{M}]\frac{\partial T_{\mathrm{M}}}{\partial [\mathrm{M}]} & [\mathrm{L}]\frac{\partial T_{\mathrm{M}}}{\partial [\mathrm{L}]} & [\mathrm{H}]\frac{\partial T_{\mathrm{M}}}{\partial [\mathrm{H}]} \\ [\mathrm{M}]\frac{\partial T_{\mathrm{L}}}{\partial [\mathrm{M}]} & [\mathrm{L}]\frac{\partial T_{\mathrm{L}}}{\partial [\mathrm{L}]} & [\mathrm{H}]\frac{\partial T_{\mathrm{L}}}{\partial [\mathrm{H}]} \\ [\mathrm{M}]\frac{\partial T_{\mathrm{H}}}{\partial [\mathrm{M}]} & [\mathrm{L}]\frac{\partial T_{\mathrm{H}}}{\partial [\mathrm{L}]} & [\mathrm{H}]\frac{\partial T_{\mathrm{H}}}{\partial [\mathrm{H}]} \end{pmatrix} \begin{pmatrix} \frac{x}{[\mathrm{M}]}\frac{\partial [\mathrm{M}]}{\partial x} \\ \frac{x}{[\mathrm{L}]}\frac{\partial [\mathrm{L}]}{\partial x} \\ \frac{x}{[\mathrm{H}]}\frac{\partial [\mathrm{H}]}{\partial x} \end{pmatrix} = \begin{pmatrix} -x\frac{\partial T_{\mathrm{M}}}{\partial x} \\ -x\frac{\partial T_{\mathrm{L}}}{\partial x} \\ -x\frac{\partial T_{\mathrm{H}}}{\partial x} \end{pmatrix} \tag{D.32}$$

The coefficients on the left-hand side are found by derivatization of the general expression (D.30). The right-hand side takes different forms according to the nature of the parameter. In this example the only parameters we take into account are the formation (stability) constants. Alternatively, a parameter may be the initial quantity of a species, or the titrant concentration. The unknown free concentrations are found by solving the equations (D.31) of mass balance. The solution consists of an iterative Newton-Raphson refinement, using:

$$\begin{pmatrix} [\mathrm{M}]\frac{\partial T_{\mathrm{M}}}{\partial [\mathrm{M}]} & [\mathrm{L}]\frac{\partial T_{\mathrm{M}}}{\partial [\mathrm{L}]} & [\mathrm{H}]\frac{\partial T_{\mathrm{M}}}{\partial [\mathrm{H}]} \\ [\mathrm{M}]\frac{\partial T_{\mathrm{L}}}{\partial [\mathrm{M}]} & [\mathrm{L}]\frac{\partial T_{\mathrm{L}}}{\partial [\mathrm{L}]} & [\mathrm{H}]\frac{\partial T_{\mathrm{L}}}{\partial [\mathrm{H}]} \\ [\mathrm{M}]\frac{\partial T_{\mathrm{H}}}{\partial [\mathrm{M}]} & [\mathrm{L}]\frac{\partial T_{\mathrm{H}}}{\partial [\mathrm{L}]} & [\mathrm{H}]\frac{\partial T_{\mathrm{H}}}{\partial [\mathrm{H}]} \end{pmatrix} \begin{pmatrix} \frac{\Delta [\mathrm{M}]}{[\mathrm{M}]} \\ \frac{\Delta [\mathrm{L}]}{[L]} \\ \frac{\Delta [\mathrm{H}]}{[\mathrm{H}]} \end{pmatrix} = \begin{pmatrix} \Delta T_{\mathrm{M}} \\ \Delta T_{\mathrm{L}} \\ \Delta T_{\mathrm{H}} \end{pmatrix} \tag{D.33}$$

D.4. The program Letagrop: the minimization of microcalorimetric data

Letagrop [82, 84, 104] was the very first computer program to be applied to the study of equilibrium systems [77]. In the present work, a minimization algorithm developed in *Fortran* and based on the Letagrop approach has been used to minimize the experimental data obtained by the microcalorimetric titrations, in order to obtain the values of the formation constants and the related enthalpies of the species present in solution.

The refinement of the microcalorimetric data (experimental heat, mJ and volume added, μL) of an equilibrium system is a quite delicate task, since the program is usually asked to calculate at the same time a relatively large number of common parameters: the formation constants and the related enthalpies of the complexes. Therefore the algorithm of the program must be quite robust in order to avoid the calculation of wrong values, especially if the minimization runs through a false-minimum of the objective function.

Peter Gans and coworkers developed a Hyperquad suite [144] suitable for the minimization of such data by means of the Gauss–Newton–Marquardt approach. In this work we instead used a Letagrop-based software specifically designed by our research group.

Letagrop calculation of the best-fit is made by means of a numerical method based on the so-called pit-mapping approach. Two main minimization routines are built in the program. Each one performs a minimization on a different type of objective function U, defined as previously as the sum of the squares residuals of the experimental values as in eqn. (D.1) and (D.2).

The set of the common parameters $p_1, p_2, \ldots p_m$ upon which the calculation of the

minimum is made, are in this case both the values of the formation constants of the complexes supposed to be present in solution (β_j), and their related enthalpies (ΔH_j).

In the first routine the minimization is made over the residuals of the experimental reaction heat, so: $f_i^{exp} = Q_i^{react}$. The program calculates the related reaction heat on the basis of the estimated parameters. Concerning the formation of the complex species at a given titration point i, the programs first calculates their molar concentrations, C_j (mol/dm^3), on the basis of the estimated values of their formation constants, as reported in eqn. (D.23). In the Letagrop version we have used, the calculation of the species concentration is made by means of the Newton-Raphson approach previously discussed. Secondly, given the estimated values of the related molar formation enthalpies, ΔH_j (kJ/mol), the program calculates the reaction heat, Q_i^{calc}, from the relationship:

$$Q_i^{calc} = V_i(\Delta H_1 C_1 + \Delta H_2 C_2 + \ldots + \Delta H_j C_j) + \Delta H_{dil} \tag{D.34}$$

Where ΔH_{dil} is the dilution heat.

In the second minimization routine the minimization process is made over the sum of residual squares of the overall complexation heat per mole of metal, Δh_v^{tot} given by:

$$\Delta h_v^{tot} = \frac{Q^{react,\,tot}}{n_M} \tag{D.35}$$

The pit-mapping approach. We introduce the idea lying behind the pit-mapping approach with a simplified example, in which we assume that the objective function U, to be minimized, is dependent on a single common parameter p_j, so is $U(p_j)$. The program first calculates $U(p_j)$ on the basis of an estimated value of p_j, then p_j is varied about a positive and a negative quantity $\pm\sigma$ chosen by the program, and the new values of the objective function, $U(p_j \pm \sigma)$ are therefore calculated. A second-order polynomial fitting of the three values of $U(p_j)$, $U(p_j \pm \sigma)$ is then made. In the diagram in Figure D.1 is reported a suggestion of such calculation. The minimum point of this curve (red in the figure) provide the new calculated value of U from which a corresponding new value of p_j is obtained and used as new estimation value in the subsequent iteration step. It is possible to demonstrate that the iterative process runs toward convergence of the true value of p_j.

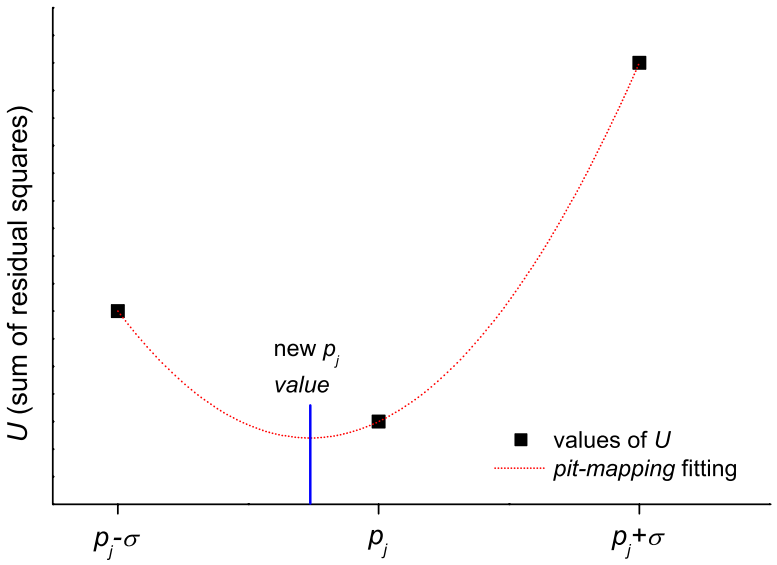

Figure D.1.: simplified example of pit-mapping minimization, in the calculation of the minimum of an objective function U (the sum of the squared residuals of the experimental and the calculated values)

Real systems with multiple equilibria, and therefore several formation constants and enthalpies to be calculated, can be treated as a generalization of the previous example. In this cases U is calculated upon a set of many common parameters p_j; in a single iteration step the program varies several of these parameters simultaneously and the fitting is made by means of a multi-dimensional parabola, where the number of dimensions depends on the number of parameters changed. Usually Letagrop changes the values of a chosen set of formation constants, and the values of the related enthalpies, alternately. The minimization process ends when an established convergence criterion is finally reached.